Theory of Nanoelectromechanical Systems: From Nanostructures to Molecules

im Fachbereich Physik

der Freien Universität Berlin

eingereichte

Dissertation

vorgelegt von

Mark Gregor Thomas

Berlin, Juli 2015

Erstgutachter (Betreuer):	Prof. Felix von Oppen, Ph.D.
Zweitgutachterin:	Prof. Dr. Tamara Nunner
Disputationstermin:	4. Mai 2015

Zusammenfassung

Aufgrund fortschreitender experimenteller Fortschritte stellen nanoelektromechanische Systeme ein faszinierendes Gebiet mit steigender Aufmerksamkeit dar. Wegen ihrer kleinen Ausmaße erlauben diese Systeme die Erforschung fundamentaler Physik und ermöglichen eine Vielzahl von Anwendungen, u.a. als Hochfrequenzresonatoren und ultrasensitiven Sensoren. Wegen starker Elektron-Phonon-Wechselwirkung sind diese Systeme ein Paradebeispiel von bosonischen Freiheitsgraden, die an eine fermionische Umgebung im Nichtgleichgewicht koppeln.

Viele der Anwendungen erfordern ein generelles Verständnis der umgebungsinduzierten Kräfte auf ein klassisches System. Indem das Nanosystem als generelle zeitabhängige Streuregion beschrieben wird, sind diese Kräfte kürzlich als Funktion der Streumatrix und seiner ersten adiabatischen Korrektur hergeleitet worden. In dieser Arbeit präsentieren wir eine effizientere und direkte Herleitung dieser Kräfte ausschließlich unter Benutzung der Streutheorie, die auf natürlich Weise solche Systeme beschreibt.

Kleine lokale Änderungen eines Streupotentials können aufgrund der Anderson Orthogonalitätskatastrophe drastische Auswirkungen auf Eigenschaften großer Quantensysteme haben. Im Gleichgewicht wurde der Orthogonalitätsexponent direkt mit dem Reibungskoeffizienten eines klassischen System, das sich in einem freien Elektronengas bewegt, verknüpft. Mit den erworbenen Kenntnissen zu den umgebungsinduzierten Kräften verallgemeinern wir diese Idee ins Nichtgleichgewicht. Hierzu untersuchen wir das Verhalten der Fidelitätsamplitude und des Loschmidt Echos, die dynamische Grössen der Orthogonalitätskatastrophe darstellen.

Ein molekularer Transistor im ultimativen Miniaturisierungslimit ist kürzlich experimentell realisiert worden. Atomar präzise Steuerspannung ist erzielt durch Repositionierung einzelner Ladungen durch Rastertunnelmikroskopie. Eine ausgeprägte Leitwertlücke anstatt des erwarteten Ladungsentartungspunktes wurde gemessen. Motiviert durch die experimentellen Beobachtungen erklären wir dieses Verhalten mit der Existenz zweier molekularer Konformationszustände, was das konventionelle Bild des Einzelelektronentunnelns durch molekulare Transistoren generalisiert.

Abstract

Due to ongoing experimental advances, nanoelectromechanical systems represent a fascinating field of study which receives increasing attention. Because of their small size, these systems allow for exploring fundamental physics and give rise to a wide range of applications such as high frequency resonators and ultra-sensitive sensors. Because of strong electron-phonon coupling, nanoelectromechanical systems provide a paradigmatic model for bosonic degrees of freedom coupled to an out-of-equilibrium fermionic environment.

Many of the applications require a general understanding of the forces which are induced by a quantum environment on a classical system. By considering the nanosystem as a generic time-dependent scatterer, these reaction forces have recently been expressed via an adiabatic expansion in terms of the scattering matrix and its first adiabatic correction. In this thesis, we present a more efficient and direct derivation of these forces by solely using scattering theory which is natural to the considered problem.

Due to the Anderson orthogonality catastrophe small local changes of a scattering potential can drastically affect properties of large quantum systems. In equilibrium, the orthogonality exponent was related to the friction coefficient of a classical particle moving in a free electron gas. Based on our knowledge on the environment-induced forces, we generalise this idea to out-of-equilibrium situations. To this end, we study the fidelity amplitude and the Loschmidt echo, which are dynamical measures of the Anderson orthogonality catastrophe.

A molecular transistor at the ultimate miniaturisation limit has recently been experimentally realised. Atomically precise gating is achieved via repositioning of individual charges by scanning tunnelling microscopy. Remarkably, a pronounced conductance gap instead of the expected charge degeneracy is observed. Motivated by the experimental observations, we explain this behaviour by the presence of two different molecular conformational states, which generalises the conventional picture of single-electron tunnelling through molecular transistors.

Contents

1. Introduction

The ultimate aim to control miniaturised devices has a long history. Famous is the talk given by Richard Feynman in 1959 at the annual meeting of the American Physical Society at the California Institute of Technology about the miniaturisation of electronic devices, where he offered $1000 to the inventor of a hard disk whose size is 25,000 times smaller than a common page in a book and which can store the information of the page itself [Feynman, 1960]. In this talk, he presented various conceptual ideas how to reduce the size of electronic devices towards the atomic scale. With ongoing experimental advances, many of the ideas of this talk have now been realised and even exceeded the proposed scale, for instance with the invention of the scanning tunnelling microscope (STM) [Binnig et al., 1982a, Binnig et al., 1982b] and the atomic force microscope [Binnig et al., 1986]. The $1000-challenge was eventually won in 1985 by Tom Newman using electron-beam lithography [Dietrich, 1986]. Nowadays this technique enables the construction of devices on the nanoscale [Park et al., 2002, Liang et al., 2002, Kubatkin et al., 2003, Roch et al., 2008, Song et al., 2009, Leturcq et al., 2009].

Beyond the construction of nanoscale systems, controlling and detecting their motion are experimental challenges. In 1959 Richard Feynman proposed a second challenge in his talk and offered "another $1000 [prize] to the first guy who makes an operating electric motor – a rotating electronic motor which can be controlled from the outside and, not counting the lead-in wires, is only 1/64 inch cube" [Feynman, 1960]. This prize was awarded already two years later, but the small machine did not contain any breakthrough ideas and creating control over the directed motion of molecular machines remained an unsolved issue [Dietrich, 1986, Feynman, 1993]. Nowadays different ways of driving nanomechanical systems into motion have been developed. In the present thesis, we focus on nanoelectromechanical systems as promising candidates with enormous capabilities [Craighead, 2000, Roukes, 2000].

Nanoelectromechanical systems are nanoscale mechanical devices which are controlled by running an electric current through the system. A strong coupling of the system's mechanical, that is vibrational, degrees of freedom to the electronic

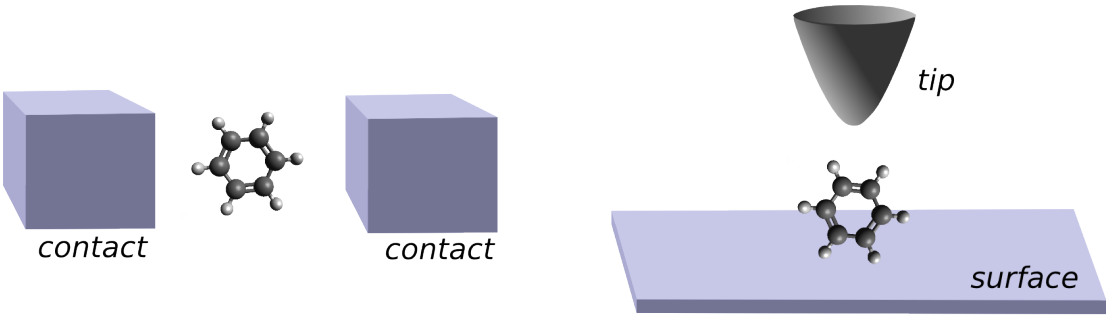

(a) (b)

Figure 1.1.: A molecule between two contacts; (a) a molecular tunnel junction; (b) a molecule on a surface with an adjacent STM tip. The tip and the substrate serve as electrodes allowing for a sensitive control of the system.

environment characterises these devices and opens a wide range of applications. Possible applications range from medical diagnostics and data storage to ultra-sensitive sensing of masses or forces or measuring displacements or charges [Craighead, 2000, Roukes, 2000, Ke and Espinosa, 2005, Cimalla et al., 2006, Eom et al., 2011]. Nanoelectromechanical systems also find applications as pH sensors [Chen et al., 2006], biosensors [Besteman et al., 2003, Cui et al., 2001], protein concentration detectors [Lee et al., 2007] and ultra-sharp tips in the context of atomic force microscopy [Bunch et al., 2004]. Due to their small size, new physical effects become important in these devices which increases the interest in nanoelectromechanical systems both at the experimental and at the theoretical level. In particular, the theoretical treatment is strongly motivated by the complexity of these systems. Due to the strong electron-phonon coupling, nanoelectromechanical systems constitute a paradigm of vibronic degrees of freedom which couple to an out-of-equilibrium fermionic quantum environment.

Nanoelectromechanical systems have been successfully realised within different contexts. Examples include suspended graphene sheets [Bunch et al., 2007], carbon nanotubes [LeRoy et al., 2004], one-dimensional wires [Krive et al., 2010] and molecular junctions [Park et al., 2000, Galperin et al., 2007]. In the latter case an individual molecule is placed between electrodes or on a substrate with an adjacent STM tip, cf. Fig. 1.1. In all these systems an electric current can induce forces on the motion of the nanomechanical system by exciting the mechanical modes. This is schematically depicted in Fig. 1.2 for the example of a nanotube. The strong electron-phonon interactions also generate the opposite effect, that is an electric current which is strongly influenced by the mechanical motion of the system. Un-

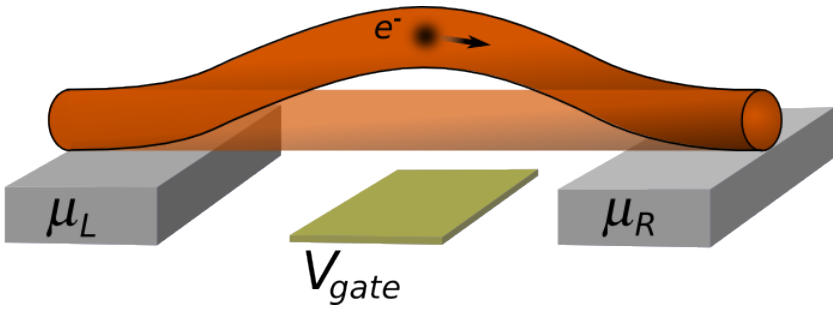

Figure 1.2.: Controlling the motion of a nanoelectromechanical system by applying a gate and bias voltage. A charge entering a nanotube distorts the tube via electric repulsion from a gate voltage, V_{gate}.

derstanding the interaction between the nanosystem and its quantum environment is of crucial importance for applications of nanoelectromechanical systems and constitutes one of the main issues of the present thesis.

Transport through nanoelectromechanical devices broadly falls into two different regimes. These regimes differ in the characteristic timescales of the electronic environment and the mechanical system and go along with different experimental phenomena. The case of a fast-moving nanomechanical system coupled to slow-moving electrons is for instance realised in the context of a single-molecule junction. Electron-phonon coupling then is a consequence of the adjustment of the nuclear configuration whenever the molecule is charged by individual electrons. The potential landscape which describes the vibrational excitations is displaced depending on the charge of the molecule. In the case of weak electron-phonon coupling this leads to side-bands due to phonon-assisted tunnelling which have been observed for instance in Refs. [Yu et al., 2004, Sapmaz et al., 2006]. For strong electron-phonon this displacement is large so that the overlap of the low-energy vibrational states is suppressed. This results in a strong suppression of electron transport at low bias voltages which is known as the Franck-Condon blockade [Koch and von Oppen, 2005, Koch et al., 2006, Leturcq et al., 2009]. On the other hand, in the opposite regime of low mechanical frequencies, many electrons travel through the nanostructure per oscillation period. The moving electrons then react to a quasistatic nanosystem but strongly influence the mechanical motion [Naik et al., 2006, Steele et al., 2009, Lassagne et al., 2009, Stettenheim et al., 2010, Bode et al., 2011, Bode et al., 2012b]. In the present thesis we investigate the interplay of the nanostructure with its quantum environment in the latter regime, that is the limit of a slowly moving nanoelectromechanical system. Moreover, we study transport through a molecular transistor.

Recently it has been shown, that for finite applied bias voltages the electrons, which travel through the device, can perform work on the nanomechanical system [Dundas et al., 2009, Brandbyge, 2009, Todorov et al., 2010, Bode et al., 2011, Bode et al., 2012b]. This principal idea opens applications for building of nanoscale devices or quantum machines and is further studied in this thesis. A prototype of a molecular motor whose motion is controlled by ac-voltage elements is described in Ref. [Fennimore et al., 2003] where a tiny rotating metal plate is connected to a suspended nanotube attached to leads. Further ac-driven nanomotors are proposed in Ref. [Ponomarev et al., 2009] and experimentally addressed in Ref. [Salger et al., 2009], while the idea of a dc-motor is proposed in Refs. [Bailey et al., 2008, Qi and Zhang, 2009]. Moreover, by placing an STM tip on top of an individual molecule both translational [Kudernac et al., 2011] and rotational motion [Tierney et al., 2011] of the molecule have been successfully induced experimentally. Directed motion is achieved by the specific atomic structure of the molecule or the tip.

The principal idea of using an electric current and the underlying strong electron-phonon interactions as control mechanisms has wide applications and is not restricted to electrically driven nanosystems or molecular motors. Heating and cooling by a current, for instance, has also attracted attention both theoretically [Pecchia et al., 2007, Arrachea et al., 2014] and experimentally [Schulze et al., 2008, Safavi-Naeini et al., 2012]. In fact, the back-action of the quantum environment on the nanomechanical system can lead to cooling of a macroscopic object down to the level where quantum effects become evident at the ultimate limit of measurement [Naik et al., 2006, Stettenheim et al., 2010].

In the seminal experiments in Refs. [Steele et al., 2009, Lassagne et al., 2009] strong electron-photon interactions have been experimentally demonstrated for a suspended carbon nanotube. Similar features have been observed in Refs. [Benyamini et al., 2014]. As these findings are crucial for applications and the theoretical understanding of nanoelectromechanical systems, the experimental results of Ref. [Steele et al., 2009] are discussed in more detail next. The set-up is shown in Fig. 1.3(a) and consists of a quantum dot which is embedded on a suspended carbon nanotube with high quality factor. The nanotube is attached to two electrodes and is used as a mechanical resonator, which is actuated into motion by applying a periodic radio frequency signal with the aid of an adjacent antenna. By varying gate and bias voltages, the current running through the tube is measured for different driving frequencies. The result is presented in Fig. 1.3(b). The upper plot (A) shows the measured current as a function of the gate voltage at fixed bias voltage and constant driving frequency. Valleys in the current reflect the Coulomb blockade regime while peaks in between the valleys are due to single-electron tunnelling. The number of electron charges on the quantum dot thus changes by one from one valley to the

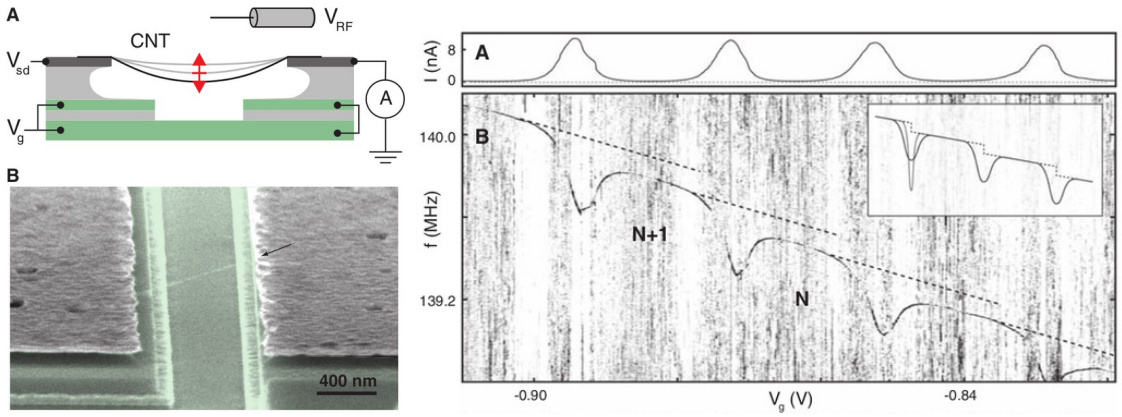

(a) (b)

Figure 1.3.: Experiment by Steele et al. (a) Schematic drawing of the experimental set-up (A) and STM image (B). (b) Current as a function of gate voltage at fixed bias and bias voltage (A) and current as a function frequency and gate voltage (B) The inset shows the behavior for different bias voltages. The figures are taken from Ref. [Steele et al., 2009] with permission from the American Association for the Advancement of Science.

next.

Below this figure, a second plot (B) in Fig. 1.3(b) depicts the main results of the experiment. In this figure the current is shown as a function of both gate voltage and driving frequency. The resonance frequency versus gate voltage is seen as a dark curve in this figure. By comparing plot (B) and (A), two main features are observed. On the one hand, a clearly detectable change in the resonance frequency is seen whenever a single charge is added to the nanotube. This is due to the fact that the addition of a single charge changes the electrostatic force acting on the nanotube. Entering charges are repelled by the electric field created by the gate voltage, which is sketched in Fig. 1.2. This results in a measurable frequency shift, which – similar to the behaviour of a guitar string – is due to a stiffening of the nanotube.

Besides a detectable frequency shift by the addition of single charges, figure (B) shows that the resonance frequency decreases in form of dips when current flows at the Coulomb blockade peaks. At the peaks, the tunnelling of single electrons exerts a time-dependent, fluctuating force on the nanotube in addition to the electrostatic force. This force changes the spring constant of the nanotube, which results in a modification of the mechanical resonance frequency and by this produces the dips.

The origin of this force can be traced back to a strong coupling between the mechanical and electronic degrees of freedom. The strong coupling between electrons and phonons is a consequence of the strong correlation between the mechanical motion and the tunnelling electrons. When the nanotube vibrates, the periodic motion pumps charges in and out of the system. The attraction of these charges to an adjacent gate voltage then results in a softening of the mechanical restoring force [Woodside and McEuen, 2002, Benyamini et al., 2014]. The inset of figure (B) shows the dependency of the dips in the resonance frequency as a function of the applied bias voltage. A more pronounced dip is observed at a smaller bias voltage. This reflects the broadening of the Coulomb blockade conductance peaks, cf. plot (A) of Fig. 1.3(b), which increases at larger bias voltages.

1.1. Theoretical modelling of nanoelectromechanical systems

Besides the high degrees of tunability and control, the experiments in Refs. [Steele et al., 2009, Lassagne et al., 2009, Benyamini et al., 2014] show the existence of forces induced by charges which enter the nanoelectromechanical system. We refer to these forces as adiabatic reaction forces in the regime of a slowly moving nanoelectromechanical system in the following. The adiabatic reaction forces provide a mechanism to control the motion of the nanosystem. Many applications require an understanding of these forces. We present a derivation of the adiabatic reaction forces in nanoelectromechanical systems or, more generally, of adiabatic reaction forces on a classically moving system induced by a quantum environment, which can be both fermionic or bosonic, later in chapter 3.

For an understanding and a description of the reaction forces and of nanoelectromechanical systems in general, a characterisation of transport through these systems is important. We note that a theoretical description of transport through nanosystems generally can be done by different approaches valid in different regimes. In the following, we characterise the approaches, which are used in the present thesis, and describe their validity.

Specifically, we treat the regimes of coherent and incoherent transport in this thesis. The coherent transport regime is studied in the context of the adiabatic reaction forces in chapter 3 and 4. Incoherent transport is used for the description of sequential tunnelling through a single-molecule transistor in chapter 5. Next, we describe these regimes, which give rise to different physical phenomena, in more detail.

1.1.1. Coherent transport

When the system is phase coherent and can be described in terms of non-interacting particles,[1] the Landauer-Büttiker approach [Landauer, 1957, Landauer, 1970, Landauer, 1975, Büttiker et al., 1985, Büttiker, 1990, Büttiker, 1992, Büttiker, 1993, Moskalets, 2011] has turned out to be a powerful tool, which fully accounts for quantum phase coherence. In this context, "coherent" means that the quantum mechanical coherence length is larger than the size of the system [Bruus and Flensberg, 2004]. This means that transport must be described at the quantum level.

In the Landauer-Büttiker approach, the nanosystem is connected to source and drain leads which are attached to electron reservoirs. The leads are assumed to be macroscopically large with a small region where the electrons enter the system, cf. Fig. 1.4. By this we assume that the incoming electrons possess the temperature and chemical potential of the reservoirs. Moreover, the leads are treated as perfectly transmitting and thus treated as semi-infinite "ideal leads" where electrons travel without scattering events. When the electrons move rapidly through the nanoelectromechanical system on a timescale faster than the decoherence time, the system gives rise to a scattering potential felt by the electrons travelling through the system. Transport is then described by the scattering matrix with its reflection and transmission coefficients.

Besides giving a simple expression of the conductance through a mesoscopic system with multiple attached leads [Büttiker, 1992, Büttiker, 1993, Moskalets, 2011], the Landauer-Büttiker approach successfully describes time-dependent transport phenomena like quantum pumping [Büttiker et al., 1994, Brouwer, 1998]. In this case periodic variations of the scattering potential in time, which can for instance be induced by a moving nanoelectromechanical system, generate a direct current through the system. Scattering matrix expressions of the pumped current through the system have been derived in Refs. [Brouwer, 1998, Avron et al., 2001] and a generalised description of an out-of-equilibrium quantum environment has been obtained in Refs. [Entin-Wohlman et al., 2002, Moskalets and Büttiker, 2005].

In this work, we make use of scattering theory to describe the adiabatic reaction forces on a general nanoelectromechanical system. We give an introduction into scattering theory in chapter 2 as it constitutes an important theoretical framework for our analysis. Due to the restriction to non-interacting particles, the many-body problem of many electrons scattering off the nanoelectromechanical system is

[1] To be more precise, by non-interacting "electrons" or "particles" we actually mean non-interacting quasiparticles of a Fermi liquid [Landau, 1957a, Landau, 1957b, Landau, 1959].

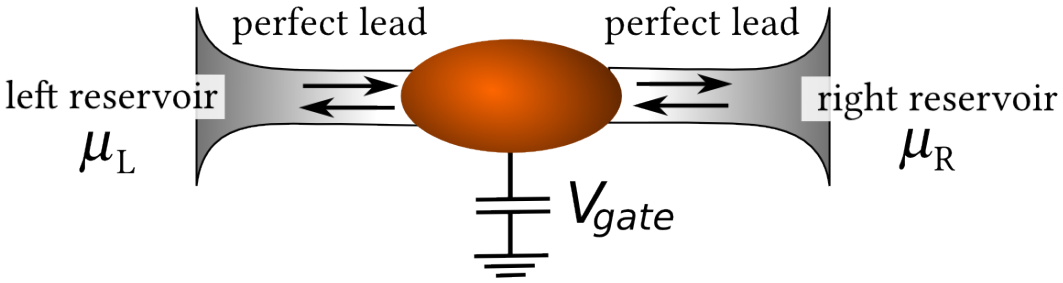

Figure 1.4.: Geometry considered in the Landauer-Büttiker approach. Incoming and outgoing waves are indicated by arrows. The attached reservoirs are kept at fixed chemical potentials μ_L and μ_R.

conceptually simplified as it effectively reduces to a single-particle problem. Interactions can be included within a mean-field theory where a varying charge distribution changes the scattering potential, see e.g. Ref. [Büttiker et al., 1994].

1.1.2. Incoherent transport

The assumption of non-interacting particles is generally reasonable for extended systems at low temperatures [Bruus and Flensberg, 2004]. Especially for smaller systems such as semiconductor quantum dots or molecular electronic devices, however, electron-electron interactions become important as the charging energy increases with decreasing system size [Rauch et al., 1998]. This increasing charging energy dramatically changes the physical properties of the system and a different theoretical description is needed. For interacting particles a general many-body approach is necessary as particles cannot be treated independently any longer. Moreover, as in small systems the single-particle energy-level spacing becomes large, electronic transport is sensitive to both energy scales, the energy-level spacing and the charging energy. The sensitivity to both the charging energy and the level spacing is reflected in the so-called Coulomb blockade [Gorter, 1951, Kouwenhoven et al., 1997], that is the suppression of conduction at sufficiently low temperatures and small applied bias voltages.

In the present thesis, we consider incoherent transport through a single-molecule transistor, which is an electronic device on the molecular scale. In this regime, similar to the Landauer-Büttiker approach, the system is attached to metallic contacts in which the electrons are assumed to be non-interacting. Within the nanostructure, however, interactions are important. Denoting the tunnelling rates between

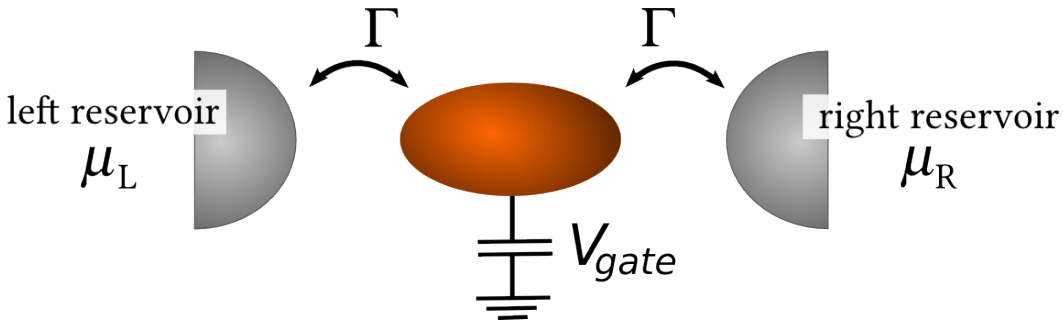

Figure 1.5.: Sketch of the sequential tunnelling regime with incoherent transport where the tunnelling rates Γ are much smaller than the temperature times the Boltzmann constant.

the system and the attached leads by Γ, we describe incoherent transport in the limit $\Gamma \ll k_B T$ with temperature T and Boltzmann constant k_B in the present thesis, cf. Fig. 1.5. Incoherent transport assumes that electrons sequentially tunnel through the device and that the timescale between two sequential tunnelling events is larger than the characteristic decoherence time of the electrons. Consequently, the electronic reduced density matrix of the system describes a statistical mixture and no coherences are taken into account. The tunnelling electrons are treated as fully decohered particles. Hence, the theoretical description in the incoherent tunnelling regime is in terms of classical probabilities which characterise occupation probabilities of the nanostructure. These probabilities fulfill the so-called Pauli master equation or rate equation which describes transitions between all possible states [Weiss, 1999, Bruus and Flensberg, 2004].

In chapter 5 we treat the sequential tunnelling regime in the limit $\Gamma \ll k_B T \ll \Delta\varepsilon$, where $\Delta\varepsilon$ is the averaged level spacing of the quantum dot, so that electrons successively tunnel through a nanostructure with well-defined energy levels. The energy levels within the nanostructure are well separated for $\Gamma \ll \Delta\varepsilon$ as this condition imposes the width of the respective energy levels to be much smaller than their averaged level spacing. The requirement $k_B T \ll \Delta\varepsilon$ models the nanostructure as a semiconductor quantum dot with discrete energy levels participating in the conduction, since $k_B T$ determines the width of the conduction window. As a consequence of these assumptions, the nanostructure can be described by a set of probabilities which describe the occupation number of single energy levels obeying the Pauli master equation. We note that the nanostructure itself can be modelled as a metallic dot with a continuous energy spectrum for $\Delta\varepsilon \ll k_B T$. In the sequential tunnelling regime or in the weak tunnelling limit, respectively, the tunnelling rates entering in the Pauli master equation are calculated with the aid of Fermi's golden rule. Out-of-equilibrium situations induced by applying a bias voltage between the leads are

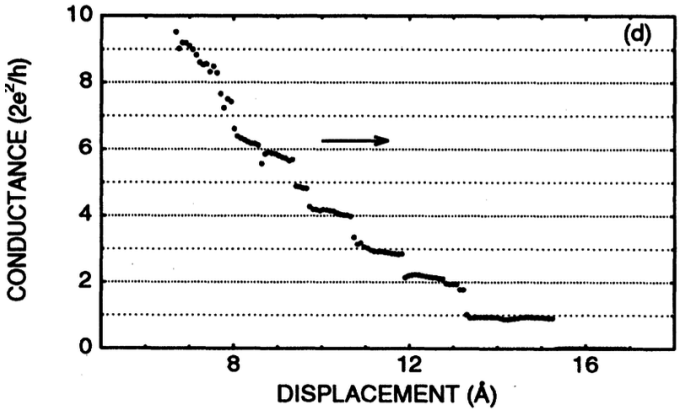

Figure 1.6.: The conductance measured for a gold contact when retracting a tungsten STM tip from a clean gold surface after crashing the tip onto the surface. The arrow indicates the direction of the tip motion. The figure is taken from Ref. [Brandbyge et al., 1995]. The experiment was performed at room temperature in ultra-high vacuum. The recording time of the curve was approximately 20 ms. Copyright (1995) by The American Physical Society.

then encapsulated in the tunnelling rates which depend on the chemical potential of the different leads. The effect of blocking current, e.g. Coulomb blockade, is generally observed at sufficiently small bias voltages and for $k_BT \lesssim \max(\Delta\varepsilon, E_C)$ with $\Gamma \ll k_BT$, $\Delta\varepsilon$ and charging energy E_C [Beenakker, 1991, Heikkilä, 2013].

The Pauli master equation successfully describes transport through molecular junctions and quantum dots [Glazman and Pustilnik, 2005, Galperin et al., 2007]. When the electrons in the nanostructure couple to vibronic degrees of freedom, further phenomena can be explained with the aid of rate equations, e.g. the observation of side-bands due to phonon-assisted tunnelling for weak electron-phonon coupling [Yu et al., 2004, Sapmaz et al., 2006] or the Franck-Condon blockade, for strong electron-phonon coupling [Koch et al., 2006, Leturcq et al., 2009]. Recently a general theory of quantum pumping has been developed for the interacting case by using a rate equation approach [Splettstoesser et al., 2006].

The transition between the coherent transport and the sequential (weak) tunnelling regime with incoherent transport has experimentally been observed by gradually decreasing the number of channels contributing to the conductance in Refs. [van Wees et al., 1988, Wharam et al., 1988, Muller et al., 1992, Krans et al., 1993, Brandbyge et al., 1995, Ohnishi et al., 1998, Yanson et al., 1998, Agraït et al., 2003]. This has been realised in some of these references for instance in an STM set-up by increasing the distance between the STM tip and the molecule or surface,

respectively, or in molecular break junctions by increasing the distance between the contacts. Recording the conductance as a function of the increasing distance, then results in a stepwise decrease of the conductance by an amount which is given by the quantum unit of conductance. An exemplary conductance curve taken from Ref. [Brandbyge et al., 1995] is depicted in Fig. 1.6 where the conductance is recorded while retracting an STM tip from a gold surface. The limit of incoherent transport describes the regime where the conductance is much smaller than the quantum conductance [Beenakker, 1991, Nazarov and Blanter, 2010]. In Fig. 1.6 this is reached at distances larger than approximately 15 Å between STM tip and surface.

1.2. Adiabatic reaction forces

Ultimately aiming at controlling nanoelectromechanical systems, an understanding of the forces on the vibrational degress of freedom induced by charges entering the nanosystem is of crucial importance. We address the derivation of the adiabatic reaction forces in the regime of coherent transport by using scattering theory. In the derivation, however, we do not restrict ourselves to electronic transport through a nanoscale object, we rather generalise the idea by considering a classical object which moves in a quantum environment. We are then interested in the forces induced by the quantum system on the classical degrees of freedom, i.e. the adiabatic reaction forces.

An early version of adiabatic environment-induced forces is treated in the seminal paper by M. Born and R. Oppenheimer in 1927 in the context of electrons moving around atomic nuclei [Born and Oppenheimer, 1927]. Due to their large difference in mass, the "heavy" nuclei move on timescales which are long compared to the characteristic timescales of the surrounding "light" electrons. To lowest order in the adiabatic expansion, the electrons see frozen nuclei and react instantaneously to the positions of the nuclei. The instantaneous energy levels of the electrons, that is the quantum environment, then give rise to a potential landscape felt by the nuclei. The environment-induced force acting on the "heavy" system, which can be extracted from the potential landscape depending on the instantaneous position of the the system itself, is called Born-Oppenheimer force.

Recent developments increased the interest in the Born-Oppenheimer force. Within a Green function approach the Born-Oppenheimer force has been shown to possibly give rise to a bistable potential and thus to switching in the case of a single electronic

level coupling to one phononic mode [Mozyrsky et al., 2006, Pistolesi et al., 2008]. Moreover, when the quantum system is driven out of equilibrium it has been shown that the Born-Oppenheimer force can be non-conservative [Dundas et al., 2009, Brandbyge, 2009, Todorov et al., 2010]. Dundas et al. proposed an application to nanoelectromechanical systems by considering forces acting on the nuclei in a wire where the quantum environment consists of electrons in the wire. The wire is attached to electrodes which can drive the system out of equilibrium by a bias voltage so that an electric current runs through the wire. It was then shown that the curl of the force as a function of the instantaneous positions of the wire atoms does not generally vanish in the presence of a bias voltage. As a consequence, the integral over a closed path is non-zero which enables the possibility of exerting work on the system. This opens a wide field of applications, e.g. building quantum motors or quantum machines based on a current running through the system. A conceptual idea for an adiabatic quantum motor is proposed in Ref. [Bustos-Marún et al., 2013].

Besides possibly non-conservative forces, going to higher order in the adiabatic parameter, allows for a description of forces which are proportional to the velocity of the slow moving system. For closed quantum systems with a finite energy spectrum an expression of a Lorentz-like force has been derived in Ref. [Berry and Robbins, 1993]. However, as the quantum environment is assumed to be finite-sized in this derivation, neither friction nor fluctuating forces are present. In nanoelectromechanical systems on the other hand, by attaching leads, the system is opened and dissipation occurs naturally. Furthermore, by the fluctuation-dissipation theorem and the probabilistic nature of the scattering process, stochastic forces are expected to appear. Indeed, expressions for both friction and stochastic forces are obtained within an influence functional theory in the literature [Lü et al., 2012]. Moreover, current-induced forces have been recently expressed in terms of Green functions and the scattering matrix including its first non-adiabatic correction in Refs. [Bode et al., 2011, Bode et al., 2012b] by relying on Keldysh Green function techniques.

In chapter 3 we provide a deeper understanding of adiabatic reaction forces by directly following the seminal derivation presented in Ref. [Berry and Robbins, 1993], however, for an open system with a continuous energy spectrum. By this, our approach is applicable to nanoelectromechanical systems. This enables a direct comparison between the two set-ups of closed and open quantum environments. We perform an adiabatic expansion purely within the methods of scattering theory and derive all quantities appearing in the equation motion to linear order in the adiabatic parameter. We rederive the expressions obtained in Refs. [Bode et al., 2011, Bode et al., 2012b] in terms of the scattering matrix and its first adiabatic expression without the detour using Keldysh Green functions. The use of scatter-

ing theory alone underlines the generality of the obtained results which hold for both fermionic and bosonic scattering environments. It can thus be applied to a description of environment-induced force in optomechanical systems [Kippenberg and Vahala, 2008] as well as cold-atom systems [Dalibard et al., 2011]. As being simple and natural to transport set-ups, scattering theory furthermore easily allows to consider symmetries of a given system as possible symmetries transfer to well-known properties of the scattering matrix.

1.3. Loschmidt echo

When dealing with adiabatic reaction forces on a nanoelectromechanical system the effect of an open quantum environment on a classical system is studied. In chapter 4 of this thesis we deepen the understanding of the interplay between a system and its environment by turning the analysis around and considering the reverse problem, that is the influence of the classical system on its quantum environment.

When a nanosystem moves in an electronic environment, different positions of the nanosystem give rise to different scattering potentials felt by the electrons which move through the nanostructure. This is schematically depicted in Fig. 1.7 for the example of a suspended nanotube which is attached to two metallic leads. Small changes of a scattering potential can have drastic consequences on properties of large quantum environments as known from the Anderson orthogonality catastrophe [Anderson, 1967]. In the seminal work in 1967 P. Anderson has shown that the ground state overlap of a free fermionic many-body state and a state in the presence of a local scattering potential vanishes as a power law in the system size so that the states become orthogonal with increasing system sizes. The power-law exponent, which describes the decay of the ground state overlap, is called Anderson orthogonality exponent.

In this thesis, we study how the Anderson orthogonality exponent and the dynamics of a classical nanosystem or a heavy particle are related. A relation between the orthogonality exponent and the dissipation coefficient of a classical heavy particle has numerically been anticipated for a quantum environment in equilibrium in Ref. [Sols and Guinea, 1987]. A few years later, for a free electron gas a direct relation between the Anderson orthogonality exponent and the friction tensor for slightly different positions of the local potential of the classical system was proven for finite quantum environments in equilibrium in Ref. [Schönhammer, 1991]. Motivated by nanoelectromechanical systems, where a finite imposed bias voltage is

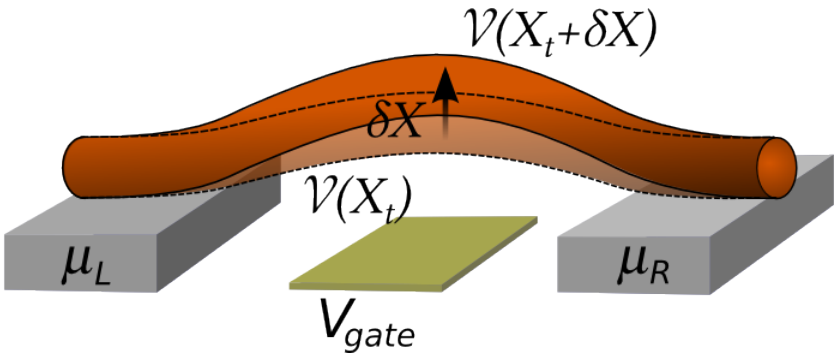

Figure 1.7.: The Loschmidt echo in the context of nanoelectromechanical systems exemplarily shown for a suspended nanotube attached to leads. Two different positions of the nanotube, X_t and $X_t+\delta X$, give rise to different scattering potentials, $\mathcal{V}(X_t)$ and $\mathcal{V}(X_t+\delta X)$, felt by the electronic environment which defines the Loschmidt echo.

crucial for an ultimate control of the system, we analyse the relation between the friction coefficient and the Anderson orthogonality in out-of-equilibrium situations and study, under which conditions the relation remains valid.

We characterise the Anderson orthogonality exponent through the fidelity amplitude and its absolute square value, the Loschmidt echo [Peres, 1984, Jalabert and Pastawski, 2001, Gorin et al., 2006]. These quantities represent dynamical measures of the Anderson orthogonality catastrophe as we detail in chapter 4. By definition, the fidelity amplitude for quantum systems describes the overlap of two many-body quantum states evolving with different Hamiltonians. In the picture of a nanoelectromechanical system this corresponds to the evolution of the states of the electronic environment with respect to two different positions of the nanodevice, cf. Fig. 1.7 for the example of a suspended nanotube. An equivalent interpretation of the fidelity amplitude is given in terms of irreversibility. The fidelity amplitude quantifies how close a system returns to its original state under forward an backward evolution with respect to two different Hamiltonians.

Specifically, we express the behaviour of the fidelity amplitude and the Loschmidt echo in the small-distance limit in terms of scattering states in chapter 4. We then make use of the acquired knowledge of the adiabatic environment-induced reaction forces of chapter 3 to generalise the relation between the orthogonality exponent and the friction tensor found in Ref. [Schönhammer, 1991] to an out-of-equilibrium situation and to infinite systems with a continuous energy spectrum. Both within the methods of scattering theory [Thomas et al., 2012] and Green functions [Bode et al., 2011, Bode et al., 2012b] we characterise the behaviour of

the fidelity amplitude and the Loschmidt echo in terms of the Born-Oppenheimer force, dissipation and fluctuations.

Besides an interpretation as a measure of irreversibility, the fidelity amplitude finds applications in quantum chaos as a quantity defining the sensitivity to perturbations [Stöckmann, 2006,Haake, 2010] as well as applications in quantum information theory. In the latter context, the fidelity amplitude has been connected to decoherence, that is the decay of the off-diagonal elements of a reduced density matrix when coupling to an environment [Zurek, 2001, Karkuszewski et al., 2002, Cucchietti et al., 2003, Gorin et al., 2004]. Generally, a coupling to an environment results in decoherence, which is intimately related to fluctuations and dissipation in the system [Weiss, 1999]. Interesting for nanoelectromechanical systems is the interpretation of the fidelity amplitude as the characteristic function of the work distribution function when suddenly changing its Hamiltonian between two configurations [Silva, 2008]. Since the Loschmidt echo and the fidelity amplitude, have various interpretations in different areas of physics, ranging from statistical mechanics to quantum chaos and to quantum information theory, a construction of miniaturised devices at the quantum level requires an understanding of their behaviour [Gorin et al., 2006].

1.4. Molecular transistors

A long-standing challenge of nanoelectronics consists in decreasing the size of electronic devices towards the construction of an electronic switching circuit with elements which are made up of single atoms or molecules [Sotthewes et al., 2014]. The construction of miniaturised transistors based on single-electron tunnelling plays a crucial role in this context as transistors can be used to control an electric current between contacts by electrical gating. Due to their small size, challenges in the construction of molecular transistors include both the connection of single molecules to macroscopic source and drain contacts [Hipps, 2001] and the realisation of atomically precise gating. Promising techniques towards their construction are provided by the break junctions [Hamill et al., 2014], cf. Fig. 1.1(a), where a nanoscale junction is created by opening and closing a narrow metallic constriction, and by electron-beam lithography. Indeed, by forming a junction through electron-beam lithography, the first single-electron transistor was experimentally realised for a metallic dot in Ref. [Fulton and Dolan, 1987]. Later, further transistors where single-electron tunnelling has been observed were constructed by using gated break junctions [Champagne et al., 2005, Perrin et al., 2013] and electron-beam lithogra-

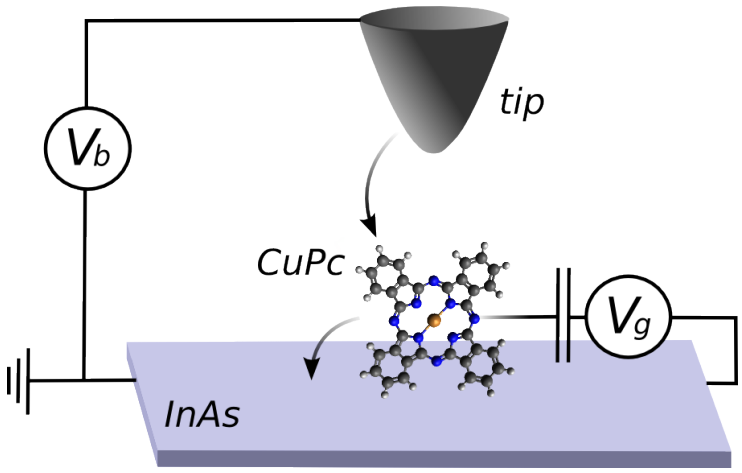

Figure 1.8.: Sketch of a molecular transistor as realised in Ref. [Martínez-Blanco et al., 2015] which consists of a single molecule, here copper phthalocyanine (CuPc), on an indium arsenide InAs(111)A-(2x2) surface and an adjacent STM tip. Electrically charged indium adatoms on the surface induce a local electrostatic potential of the the CuPc and hence serve as an analogue of a gate voltage (V_g). By applying a bias voltage (V_b) between tip and surface the indium adatom gate electrode controls the current running through the system.

phy [Park et al., 2002,Liang et al., 2002,Kubatkin et al., 2003,Roch et al., 2008,Song et al., 2009, Leturcq et al., 2009]. Atomically precise gating, however, cannot be reached with these techniques.

In chapter 5 of this thesis we present the theoretical modelling and description of an experiment performed in Ref. [Martínez-Blanco et al., 2015] which provides a different technique for the construction of a single-molecule transistor at the ultimate limit of miniaturisation. The basic mechanism behind achieving atomically precise gating relies on repositioning individual electric charges on a surface by using scanning tunnelling microscopy of individual atoms and molecules [Stroscio and Eigler, 1991]. The main element of the transistor realised in Ref. [Martínez-Blanco et al., 2015] is a phthalocyanine molecule [Engel, 1997,Wang et al., 2012], in particular free base phthalocyanine and copper phthalocyanine, which are adsorbed on an indium arsenide InAs(111)A-(2×2) surface and are in close vicinity to an STM tip. The set-up is schematically depicted in Fig. 1.8. An analogue of a gate electrode is formed by charged indium adatoms on the surface which induce an electrostatic potential on the molecule. As the adatoms are weakly bound to the substrate, they can be moved by the STM tip which enables a fine-tuning of the molecule's electrostatic potential and thus atomically precise gating. A bias voltage applied

between the InAs surface and the STM tip creates an electric current running through the system, which is controlled by the position of the indium adatoms.

With the high degree of tunability of the gate voltage by repositioning individual charges, the phthalocyanine molecule is tuned into the sequential tunnelling regime. By modelling the molecule as a quantum dot, which is attached to two electron reservoirs formed by the tip and the substrate, the conventional picture of sequential tunnelling predicts a current-voltage diagram which is reminiscent of Coulomb diamonds [Beenakker, 1991, Nazarov and Blanter, 2010]. Remarkably, the observed current-voltage diagram in Ref. [Martínez-Blanco et al., 2015] shows a pronounced conductance gap instead of the expected charge degeneracy point.

We explain this behaviour by the presence of two conformational states of the molecule in the present thesis. The molecule can switch its conformational state by thermally induced transitions and individual electrons change the charge state of the molecule when tunnelling through the device. By assuming that the ground state conformations of the neutral and the charged molecules are different, we detail in chapter 5 that a gap naturally opens in the current-voltage characteristics. We quantitatively confirm this conclusion by setting up a master equation, which includes thermal transition rates between the conformations, which keep the charge state of the molecule unchanged, and electronic transition rates, which change the charge state at a fixed conformation. The solution of the stationary master equation determines the stationary current, which verifies the occurrence of the gap. Our results show that in the case of strong coupling between charge states and conformational degrees of freedom, new physics arise due to a modification of the conventional picture of sequential tunnelling through molecular transistor.

1.5. Fabrication of nanoelectromechanical systems

A molecular transistor, one-dimensional wires and molecular break junctions are different examples of nanoelectromechanical systems. A large group of nanoelectromechanical devices is formed by suspended mechanical objects. In the following, we sketch how such suspended objects can be fabricated by using different experimental techniques. In principle, these systems can be fabricated by two different approaches [Madou, 1997, Craighead, 2000, Ke and Espinosa, 2005]. One approach, commonly known as the top-down approach, starts from the fabrication of larger bulk materials out of which nanoelectromechanical systems can be constructed for instance by a combined method of using high-resolution electron-beam lithography

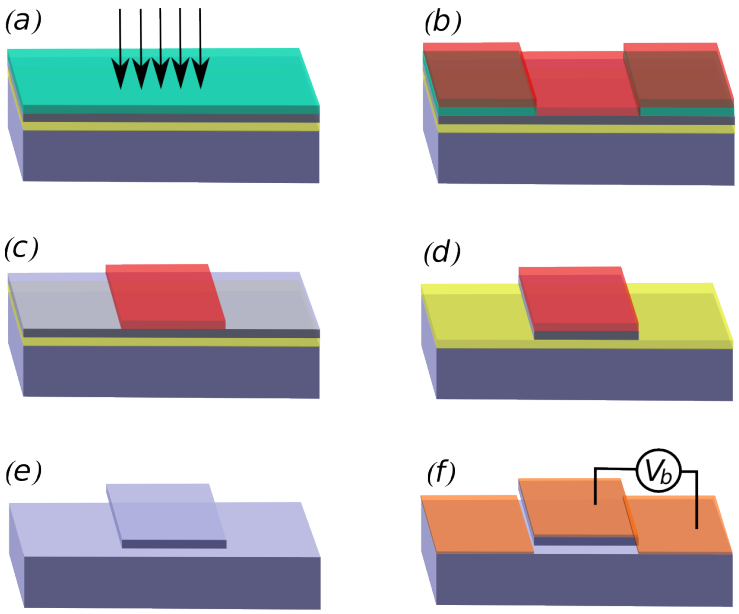

Figure 1.9.: Sketch of the fabrication process of a suspended nanoelectromechanical system. (a) A polymeric polymethylmethacrylate layer (cyan) on a silicon oxide film (yellow) in between silicon (grey) is exposed to an electron-beam (arrows); (b) deposition of metal which is followed by (c) lift-off; (d) dry-etch transfer through the silicon layer on top and (e) wet-etch through the silicon oxide film; (f) a contact metal (orange) is evaporated; applying a bias voltage, V_b, for instance can drive the system into motion. [Craighead, 2000].

and surface micromachining, cf. Fig. 1.9. A thin polymeric polymethylmethacrylate film is put as a resist on a wafer which is composed of a layer of silicon dioxide in between a silicon substrate and a thin layer of silicon. In order to define the shape of the device the polymeric thin is then exposed to an electron beam with energies of the order of keV which changes the chemical composition of the resist. Via metal decomposition and lift-off the sample is subsequently prepared for a dry- and wet-etch through the silicon and the silicon oxide layer, respectively. An evaporation of the contact metal finally defines the nanoelectromechanical device. This process however is limited for example by the roughness induced by the etching process as well as by the resolution of the electron-beam lithography. Due to these limitations, a different manufacturing approach called bottom-up approach widens the fabrication possibilities which allows for producing devices made up of a few atoms or molecules and is nowadays feasible. It consists in sequentially assembling individual atoms or molecules which form the components and building blocks of the nanoscale device. For the construction of larger devices with increasing complexity of assembling this approach however becomes less controllable and effective.

For this reason a combination of both the top-down and the bottom-up approach is nowadays widely used for the creation of nanoelectromechanical systems which for instance is done in Ref. [Husain et al., 2003].

With ongoing experimental advances and theoretical achievements in the recent years, strong attention has been paid to the class of suspended nanotubes as ultra-high frequency resonators which are cylinders on a molecular scale made up of atoms. Particularly interesting are nanotubes made up of carbon atoms due to their extraordinary electronic and mechanical properties [Iijima, 1991] and their possible commercial implementations [De Volder et al., 2013]. Because of the sp^2-hybridised bonds between the carbon atoms, carbon nanotubes – concomitant with their general lightness – posses a high intrinsic carrier mobility and conductivity. Moreover, they possess an extremely high strength and stiffness along their longitudinal axis, while they are flexible and elastic along the tube waist [Terrones, 2003]. The specific structure of the carbon nanotubes allows for further different fabrication techniques such as catalytic vapor deposition methods [Li et al., 1996], laser ablation methods [Thess et al., 1996] and arc evaporation methods [Ebbesen and Ajayan, 1992, Journet et al., 1997]. These methods are nowadays very advanced so that carbon nanotubes with high quality factors of the order $Q \sim 10^5$ can be produced [Hüttel et al., 2009, Laird et al., 2011].

1.6. Alternative methods: Brownian motors

Nanoelectromechanical systems form a class of systems where the idea of controlling the motion of a nanoobject is via running an electric current through the system. There are alternative methods which provide different ways of driving nanomechanical systems into motion. In the following, we sketch the conceptual idea of such an alternative, that is a Brownian motor.

As the motion in the nanoscale range is dictated by fluctuations and stochastic forces, the conceptual idea of a Brownian motor is to convert a stochastic input signal into a directed motion of a particle or system [Reimann, 2002, Hänggi and Marchesoni, 2009, Craig and Linke, 2009]. The basic mechanism behind gaining useful work out of Brownian motion can be understood at a classical level by the principle of a Smoluchowski-Feynman ratchet which is also known as a Brownian ratchet [Feynman et al., 1963]. Such a system is schematically drawn in Fig. 1.10 and consists of an axle which has a paddle at one end and a ratchet which has the shape of a circular saw with an asymmetric sawtooth wave. A pawl is linked to the

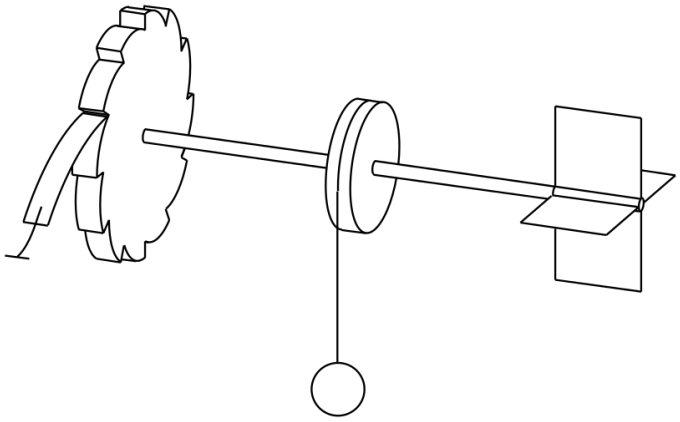

Figure 1.10.: Sketch of the classical analogue of a Brownian ratchet. The pawl on the left-hand side translates the stochastic collision of the surrounding gas with the paddle on the right-hand side into a directed motion. This figure is taken from Ref. [Reimann, 2002] and reprinted with permission from Elsevier.

ratchet preventing it from turning into one direction while allowing rotations of the axle in the opposite direction. The fundamental concept of this set-up is the fact that the entire machine is surrounded by a gas or particles which randomly collide with the paddles on one end of the axle and hence induce a rotational motion by transferring momentum from the gas to the paddle. This motion however is undirected, as otherwise a perpetuum mobile would be created which contradicts the second law of thermodynamics.

Indeed, such a ratchet has been realised on a molecular scale which revealed an undirected motion [Kelly et al., 1997, Kelly et al., 1998, Sebastian, 2000]. Directing the motion may be achieved by keeping the gas which surrounds the paddle at a different temperature T_1 compared to the ratchet and the pawl which are held at temperature T_2 by contacting the two ends of the axle to different baths. Energy can then be converted from the the temperature gradient between the two thermal reservoirs into mechanical work. In fact, it can be shown that for $T_1 > T_2$ the axle rotates in the above described manner while for $T_1 < T_2$ the rotation is expected to be inverted and thus against the pawl [Reimann, 2002]. Due to the small scale of the set-up where thermal fluctuations are dominant an experimental realisation of a molecular Smoluchowski-Feynman ratchet with different temperatures at both ends of the system remains a strong challenge.

1.7. Outline of the thesis

As we use the Landauer-Büttiker approach and, in this context, scattering theory as a basic mathematical tool for a theoretical description of electronic transport through nanoelectromechanical systems, we give an introduction to scattering theory in chapter 2. In this chapter, we derive several formulas which are needed for the derivation of the adiabatic reaction forces in terms of the scattering matrix and its adiabatic correction in chapter 3. The derivation of the reaction forces solely relies on the fundamentals of scattering theory and includes an adiabatic expansion within this theory. Thereafter, we address the question on how the nanosystem itself affects the evolution of the quantum environment. In particular, we study how the Anderson orthogonality exponent and the dynamics of a classical particle, which moves in a quantum environment, are related via calculating the Loschmidt echo and the fidelity amplitude in chapter 4. While we use the limit of coherent transport for describing a classical nanosystem moving in a quantum environment, we consider the regime of incoherent transport in chapter 5 to model sequential electron tunnelling through a molecular transistor as realised in Ref. [Martínez-Blanco et al., 2015]. We conclude in chapter 6.

We set $\hbar = 1$ and $k_B = 1$ throughout the thesis.

2. Scattering theory

This chapter is devoted to an introduction to scattering theory which constitutes the basic mathematical tool in our analysis of coherent transport through nanoelectromechanical systems. In particular, scattering theory is used for the derivation of the adiabatic reaction forces. In this derivation, we frequently refer to the formulas derived below in this chapter. The expressions presented in this chapter are well known in the literature,[1] see for instance Refs. [Roman, 1965, Sakurai, 1994, Mello and Kumar, 2004, Moskalets, 2011].

The concept of scattering theory is valid for a generic non-interacting Hamiltonian which can be split into a "free" part and a term including the "scattering potential" which is confined to a finite region. It is a powerful tool to address various topics in physics. These topics range from the description of measurements aiming at analysing a system's structure, e.g. X-ray diffraction experiments or high energy collisions of particles, to theoretical descriptions of, for instance, electron scattering off impurities in a metal, which governs its electrical resistivity. In fact, many of the formulas derived below apply to a huge variety of problems as we keep the considered Hamiltonian quite general.

Later in the thesis, we particularly apply the formalism of scattering theory to nanoelectromechanical systems within the derivation of the adiabatic reaction forces. Nanoelectromechanical systems are in contact with source and drain electrodes, which form electronic leads. According to the framework of scattering theory, the leads are treated as ideal in the sense that electrons move in the leads without any scattering events. Moreover, we assume the leads to be macroscopically large so that they possess a continuous energy spectrum. By imposing a bias voltage, which gives rise to different chemical potentials in the respective leads and hence out-of-equilibrium conditions, electrons travel through the nanosystem. The nanosystem itself acts as a scattering potential felt by the moving electrons, cf. Figs. 1.7 and 2.1.

[1] The formalism introduced here is mainly based on the lecture notes for Advanced Quantum Mechanics by Prof. Piet W. Brouwer, Freie Universität Berlin, winter 2012/2013.

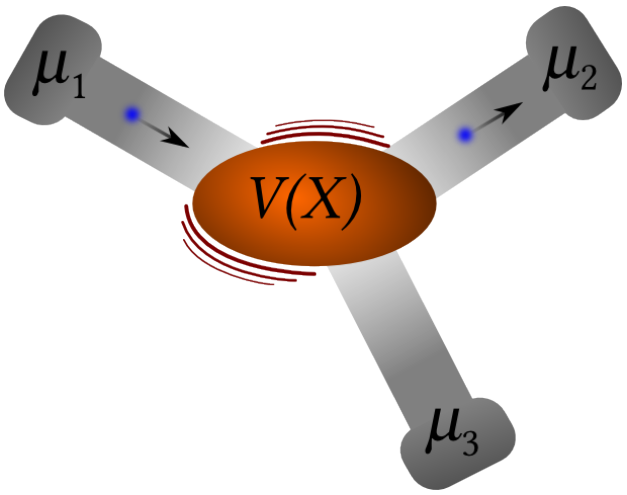

Figure 2.1.: A scattering potential $V(X)$ attached to three leads, each with chemical potential μ_j. An electron entering from a certain lead scatters off the potential and gets reflected into the same lead or transmitted into a different lead.

The electrons in the leads are described by propagating wave packets. Initially, we assume the electrons to be far away from the scattering region and hence we expect no initial interaction with the scattering potential. This means, that the initial state consists of a free wave packet approaching the scatterer. Eventually, the electron reaches the scattering region and the interaction with the nanosystem, i.e. the scatterer, changes its state. After the interaction the final state is a linear superposition of free wave packets in each lead, which travel away from the scattering region, since there is no interaction between the electron and the scatterer once the electron is far away. The free wave packets appear with a certain scattering amplitude called transmission or reflection coefficients depending on the initial state. The absolute square value of the scattering amplitude determines the probability to find the scattered particle in the respective lead, which can be the same lead or a different attached one, cf. Fig. 2.1. When the energy of the scattering particle remains unchanged by the scattering process, one speaks of elastic scattering, while an inherent energy change is dubbed inelastic scattering.

Physically, we are interested in the transformation, which changes the incoming into the outgoing states. The operator which effects this transformation is called scattering matrix or S-matrix. The scattering matrix contains all relevant information on the scattering process and constitutes the central quantity of scattering theory.

In the remainder of this section, we introduce the general mathematical description

of a single-particle scattering process including the definition of scattering states. We define the scattering matrix and deduce some of its properties. Finally, we illustrate the concept and basic principles of scattering with wave packets by discussing a one-dimensional problem where two leads are attached to the scatterer.

2.1. Scattering states

We model transport through the nanoelectromechanical system by assuming non-interacting electrons (i.e. non-interacting quasi-particle excitations of a Fermi liquid) which scatter off a scattering potential. As we will see later , this allows for an effective treatment as single-particle scattering. We introduce the Hamiltonian felt by a single electron, H, which encompasses an effective single-particle description of the leads, H_0, and the effective local scattering potential, V. The idea of scattering theory is to describe the *dynamical* process of a scattering of wave packets by *stationary* solutions of the corresponding Schrödinger equation. In order to enable a description in terms of stationary states, we consider the Hamiltonian

$$H = H_0 + V(t)\,, \quad V(t) = V\, e^{-\eta|t|} \tag{2.1}$$

with $\hbar = 1$, where the scattering potential V is slowly switched on and off with a rate given by the positive parameter η. By "slow" we mean that the switching process happens on timescales which are large compared to the dwell time, τ_D, of the scattering process. The dwell time describes the timescale that the scattering particles remain in the scattering region. The slow time dependence of the scattering potential thus has no effect on the description of the scattering potential, as it can be viewed as unchanged during the scattering process. The introduction of the small $\eta \ll 1/\tau_D$ is rather a mathematical trick: Stationary states become slowly time-dependent. By introducing the slowly time-dependent potential $V(t)$, a "stationary" state gets transformed from an initial free stationary state at infinite negative times $t \to -\infty$ to the scattering state at $t \approx 0$, where the potential is completely switched on, and to a free final stationary state at $t\ rightarrow\infty$ after the scattering process. For a description of a scattering process we are interested in the three limits $t \to -\infty$, $t \approx 0$ and $t \to \infty$.

We introduce the eigenstates, $|\Phi_m(\varepsilon, t)\rangle$, of the free Hamiltonian H_0, which represent the free states. Here, m is a combined channel-lead index and ε denotes the corresponding energy. Their time dependence is given by

$$|\Phi_m(\varepsilon, t)\rangle = e^{-i\varepsilon t}\, |\phi_m(\varepsilon)\rangle\,. \tag{2.2}$$

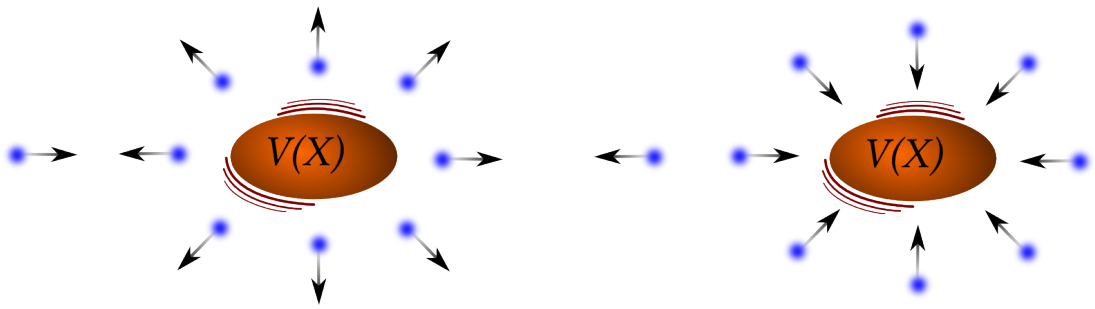

Figure 2.2.: Depiction of (a) a retarded scattering state and (b) an advanced scattering state. While a retarded scattering state is initially at large negative times a free state propagating towards the scatterer, the advanced scattering state is a free state travelling away from the scattering region at large positive times. Arrows indicate time evolution and propagation directions. The leads are not explicitly drawn in this figure.

with $H_0\,|\phi_m(\varepsilon)\rangle = \varepsilon\,|\phi_m(\varepsilon)\rangle$. We normalise the free states as

$$\langle\phi_m(\varepsilon)|\phi_{m'}(\varepsilon')\rangle = 2\pi\,\delta_{mm'}\,\delta(\varepsilon-\varepsilon')\,. \tag{2.3}$$

The single-particle scattering states, which we denote by $|\Psi_m^{\pm}(\varepsilon,t)\rangle$, are solutions of the Schrödinger equation

$$i\,\partial_t|\Psi_m^{\pm}(\varepsilon,t)\rangle = H\,|\Psi_m^{\pm}(\varepsilon,t)\rangle\,. \tag{2.4}$$

The superscript $\pm$ distinguishes between retarded $(+)$ and advanced scattering states $(-)$. Both the retarded and advanced scattering states evolve in time with respect to the same Schödinger equation, they differ however in their boundary conditions at large times. For the scattering states, the introduction of the slow time dependence of the potential is crucial. For large times before and after the potential is switched on and off, the respective retarded (at $t\to-\infty$) and advanced (at $t\to\infty$) scattering state is assumed to be in a free state, which does not interact with the scatterer. More precisely,

$$|\Psi_m^{\pm}(\varepsilon,t\to\mp\infty)\rangle = |\Phi_m(\varepsilon,t)\rangle\,. \tag{2.5}$$

While the retarded scattering state describes a state which initially at $t\to-\infty$ consists of an incident free state, the advanced scattering state is a free state leaving the scattering region at $t\to+\infty$ as shown in Fig. 2.2. Slowly switching on the potential then means that the free state slowly begins to feel the potential V until the potential is completely switched on at $t=0$. Thus we are interested in the general solution of the Schrödinger equation (2.4) in the vicinity of $t=0$ where the

scattering process takes place. At general times, the full solutions of the Schrödinger equation reads for the retarded and advanced scattering state

$$|\Psi_m^+(\varepsilon,t)\rangle = |\Phi_m(\varepsilon,t)\rangle - i\int_{-\infty}^{t} \mathrm{d}t'\, e^{-iH_0(t-t')}\, V(t')\, |\Psi_m^+(\varepsilon,t')\rangle \tag{2.6}$$

$$|\Psi_m^-(\varepsilon,t)\rangle = |\Phi_m(\varepsilon,t)\rangle - i\int_{t}^{\infty} \mathrm{d}t'\, e^{-iH_0(t-t')}\, V(t')\, |\Psi_m^-(\varepsilon,t')\rangle\,, \tag{2.7}$$

which fulfil the boundary conditions in Eq. (2.5). In order to evaluate these time integrals we recall that the scattering particles spend a finite time in the scattering region, given by the dwell time. Hence the time interval in the above integration is effectively finite. For small $\eta \ll 1/\tau_D$ we can assume the scattering potential $V(t)$ in Eq. (2.1) to be constant within this finite time range and we can consider the scattering states to be stationary. This allows us to replace $|\Psi_m^\pm(\varepsilon,t')\rangle \to e^{-i\varepsilon(t'-t)}\,|\Psi_m^\pm(\varepsilon,t)\rangle$ in the above integral. The scattering states appearing in the above integral equations (2.6) are thus evaluated at the same time, which enables an evaluation of the time integrals. An integration yields

$$|\Psi_m^+(\varepsilon,t)\rangle = |\Phi_m(\varepsilon,t)\rangle + G_0^R(\varepsilon)\, V\, e^{+\eta t}\, |\Psi_m^+(\varepsilon,t)\rangle\,, \quad t \le 0 \tag{2.8}$$

$$|\Psi_m^-(\varepsilon,t)\rangle = |\Phi_m(\varepsilon,t)\rangle + G_0^A(\varepsilon)\, V\, e^{-\eta t}\, |\Psi_m^-(\varepsilon,t)\rangle\,, \quad t \ge 0 \tag{2.9}$$

where we introduced the respective retarded and advanced Green function of the free Hamiltonian

$$G_0^{R/A}(\varepsilon) = \frac{1}{\varepsilon - H_0 \pm i\eta}\,. \tag{2.10}$$

We are interested in the solutions in the vicinity of $t = 0$ for the stationary states. We extract the dynamical phase

$$|\Psi_m^\pm(\varepsilon,t)\rangle = e^{-i\varepsilon t}\, |\psi_m^\pm(\varepsilon)\rangle \tag{2.11}$$

so that at $t = 0$ Eqs. (2.8) and (2.9) become

$$|\psi_m^\pm(\varepsilon)\rangle = |\phi_m(\varepsilon)\rangle + G_0^{R/A}(\varepsilon)\, V\, |\psi_m^\pm(\varepsilon)\rangle\,. \tag{2.12}$$

This equation is called Lippmann-Schwinger equation in the literature. It constitutes the basic equation for both the retarded and the advanced scattering state. We note that the Lippmann-Schwinger equation is an implicit equation as the scattering state appears on both sides of the equation. On a formal level however, we can present a solution of this equation. By iteratively substituting the left-hand side of Eq. (2.12) into the expression on the right-hand side we can sum up all the terms appearing on the right-hand side. Introducing the retarded and advanced Green function of the full Hamiltonian H at $t = 0$

$$G^{R/A}(\varepsilon) = \frac{1}{\varepsilon - H \pm i\eta} = G_0^{R/A}(\varepsilon) + G_0^{R/A}(\varepsilon)\, V\, G^{R/A}(\varepsilon) \tag{2.13}$$

we can write the solution of the Lippmann-Schwinger equation as

$$|\psi_m^{\pm}(\varepsilon)\rangle = \left(1 + G^{R/A}(\varepsilon)\, V\right) |\phi_m(\varepsilon)\rangle\,. \tag{2.14}$$

This equation is one of the main equations of this introductory section and has many implications. It states that the scattering state is composed of a free state and a scattered state. We can use the Lippmann-Schwinger equation (2.12) and its solution (2.14) to show that the scattering states are normalised in the same way as the free states. To this end, we write

$$\begin{aligned}
\langle\psi_m^{\pm}(\varepsilon)|\psi_{m'}^{\pm}(\varepsilon')\rangle &= \langle\phi_m(\varepsilon)|\left(1 + V\, G^{A/R}(\varepsilon)\right)|\psi_{m'}^{\pm}(\varepsilon')\rangle \\
&= \langle\phi_m(\varepsilon)|\left(1 + \frac{V}{\varepsilon - \varepsilon' \mp i\eta}\right)|\psi_{m'}^{\pm}(\varepsilon')\rangle \\
&= \langle\phi_m(\varepsilon)|\left(1 - G_0^{R/A}(\varepsilon')\, V\right)|\psi_{m'}^{\pm}(\varepsilon')\rangle \\
&= \langle\phi_m(\varepsilon)|\phi_{m'}(\varepsilon')\rangle \\
&= 2\pi\, \delta_{mm'}\, \delta(\varepsilon - \varepsilon')\,,
\end{aligned} \tag{2.15}$$

where the last line is the normalisation of the free states in Eq. (2.3). Finally, we note the completeness relation of the scattering states, i.e.

$$\sum_m \int \frac{\mathrm{d}\varepsilon}{2\pi} |\psi_m^{\pm}(\varepsilon)\rangle\langle\psi_m^{\pm}(\varepsilon)| = 1\,. \tag{2.16}$$

Both the retarded and the advanced scattering states span the full Hilbert space given by the Hamiltonian H.

2.2. The S-matrix

The S-matrix represents a key element of scattering theory. It connects the incoming free states to the scattered outgoing states and contains all necessary information on the scattering process. Making use of the fact that after the scattering process the scattering state is a superposition of free states, the S-matrix is defined as the on-shell overlap of the scattering states and the free states at large times,

$$2\pi\, S_{mm'}(\varepsilon)\, \delta(\varepsilon - \varepsilon') = \lim_{t\to\infty} \langle\Phi_m(\varepsilon, t)|\Psi_{m'}^{+}(\varepsilon', t)\rangle\,. \tag{2.17}$$

Expressing the asymptotic (retarded) scattering state at large times as a superposition of free states, we deduce from Eq. (2.17) that the elements of the S-matrix are the amplitudes of each free state after the scattering event. In order to make

this statement more precise, we use Eq. (2.17) and the completeness relation of the free states to write

$$\lim_{t\to\infty} |\Psi_m^+(\varepsilon,t)\rangle = e^{-i\varepsilon t}\sum_n S_{nm}(\varepsilon)\,|\phi_n(\varepsilon)\rangle\,. \tag{2.18}$$

Equivalently, the S-matrix can be defined using the advanced scattering state through $2\pi\, S_{mm'}(\varepsilon)\,\delta(\varepsilon-\varepsilon') = \lim_{t\to-\infty}\langle\Psi_m^-(\varepsilon,t)|\Phi_{m'}(\varepsilon',t)\rangle$, since the advanced scattering state is assumed to be in a superposition of free states for large negative times. Similarly we write for the advanced scattering state

$$\lim_{t\to-\infty} |\Psi_m^-(\varepsilon,t)\rangle = e^{-i\varepsilon t}\sum_n S_{nm}^*(\varepsilon)\,|\phi_n(\varepsilon)\rangle\,, \tag{2.19}$$

where the symbol * indicates complex conjugation. We note that the S-matrix does not depend on time as both the scattering states and the free states are stationary states with trivial time dependence and $e^{i(\varepsilon-\varepsilon')t} = 1$ for $\varepsilon = \varepsilon'$ as imposed by the δ-distribution.

In the following we present some general properties of the S-matrix. We begin by observing that the S-matrix can be expressed as the overlap of retarded and advanced scattering states. This represents a useful tool and will be frequently used below. In order to see this, we make use of the boundary condition of the advanced scattering state, cf. Eq. (2.5), as well as the fact that the scalar product of retarded and advanced scattering states does not depend on time as they fulfil the same Schrödinger equation. Hence

$$\begin{aligned} 2\pi\, S_{mm'}(\varepsilon)\,\delta(\varepsilon-\varepsilon') &= \lim_{t\to\infty}\langle\Phi_m(\varepsilon,t)|\Psi_{m'}^+(\varepsilon',t)\rangle \\ &= \lim_{t\to\infty}\langle\Psi_m^-(\varepsilon,t)|\Psi_{m'}^+(\varepsilon',t)\rangle \\ &= \langle\psi_m^-(\varepsilon)|\psi_{m'}^+(\varepsilon')\rangle\,. \end{aligned} \tag{2.20}$$

From the normalisation of the scattering states in Eq. (2.15) and the last line in Eq. (2.20) we deduce that the S-matrix is a unitary matrix, that is

$$\sum_n S_{mn}(\varepsilon)\,S_{m'n}^*(\varepsilon) = \delta_{mm'}\,. \tag{2.21}$$

The unitarity of the S-matrix means that the normalisation of the states is unchanged after the scattering process. This is expected as we deduce from the definition of the S-matrix that it describes a change of basis.

2.3. Time-reversal

Next we study the effect of time reversal, i.e. the transformation $t \to -t$, on the scattering matrix. The Hamiltonian in Eq. (2.1) is invariant under time reversal. However, the time derivative in the Schrödinger equation (2.4) changes its sign. Using the hermiticity $H = H^\dagger$ of the full Hamiltonian we then deduce that $|\Psi_m^\pm(\varepsilon, -t)\rangle^*$ fulfils the same equations as $|\Psi_m^\pm(\varepsilon, t)\rangle$, that is $i\,\partial_{(-t)}|\Psi_m^\pm(\varepsilon, -t)\rangle^* = H\,|\Psi_m^\pm(\varepsilon, -t)\rangle^*$. We note that when t changes its sign, the velocity of the scattering particles changes such that the particles move in the opposite direction. Thus, outgoing states become incoming states and vice versa. Referring to Eq. (2.18) we then define the incoming state $|\Psi_m^{\rm in}(\varepsilon, t)\rangle$ as

$$|\Psi_m^{\rm in}(\varepsilon, t)\rangle = \lim_{t\to\infty} |\Psi_m^+(\varepsilon, -t)\rangle^* = e^{-i\varepsilon t} \sum_n S_{nm}^*(\varepsilon)\, |\phi_n(\varepsilon)\rangle^* \,. \tag{2.22}$$

The outgoing state on the other hand is just the free state

$$|\Psi_m^{\rm out}(\varepsilon, t)\rangle = e^{-i\varepsilon t}\, |\phi_m(\varepsilon)\rangle^* \,. \tag{2.23}$$

The S-matrix connects these incoming and outgoing states. We write $|\Psi_m^{\rm in}(\varepsilon, t)\rangle = \sum_n (S^{-1}(\varepsilon))_{nm}\, |\Psi_n^{\rm out}(\varepsilon, t)$ for large t by definition of the scattering matrix. Inserting the above expression then yields

$$e^{-i\varepsilon t} \sum_n S_{nm}^*(\varepsilon)\, |\phi_n(\varepsilon)\rangle^* = e^{-i\varepsilon t} \sum_n (S^{-1}(\varepsilon))_{nm}\, |\phi_n(\varepsilon)\rangle^* \,. \tag{2.24}$$

We conclude that time-reversal symmetry implies that $S^*(\varepsilon) = S^{-1}(\varepsilon)$. Due to unitarity of the S-matrix, cf. Eq. (2.21), we then deduce that

$$S(\varepsilon) = S^T(\varepsilon) \tag{2.25}$$

in time-reversal invariant systems [Moskalets, 2011].

2.4. The T-matrix

In the absence of a scattering potential, the scattering matrix is given by the unit matrix. In scattering experiments one is often interested in transitions between *different* incoming and outgoing states. This motivates us to subtract the unit matrix from the scattering matrix and to define the transition matrix (T-matrix or reaction matrix) as

$$S_{mm'}(\varepsilon) = \delta_{mm'} - i\, T_{mm'}(\varepsilon) \,. \tag{2.26}$$

The T-matrix gives precisely that part of the scattering matrix which describes transitions between different states during the scattering process. We note that this does not mean that the diagonal elements of the T-matrix vanish, cf. Eq. (2.41). As the scattering matrix can be written as the overlap of retarded and advanced scattering states, cf. Eq. (2.20), we conclude with the aid of the Lippmann-Schwinger equation (2.14) and the normalisation of the scattering states (2.15) that

$$\begin{aligned} 2\pi\, S_{mm'}(\varepsilon)\,\delta(\varepsilon-\varepsilon') &= \langle\psi_m^-(\varepsilon)|\psi_{m'}^+(\varepsilon')\rangle \\ &= \langle\psi_m^+(\varepsilon)|\psi_{m'}^+(\varepsilon')\rangle + \left(\langle\psi_m^-(\varepsilon)| - \langle\psi_m^+(\varepsilon)|\right)|\psi_{m'}^+(\varepsilon')\rangle \\ &= 2\pi\,\delta_{mm'}\,\delta(\varepsilon-\varepsilon') + \langle\phi_m(\varepsilon)|V\left(G^R(\varepsilon)-G^A(\varepsilon)\right)|\psi_{m'}^+(\varepsilon')\rangle \\ &= 2\pi\,\left(\delta_{mm'} - i\,\langle\phi_m(\varepsilon)|\,V\,|\psi_{m'}^+(\varepsilon)\rangle\right)\,\delta(\varepsilon-\varepsilon')\,, \end{aligned} \tag{2.27}$$

where it has been used that $(\varepsilon-\varepsilon'+i\eta)^{-1}-(\varepsilon-\varepsilon'-i\eta)^{-1} = -2\pi i\delta(\varepsilon-\varepsilon')$. We read off that the T-matrix can be expressed as the overlaps

$$T_{mm'}(\varepsilon) = \langle\phi_m(\varepsilon)|\,V\,|\psi_{m'}^+(\varepsilon)\rangle = \langle\psi_m^-(\varepsilon)|\,V\,|\phi_{m'}(\varepsilon)\rangle\,. \tag{2.28}$$

The last identity can be obtained by performing analogous steps for the retarded scattering state in the first line of Eq. (2.27). We stress that the overlaps defining the T-matrix contain the scattering potential V. On the one hand we conclude that in the absence of the scattering potential the T-matrix naturally vanishes, which is reasonable since the scattering state remains unchanged for $V=0$. Moreover, we note that due to the locality of the scattering potential V the overlaps in Eq. (2.28) do not diverge although the overlap is evaluated for states at the same energy ε.

2.5. Scattering in one dimension

To illustrate the above concepts, we consider the scattering of a spinless particle, e.g. an electron, off a one-dimensional local potential $V(x)$. The aim of treating the one-dimensional case is twofold. On the one hand, it shows how to deal with scattering wave packets, which are a superposition of free waves. Moreover, it highlights the elements of the scattering matrix by interpreting them as reflection and transmission amplitudes. Accordingly, we consider the Hamiltonian in Eq. (2.1) with

$$H_0 = \frac{p^2}{2m} \quad \text{and} \quad V = V(x) \tag{2.29}$$

in position representation. Here $p = -i\,\partial/\partial_x$ is the momentum and m the mass of the particle. The only constraint on the scattering potential is that it vanishes at $|x| > x_0$. The eigenstates of the free Hamiltonian H_0 possess the energy

$\varepsilon_k = k^2/(2m)$ and as the Hamiltonian is time independent, they evolve in time as $\langle x|\Phi(k,t)\rangle = \Phi(k,x,t) = e^{-i\varepsilon_k t}\,\phi(k,x)$ with the plane wave solutions

$$\phi(k,x) = \langle x|\phi(k)\rangle = \frac{1}{\sqrt{v}}\,e^{ikx}\,. \tag{2.30}$$

Dividing by the square root of the velocity $v = \partial\varepsilon_k/\partial_k = k/m$ accounts for unit flux normalisation. This implies the orthonormality

$$\langle\phi(k)|\phi(k')\rangle = 2\pi\,\delta(\varepsilon_k - \varepsilon_{k'})\,. \tag{2.31}$$

According to the boundary conditions in Eq. (2.5), the retarded scattering state at $t \to -\infty$ is a wave packet with wave vector k_i and thus consists of a linear superposition of plane waves, that is

$$|\Phi_{k_i}(t)\rangle = \int \mathrm{d}k\, f_{k_i}(k)\,|\Phi(k,t)\rangle\,. \tag{2.32}$$

The advanced scattering state on the other hand is described by $|\Phi_{k_i}(t)\rangle$ for positive $t \to \infty$. The functions $f_{k_i}(k)$ determine the shape of the wave packet and are in principle quite general. In the following we restrict to a Gaussian wave packet with $f_{k_i}(k) = \exp[-(k-k_i)^2/(2\sigma)^2]/\sqrt{2\pi\sigma}$ to keep the analysis more simple. Hence the momentum of the wavepacket has an uncertainty given by the width σ of the Gaussian functions. In position representation we have

$$\Phi_{k_i}(x,t) = \langle x|\Phi_{k_i}(t)\rangle = \int \mathrm{d}k\, f_{k_i}(k)\,\phi(k,x)\,e^{-i\varepsilon_k t}\,. \tag{2.33}$$

We consider the limit of small momentum uncertainty, i.e. $\sigma \ll |k_i|$. The velocity of the wave packet then is $v_i = k_i/m$ and we expand the energy ε_k to linear order as $\varepsilon_k = k_i^2/(2m) + v(k-k_i)$. Within this approximation the wavepacket does not disperse. Moreover we assume $k_i > 0$, which means that $\Phi_{k_i}(x,t)$ is a wave packet moving to the right, whereas $\Phi_{-k_i}(x,t)$ travels to the left. This allows us to distinguish between the two initial (retarded) states $|\Psi^+_{k_i}(t \to -\infty)\rangle = |\Phi_{k_i}(t)\rangle$ at distances much to the left of the scattering potential and $|\Psi^+_{-k_i}(t \to -\infty)\rangle = |\Phi_{-k_i}(t)\rangle$ at distances $x \gg x_0$.

The (retarded) scattering state is a linear superposition of the eigenstates $\psi^+(k,x) = \langle x|\psi^+(k)\rangle$ of the full Hamiltonian H in Eq. (2.1) with energy ε_k

$$\Psi^+_{k_i}(x,t) = \langle x|\Psi^+_{k_i}(t)\rangle = \int \mathrm{d}k\, f_{k_i}(k)\,\psi^+(k,x)\,e^{-i\varepsilon_k t}\,. \tag{2.34}$$

As the potential vanishes for $|x| > x_0$, the states $\psi^+(k,x)$ consist of plane waves outside the scattering region. We introduce the coefficients $a(k)$, $b(k) \in \mathbb{C}$ and

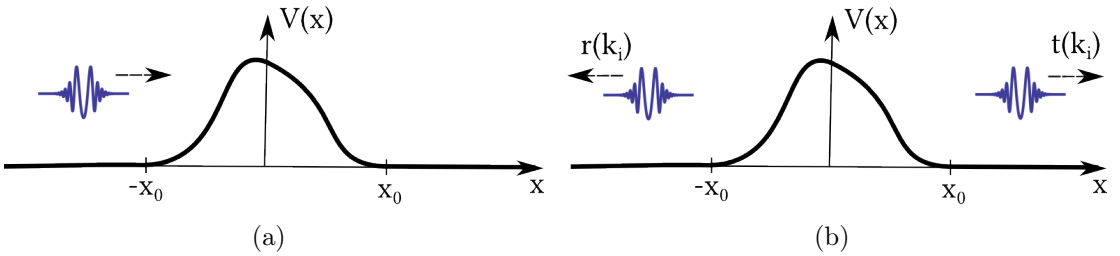

Figure 2.3.: Illustration of a retarded scattering state in one dimension as a wave packet incident from the left at large negative times with wavevector k_i; (a) initial state; (b) final state. The coefficients $r(k_i)$ and $t(k_i)$ give the respective reflection and transmission amplitudes.

write the general solution outside the scattering region as

$$\psi^+(k,x) = \frac{1}{\sqrt{v}} \begin{cases} a(k)\,[e^{ikx} + r(k)\,e^{-ikx}] + b(k)\,t'(k)\,e^{-ikx} & \text{, for} \quad x < -x_0 \\ a(k)\,t(k)\,e^{ikx} + b(k)\,[e^{-ikx} + r'(k)\,e^{ikx}] & \text{, for} \quad x > x_0 \end{cases} . \tag{2.35}$$

The coefficients $r(k)$, $r'(k)$, $t(k)$ and $t'(k)$ are determined by the Schrödinger equation. As we consider small $\sigma \ll |k_i|$ we approximate these coefficients as evaluated at the initial wave vector k_i. We determine $a(k)$, $b(k)$ by the boundary condition that the initial retarded scattering state matches the free incoming wave. We get $a(k) = 1$, $b(k) = 0$ for a wave incoming from the left, so that

$$\Psi^+_{k_i}(x,t) = \int \mathrm{d}k\, f_{k_i}(k)\, e^{-i\varepsilon_k t} \times \frac{1}{\sqrt{v}} \begin{cases} e^{ikx} + r(k_i)\,e^{-ikx} & \text{, for} \quad x < -x_0 \\ t(k_i)\,e^{ikx} & \text{, for} \quad x > x_0 \end{cases} . \tag{2.36}$$

An initial state approaching from the right at $t \to -\infty$ however implies that $a(k) = 0$, $b(k) = 1$. We denote the state incident from the right with a subscript $-k_i$. Consequently,

$$\Psi^+_{-k_i}(x,t) = \int \mathrm{d}k\, f_{-k_i}(k)\, e^{-i\varepsilon_k t} \times \frac{1}{\sqrt{v}} \begin{cases} t'(k_i)\,e^{-ikx} & \text{, for} \quad x < -x_0 \\ e^{-ikx} + r'(k_i)\,e^{ikx} & \text{, for} \quad x > x_0 \end{cases} . \tag{2.37}$$

From Eqs. (2.36) and (2.37) we can deduce the final (retarded) states at $t \to \infty$ and $|x| \gg x_0$. For the retarded scattering approaching the scatterer initially from the left we deduce

$$\Psi^+_{k_i}(x, t \to \infty) = t(k_i)\,\Phi_{k_i}(x,t) + r(k_i)\,\Phi_{-k_i}(x,t)\,. \tag{2.38}$$

Similarly for the state incident from the right we get

$$\Psi^+_{-k_i}(x, t \to \infty) = t'(k_i)\,\Phi_{-k_i}(x,t) + r'(k_i)\,\Phi_{k_i}(x,t)\,. \tag{2.39}$$

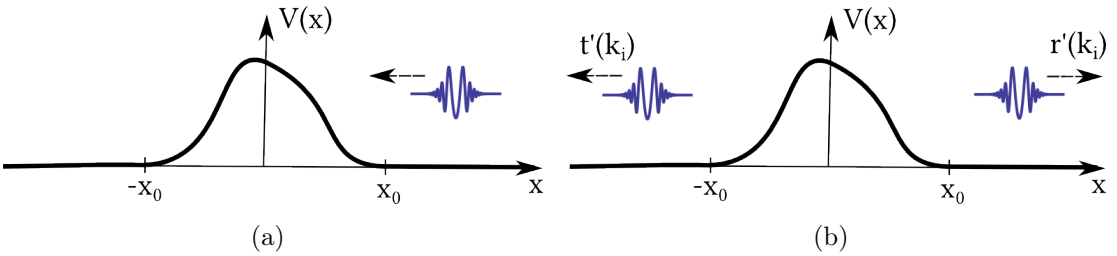

Figure 2.4.: Picture of a retarded scattering state in one dimension as a wave packet initially approaching the scatterer from the right with wavevector k_i; (a) initial state; (b) final state. The respective reflection and transmission amplitudes are represented by the coefficients $r'(k_i)$ and $t'(k_i)$.

After the scattering process the states therefore consist of a superposition of free waves travelling to the left and right. Equations (2.38) and (2.39) allow us to read off the meaning of the coefficients introduced in Eq. (2.35). An initial wave packet approaching the scattering region with wavevector k_i from the left gets reflected with amplitude $r(k_i)$ and transmitted with amplitude $t(k_i)$ as schematically depicted in Fig. 2.3. The coefficients $r'(k_i)$ and $t'(k_i)$ describe the analogue for an incoming particle from the right, cf. Fig. 2.4. The advanced scattering state is treated in complete analogy. Comparing to Eq. (2.18) shows that the elements of the S-matrix precisely represent these reflection and transmission coefficients. We conclude that

$$S(k_i) = \begin{pmatrix} t(k_i) & r'(k_i) \\ r(k_i) & t'(k_i) \end{pmatrix} . \tag{2.40}$$

The unitarity of the S-matrix implies that $|r(k_i)|^2 + |t(k_i)|^2 = 1$ as well as $|r'(k_i)|^2 + |t'(k_i)|^2 = 1$ which represents the fact that the reflection and transmission probabilities of the scattering particle must add to one. The T-matrix is obtained by referring to its definition in Eq. (2.26). We readily have

$$T(k_i) = -i \begin{pmatrix} 1 - t(k_i) & -r'(k_i) \\ -r(k_i) & 1 - t'(k_i) \end{pmatrix} . \tag{2.41}$$

We can determine the reflection and transmission coefficients from the Lippmann-Schwinger equation in position representation. For the sake of convenience, we present here the result for a symmetric potential,

$$t(k_i) = 1 - \frac{i}{v} \int_{-x_0}^{x_0} \mathrm{d}x \, V(x) \,, \tag{2.42}$$

$$r(k_i) = -\frac{i}{v} \int_{-x_0}^{x_0} \mathrm{d}x \, V(x) \, e^{2ik_i x} \,. \tag{2.43}$$

We note that a symmetric potential means that the reflection and transmission amplitudes are the same for particles approaching the scatterer from the left and the right, hence $r(k_i) = r'(k_i)$ and $t(k_i) = t'(k_i)$.

3. Scattering theory of adiabatic reaction forces

In this chapter we derive the forces induced by the backaction of a quantum environment on a classical system purely within the framework of scattering theory. Motivated by recent advances both in nanoelectromechanical systems [Pistolesi et al., 2008, Bennett et al., 2010, Lü et al., 2010, Lü et al., 2011, Bode et al., 2011, Bode et al., 2012b, Bode, 2012, Bunch et al., 2007, Lassagne et al., 2009, Steele et al., 2009] and in spintronics devices [Tserkovnyak et al., 2002, Kupferschmidt et al., 2006, Brataas et al., 2008, Brataas et al., 2011, Bode et al., 2012a, Fert, 2008, Ralph and Stiles, 2008, Misiorny and Barnaś, 2009] the quantum environment is considered as an open system with a continuous energy spectrum. By this, we naturally include fluctuations and dissipation in our description. We consider the case where the system is driven out of equilibrium.

We are interested in the backaction of the quantum environment on the classical system. We denote the classical system by the classical parameters $\mathbf{X}(t) = \mathbf{X}_t$, which we also call classical degrees of freedom in the following. The dynamics of the classical system, which moves in a quantum environment, is governed by the Langevin equation

$$\dot{P}_\alpha - F^{cl}_\alpha = F_\alpha - \sum_\beta \gamma_{\alpha\beta}\,\dot{X}_\beta + \xi_\alpha \tag{3.1}$$

with the classical momentum, $\mathbf{P}$, the classical external force, $\mathbf{F}^{cl}$, and α (β) denotes the component of the classical degree of freedom. On the right-hand side of Eq. (3.1) the environment-induced adiabatic reaction forces are collected. To lowest order in the adiabatic parameter the classical system experiences the Born-Oppenheimer force, $\mathbf{F}(\mathbf{X}_t)$, which depends on the instantaneous position of the classical parameter. To next order in the adiabatic expansion forces proportional to the velocity occur, which are described by the tensor, $\boldsymbol{\gamma}(\mathbf{X}_t)$. The antisymmetric part of the tensor $\boldsymbol{\gamma}(\mathbf{X}_t)$ corresponds to a Lorentz-like force, while the symmetric part describes dissipation. The fluctuating stochastic forces are characterised by $\boldsymbol{\xi}$.

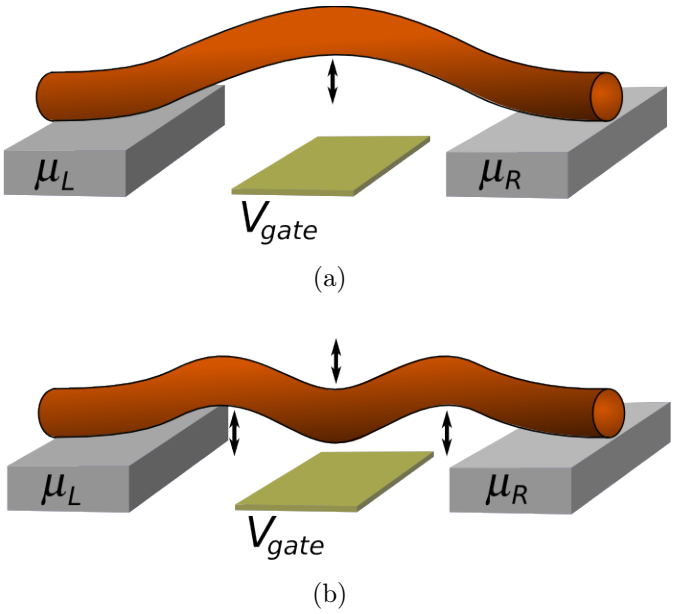

Figure 3.1.: Different vibrational modes of a nanotube attached to leads; (a) one vibrational degree of freedom X_t, (b) three vibrational degrees of freedom $\mathbf{X}_t$. Oscillating nanotubes are a paradigm of nanoelectromechanical systems where a classical system couples to a fermionic environment.

An exemplary set-up in the context of nanoelectromechanical systems is depicted in Fig. 3.1 where the classical coordinates $\mathbf{X}_t$ correspond to different vibrational degrees of freedom of a suspended nanotube which is attached to leads. The quantum environment consists of electrons moving through the nanotube and can be driven out of equilibrium by applying a bias voltage. A more general set-up is schematically shown in Fig. 2.1 which leaves the interpretation of nanoelectromechanical systems and depicts an arbitrary degree of freedom $\mathbf{X}_t$. The scattering region felt by a quantum environment then depends on the position $\mathbf{X}_t$.

In this chapter, we find expressions of the environment-induced forces on the right-hand side of the Langevin equation (3.1) in terms of the scattering matrix and its first adiabatic correction. Before we detail the derivation, however, we first present the results in Sec. 3.1 in order to simplify further reading. In Sec. 3.2, we then present the adiabatic expansion of scattering states, which provides the mathematical input for a derivation of the reaction forces. Together with this expansion, we present an explicit expression for the first adiabatic correction term of the scattering matrix in terms of adiabatic scattering states. This is then used to derive the adiabatic reaction forces in Sec. 3.3. Thereafter we connect our approach

to the Green function approach in Refs. [Bode et al., 2011, Bode et al., 2012b] by applying our formalism to the description of a generic quantum dot coupled to leads in Sec. 3.4. Finally, we conclude in Sec. 3.5

This chapter is based on Ref. [Thomas et al., 2012]. [1]

3.1. Adiabatic reaction forces

The adiabatic reaction forces appearing in the Langevin equation are the consequence of the backaction of the quantum environment on the classical degree of freedom. We describe the environment by the non-interacting *many-body* Hamiltonian, $\mathcal{H}_t = \mathcal{H}(\mathbf{X}_t)$, which depends on time via the classical parameter $\mathbf{X}_t$. This represents the coupling between the classical system and the quantum environment. Our findings apply to any coupling strength between the classical parameter and the quantum environment. For non-interacting particles, the many-body Hamiltonian can be represented by a one-particle operator. This enables a reduction to a single particle problem and hence we can use the Landauer-Büttiker approach for a description of transport through the system. By this, the above developed tools on scattering theory can be applied. The treatment of interacting particles is beyond of the scope of this thesis.

We express the adiabatic reaction forces in terms of the scattering matrix and its first adiabatic correction below. We begin with the Born-Oppenheimer force. We find [Bode et al., 2011, Bode et al., 2012b]

$$F_\alpha(\mathbf{X}_t) = \int \frac{\mathrm{d}\varepsilon}{2\pi i} \sum_n f_n(\varepsilon) \mathrm{tr} \left\{ \Pi_n S_t^\dagger(\varepsilon) \partial_\alpha S_t(\varepsilon) \right\} \tag{3.2}$$

with $\partial_\alpha = \partial/\partial X_\alpha(t)$. The energy ε describes the initial energy of the scattering particles and the index n is a combined channel-lead index. The leads are kept at chemical potentials μ_n with distribution functions $f_n(\varepsilon)$. The trace $\mathrm{tr}\{\ldots\}$ is over the leads and scattering channels and Π_n is a projector onto lead n. The index t of the scattering matrix $S_t(\varepsilon)$ describes the dependence of the scattering matrix on time via the classical parameter $\mathbf{X}_t$. We call this scattering matrix the frozen scattering matrix as it gives the adiabatic limit with frozen classical degrees of freedom $\mathbf{X}_t$.

[1] In particular, this chapter is based on a collaboration with T. Karzig. M. Thomas and T. Karzig contributed equally to the work. Some of the results of the collaboration are reported in Ref. [Karzig, 2012].

We can read off from the expression in Eq. (3.2) that the Born-Oppenheimer force is conservative in equilibrium. When the system however is driven out of equilibrium, Eq. (3.2) shows that the Born-Oppenheimer force can be non-conservative. By this, work can be exerted on the system, which is the fundamental idea of the construction of quantum machines or motors [Dundas et al., 2009, Brandbyge, 2009, Todorov et al., 2010]. For a system where the classical particle moves on a closed path it has been shown in Ref. [Bustos-Marún et al., 2013] that there is a direct relation between the Born-Oppenheimer force and the charge Q_P, which is pumped through the system by adiabatically varying the parameter $\mathbf{X}_t$ [Brouwer, 1998]. Specifically, it has been shown in this reference that the integral along a closed trajectory reads $\oint \mathrm{d}\mathbf{X}_t \cdot \mathbf{F}(\mathbf{X}_t) = Q_P\, V_b$ to linear response in the bias voltage V_b. This relation constitutes the fundamental identity for an adiabatic quantum motor [Bustos-Marún et al., 2013].

Next, we consider the symmetric part of the tensor $\boldsymbol{\gamma}(\mathbf{X}_t)$ with respect to the indices α and β which describes dissipation. We denote the symmetric part by a superscript s and find [Bode et al., 2011, Bode et al., 2012b]

$$\begin{aligned}\gamma^s_{\alpha\beta}(\mathbf{X}_t) = &\int \frac{\mathrm{d}\varepsilon}{4\pi} \sum_n [-\partial_\varepsilon f_n(\varepsilon)] \mathrm{tr}\left\{\Pi_n \partial_\alpha S_t^\dagger(\varepsilon) \partial_\beta S_t(\varepsilon)\right\}_s \\ &+ \int \frac{\mathrm{d}\varepsilon}{2\pi i} \sum_n f_n(\varepsilon) \mathrm{tr}\left\{\Pi_n \left[\partial_\alpha S_t^\dagger(\varepsilon) A_t^\beta(\varepsilon) - A_t^{\beta\dagger}(\varepsilon) \partial_\alpha S_t(\varepsilon)\right]\right\}_s .\end{aligned} \tag{3.3}$$

The matrix A_t (A-matrix) denotes the first adiabatic correction of the frozen scattering matrix. We give an explicit expression of this matrix in terms of scattering states in Eqs. (3.28) and (3.35).

We point out that the first line in Eq. (3.64) is positive definite, while the second line is not. The second line vanishes in equilibrium. This immediately leads to a positive friction coefficient in equilibrium. When the quantum system however is driven out of equilibrium, negative friction can occur. A necessary condition for negative friction is a non-vanishing A-matrix, which is indeed realisable for at least two modes $\mathbf{X}_t$ [Bode et al., 2012b]. An example where negative friction has been measured is shown in Ref. [Lotze et al., 2012], where a macroscopic cantilever is driven into motion by the fluctuations of an adjacent H_2-molecule.

We denote the Lorentz-like force, which corresponds to the antisymmetric part of the tensor $\boldsymbol{\gamma}(\mathbf{X}_t)$ with the superscript a. It reads [Bode et al., 2011, Bode et al., 2012b]

$$\gamma^a_{\alpha\beta}(\mathbf{X}_t) = \int \frac{\mathrm{d}\varepsilon}{2\pi i} \sum_n f_n(\varepsilon)\, \mathrm{tr}\left\{\Pi_n \left[S_t^\dagger(\varepsilon) \partial_\beta A_t^\alpha(\varepsilon) - \partial_\beta A_t^{\alpha\dagger}(\varepsilon) S_t(\varepsilon)\right]\right\}_a . \tag{3.4}$$

The antisymmetric tensor $\gamma^a_{\alpha\beta}$ represents an effective magnetic field in the Langevin equation which acts on the classical degree of freedom. By definition, it naturally vanishes in one dimension. Furthermore it vanishes under time-reversal symmetry in thermal equilibrium [Bode et al., 2011, Bode et al., 2012b], since $S(\varepsilon) = S^T(\varepsilon)$ and $A(\varepsilon) = -A^T(\varepsilon)$, cf. Sec. 2.3.

We conclude with the white-noise correlator of the fluctuating force, $D_{\alpha\beta}(\mathbf{X}_t)$. It is given by

$$D_{\alpha\beta}(\mathbf{X}_t) = \sum_{nm} \int \frac{\mathrm{d}\varepsilon}{2\pi} f_n(\varepsilon)\, [1 \mp f_m(\varepsilon)]\, \mathrm{tr} \left\{ \Pi_n \left[S_t^\dagger(\varepsilon)\, \partial_\alpha S_t(\varepsilon) \right]^\dagger \Pi_m\, S_t^\dagger(\varepsilon)\, \partial_\beta S_t(\varepsilon) \right\}_s , \tag{3.5}$$

where the minus sign refers to a fermionic environment and the plus sign to a bosonic environment. The correlator $D_{\alpha\beta}(\mathbf{X}_t)$ is positive definite, which can be shown by changing to a basis where the correlator is diagonal and using of the cyclic invariance of the trace [Bode et al., 2011]. Moreover, in equilibrium we have by comparing to the expression of the friction tensor in Eq. (3.3) and with the aid of $-\partial_\varepsilon f(\varepsilon) = \beta\, f(\varepsilon)\,[1 - f(\varepsilon)]$ with inverse temperature β that friction and the noise correlator are related via $\mathbf{D} = 2T\boldsymbol{\gamma}_s$. This is a manifestation of the fluctuation-dissipation theorem.

The obtained results were derived in Refs. [Bode et al., 2011, Bode et al., 2012b] for a fermionic quantum environment using Keldysh Green functions. Below, we present a rederivation of these expressions – including the generalisation to a bosonic environment – within the framework of scattering theory. This has several advantages: (i) Our derivation is much more direct compared to the derivation in Refs. [Bode et al., 2011, Bode et al., 2012b] and (ii) by this allows a comparison to the seminal work in Ref. [Berry and Robbins, 1993] calculating the adiabatic reaction forces for a closed quantum environment. (iii) The usage of scattering theory generalises previous results to quantum environments which can be either fermionic or bosonic. Before we enter the derivation, however, we formulate the necessary mathematical input.

3.2. Adiabatic expansion

This section is devoted to the adiabatic expansion of the Lippmann-Schwinger equation as developed in Ref. [Thomas et al., 2012]. This provides the basic mathematical input for a derivation of the reaction forces within scattering theory. As in

the introductory section on scattering theory in chapter 2, we consider the single-particle Hamiltonian

$$H = H_0 + V(t)\,, \tag{3.6}$$

which – similar to Eq. (2.1) – consists of a free part H_0 and a part given by the spatially confined scattering potential $V(t)$. In this chapter, however, we allow for time dependence of the scattering potential via the classical degree of freedom $\mathbf{X}_t$.

The adiabatic expansion consists in assuming a slowly varying classical degree of freedom $\mathbf{X}_t$. Generally, we characterise the time dependence on $\mathbf{X}_t$ by a typical frequency Ω. By "slow" we then mean $\Omega \ll 1/\tau_D$ where τ_D is the dwell time, that is the time that the scattering particles spend within the scattering region V_τ [Wigner, 1955]. In the context of nanoelectromechanical systems, "slow" means that many electrons travel through the system per oscillation period of the nanosystem. This assumption allows for an expansion of the scattering potential $V(t)$ in Eq. (3.6) in terms of time derivatives of the classical degree of freedom. To linear order in the adiabatic parameter, we have

$$V(t) = \left[V_\tau + \nabla_{X_\tau} V_\tau \cdot \dot{\mathbf{X}}_\tau\,(t-\tau) + \ldots\right] e^{-\eta|t|} \tag{3.7}$$

with $V_\tau = V(\mathbf{X}_\tau)$. While the first term of the potential $V(t)$ in Eq. (3.7) describes scattering with respect to a static configuration $\mathbf{X}_\tau$, the second term in the potential constitutes the next order expression by including small changes in the classical parameter. By this, the second term is proportional to the velocity $\dot{\mathbf{X}}_\tau$. The time τ in Eq. (3.7) is defined as the time, which gives rise to the classical configuration $\mathbf{X}_\tau$. We call this time central time hereafter.

When considering finite quantum systems an adiabatic expansion is conveniently performed under the condition that Ω is much smaller than the typical level-spacing $\Delta\varepsilon$ of the quantum system [Berry and Robbins, 1993]. As we however attach leads to our system which gives rise to an infinite system with a continuous energy spectrum and thus a vanishing single-particle level spacing, the condition $\Omega \ll \Delta\varepsilon$ cannot be fulfilled. Instead, for systems with a continuous energy spectrum the adiabatic condition states that the classical frequency Ω is much smaller than the inverse dwell time $1/\tau_D$.

3.2.1. Scattering states

Our aim in the following is to perform an adiabatic expansion of the scattering states. We denote the respective *time-dependent* retarded and advanced scattering

states by $|\Psi_m^{\pm}(\varepsilon,t)\rangle$ with combined channel-lead index m, similar to the description in chapter 2. The energy ε describes the initial energy of the incident scattering particle for the retarded scattering states and the final energy of the outgoing particle for the advanced scattering states. These scattering states represent the solutions of the full *time-dependent* Schrödinger equation

$$i\,\frac{\mathrm{d}}{\mathrm{d}t}\big|\Psi_m^{\pm}(\varepsilon,t)\big\rangle = H\,\big|\Psi_m^{\pm}(\varepsilon,t)\big\rangle\,. \tag{3.8}$$

The scattering states fulfil the boundary conditions in Eq. (2.5). This means that they evolve from/to free states at infinite times, which are solutions of the free Hamiltonian H_0. Similar to the treatment in chapter 2 we extract the dynamical phase

$$|\Psi_m^{\pm}(\varepsilon,t)\rangle = e^{-i\varepsilon t}\,|\psi_m^{\pm}(\varepsilon,t)\rangle\,, \tag{3.9}$$
$$|\Phi_m(\varepsilon,t)\rangle = e^{-i\varepsilon t}\,|\phi_m(\varepsilon)\rangle \tag{3.10}$$

of both the scattering states and the free states, $|\Phi_m(\varepsilon,t)\rangle$. The free states are normalised as in Eq. (2.3).

In order to perform an adiabatic expansion of the scattering states $|\Psi_m^{\pm}(\varepsilon,t)\rangle$ we introduce the notation [Entin-Wohlman et al., 2002]

$$|\psi_k^{\pm}(\varepsilon,t)\rangle = |\psi_k^{\mathbf{X}_\tau\pm}(\varepsilon)\rangle + |\delta\psi_k^{\mathbf{X}_\tau\pm}(\varepsilon)\rangle + \ldots \tag{3.11}$$

where the scattering states $|\psi_k^{\mathbf{X}_\tau\pm}(\varepsilon)\rangle$ give the adiabatic limit with frozen classical degree of freedom $\mathbf{X}_\tau$. The states $|\delta\psi_k^{\mathbf{X}_\tau\pm}(\varepsilon)\rangle$ denote the first order correction term in the adiabatic expansion and thus are proportional to the classical velocity $\dot{\mathbf{X}}_\tau$. In the adiabatic limit, the scattering potential V_τ can be treated as static as it depends on time only via the classical parameter. Hence the scattering states are stationary states and fulfil the Lippmann-Schwinger equation, cf. Eq. (2.14),

$$\big|\psi_m^{\mathbf{X}_\tau\pm}(\varepsilon)\big\rangle = \big|\phi_m(\varepsilon)\big\rangle + G_\tau^{R/A}(\varepsilon)\,V_\tau\,\big|\phi_m(\varepsilon)\big\rangle\,. \tag{3.12}$$

The index τ of the retarded and advanced Green functions indicates the frozen configuration $\mathbf{X}_\tau$,

$$G_\tau^{R/A}(\varepsilon) = \frac{1}{(\varepsilon - H_\tau \pm i\eta)} \tag{3.13}$$

with the notation $H_\tau = H_0 + V_\tau$ and $\eta \to 0^+$. A derivation of the Lippmann-Schwinger equation is presented in Sec. 2.

In order to find an expression of the first adiabatic correction $|\delta\psi_k^{\mathbf{X}_\tau\pm}(\varepsilon)\rangle$ in Eq. (3.11), we explicitly consider the next order term, which is proportional to the velocity $\dot{\mathbf{X}}_\tau$

in Eq. (3.7), as a perturbation. To make intermediate steps more transparent we briefly introduce a new notation which, however, is limited to the present discussion in this section. The advantage of this notation is that is enables a direct comparison to the treatment in the previous chapter. Accordingly we rewrite the Hamiltonian in Eq. (3.7) as

$$H = H_\tau^{(a)}(t) + V_\tau^{(1)}(t)\,, \quad H_\tau^{(a)}(t) = H_0 + V_\tau\, e^{-\eta|t|} \tag{3.14}$$

and $V_\tau^{(1)}(t) = \nabla_{X_\tau} V_\tau \cdot \dot{\mathbf{X}}_\tau\,(t-\tau)\, e^{-\eta|t|}$. Here, $H_\tau^{(a)}(t)$ denotes the Hamiltonian with respect to the frozen configuration which gives rise to the adiabatic Lippmann-Schwinger equation given in Eq. (3.12). The solution of the Schrödinger equation (3.8) can then be written for the retarded and advanced scattering state as the integral equation [analogous to Eq. (2.6)]

$$|\Psi_m^+(\varepsilon,t)\rangle = |\Psi_m^{\mathbf{X}_\tau +}(\varepsilon,t)\rangle - i\int_{-\infty}^{t} \mathrm{d}t'\, e^{i\int_t^{t'} \mathrm{d}s\, H_\tau^{(a)}(s)}\, V_\tau^{(1)}(t')\, |\Psi_m^+(\varepsilon,t')\rangle\,, \tag{3.15}$$

$$|\Psi_m^-(\varepsilon,t)\rangle = |\Psi_m^{\mathbf{X}_\tau -}(\varepsilon,t)\rangle - i\int_{t}^{\infty} \mathrm{d}t'\, e^{i\int_t^{t'} \mathrm{d}s\, H_\tau^{(a)}(s)}\, V_\tau^{(1)}(t')\, |\Psi_m^-(\varepsilon,t')\rangle\,, \tag{3.16}$$

where $|\Psi_k^{\mathbf{X}_\tau +}(\varepsilon,t)\rangle$ characterises the solution with respect to the Hamiltonian $H_\tau^{(a)}(t)$. We note that the boundary conditions of the scattering states are fulfilled in the above integral equations as $|\Psi_k^{\mathbf{X}_\tau \pm}(\varepsilon, t\to\mp\infty)\rangle = |\Phi_k(\varepsilon,t)\rangle$. We are interested in the first order correction term to the adiabatic limit. Similar to the treatment of the static scattering problem in chapter 2, we replace $|\Psi_m^\pm(\varepsilon,t')\rangle \to e^{-i\varepsilon(t'-t)}\,|\Psi_m^{\mathbf{X}_\tau \pm}(\varepsilon,t)\rangle$ within the integral. We note that the integrand is already proportional to $V_\tau^{(1)}$ so that this replacement is allowed in the regime $\Omega \ll \eta \ll 1/\tau_D$ to linear order in the adiabatic parameter. Moreover, we note that due to the restriction $\eta \ll 1/\tau_D$ we can expand the exponent in the exponential as $i\int_t^{t'} \mathrm{d}s\, H_\tau^{(a)}(s) \approx -i(H_0+V_\tau)\,(t-t') = -iH_\tau\,(t-t')$ to lowest order. We conclude to linear order in the adiabatic parameter that

$$|\Psi_m^+(\varepsilon,t)\rangle = |\Psi_m^{\mathbf{X}_\tau +}(\varepsilon,t)\rangle - i\int_{-\infty}^{t} \mathrm{d}t'\, e^{i(\varepsilon-H_\tau)(t-t')}\, V_\tau^{(1)}(t')\, |\Psi_m^{\mathbf{X}_\tau +}(\varepsilon,t)\rangle\,, \tag{3.17}$$

$$|\Psi_m^-(\varepsilon,t)\rangle = |\Psi_m^{\mathbf{X}_\tau -}(\varepsilon,t)\rangle - i\int_{t}^{\infty} \mathrm{d}t'\, e^{i(\varepsilon-H_\tau)(t-t')}\, V_\tau^{(1)}(t')\, |\Psi_m^{\mathbf{X}_\tau -}(\varepsilon,t)\rangle\,. \tag{3.18}$$

With these considerations, the integration with respect to time can now be performed. Using of $t'\, e^{\eta t'} = \partial_\eta e^{\eta t'}$ we get

$$|\Psi_m^+(\varepsilon,t)\rangle = |\Psi_m^{\mathbf{X}_\tau +}(\varepsilon,t)\rangle + \frac{\partial}{\partial\eta}\left(\frac{e^{+\eta t}}{\varepsilon - H_\tau + i\eta}\right) \nabla_{X_\tau} V_\tau\, |\Psi_m^{\mathbf{X}_\tau +}(\varepsilon,t)\rangle \cdot \dot{\mathbf{X}}_\tau\,, \quad t\le 0 \tag{3.19}$$

$$|\Psi_m^-(\varepsilon,t)\rangle = |\Psi_m^{\mathbf{X}_\tau -}(\varepsilon,t)\rangle - \frac{\partial}{\partial\eta}\left(\frac{e^{-\eta t}}{\varepsilon - H_\tau - i\eta}\right) \nabla_{X_\tau} V_\tau\, |\Psi_m^{\mathbf{X}_\tau -}(\varepsilon,t)\rangle \cdot \dot{\mathbf{X}}_\tau\,, \quad t\ge 0\,. \tag{3.20}$$

We are interested in the solution at $t \to 0$, cf. chapter 2. Hence we can neglect the terms $e^{\pm\eta t}$ in the above expressions. With the notation introduced in Eq. (3.11) and extracting the dynamical phase as in Eq. (3.9), we conclude to first order in the adiabatic parameter

$$|\psi_m^{\pm}(\varepsilon,t)\rangle = |\psi_m^{\mathbf{X}_\tau\pm}(\varepsilon)\rangle - i\left(G_\tau^{R/A}(\varepsilon)\right)^2 \dot{V}_\tau\,|\psi_m^{\mathbf{X}_\tau\pm}(\varepsilon)\rangle + \dots \tag{3.21}$$

with $\dot{V}_\tau = \nabla_{X_\tau} V_\tau \cdot \dot{\mathbf{X}}_\tau$ and the frozen Green functions presented in Eq. (3.13) as well as by defining $|\psi_m^{\mathbf{X}_\tau\pm}(\varepsilon)\rangle = |\psi_m^{\mathbf{X}_\tau\pm}(\varepsilon, t\to 0)\rangle$. In Eq. (3.21) we have omitted the term $-\tau\, G_\tau^{R/A}(\varepsilon)\,\dot{V}_\tau\,|\psi_m^{\mathbf{X}_\tau\pm}(\varepsilon)\rangle$ as it is irrelevant in defining the scattering matrix and its first adiabatic correction, the A-matrix [see below, cf. Eq. (3.29)]. Hereafter we will replace $\tau \to t$ for notational reasons as τ is the only remaining time argument after performing the adiabatic expansion. Equation (3.21) is the main result of this section as it expresses the adiabatic correction terms of the full time-dependent scattering states completely in terms of the frozen scattering states. It thus enables an adiabatic expansion of the full time-dependent scattering matrix which is done next.

3.2.2. Scattering matrix and A-matrix

Our next goal is an adiabatic expansion of the *exact* scattering matrix of the time-dependent scattering problem which is defined as

$$\mathcal{S}_{nk}(\varepsilon',\varepsilon) = \langle \Psi_n^-(\varepsilon',t_0)|\Psi_k^+(\varepsilon,t_0)\rangle\,. \tag{3.22}$$

We note that the time t_0 in the above overlap can be freely chosen. With the aid of the Schrödinger equation, cf. Eq. (3.8), we readily show that the time derivative with respect to t_0 of the full scattering matrix vanishes. This enables us to later choose t_0 as the central time, which is defined as the time which gives rise to the conformation $\mathbf{X}_t$.

As a consequence of the normalisation condition for the scattering states, the exact scattering matrix is unitary, that is

$$\sum_n \int \frac{d\varepsilon}{2\pi} \mathcal{S}_{mn}(\varepsilon',\varepsilon)\mathcal{S}_{nk}(\varepsilon,\varepsilon'') = 2\pi\delta(\varepsilon'-\varepsilon'')\delta_{mk}\,. \tag{3.23}$$

In the adiabatic limit with frozen $\mathbf{X}_t$, the overlap in Eq. (3.22) reduces to the overlap of the frozen retarded and advanced scattering states. We call the scattering matrix in the adiabatic limit frozen scattering matrix and denote it with a subscript t, i.e.

$$S_t^{nk}(\varepsilon)\,2\pi\,\delta(\varepsilon-\varepsilon') = \langle \psi_n^{\mathbf{X}_t-}(\varepsilon')|\psi_k^{\mathbf{X}_t+}(\varepsilon)\rangle\,, \tag{3.24}$$

which is in accordance with the definition in Eq. (2.20). In order to get an expression of the first order correction term in the adiabatic expansion it is convenient to use the Wigner representation

$$\mathcal{S}(\varepsilon,t) = \int \frac{\mathrm{d}\tilde{\varepsilon}}{2\pi}\, \mathrm{e}^{-i\tilde{\varepsilon}t}\, \mathcal{S}\left(\varepsilon+\tilde{\varepsilon}/2, \varepsilon-\tilde{\varepsilon}/2\right) \tag{3.25}$$

of the full scattering matrix. We can then write the time-dependent scattering matrix for a slowly varying scattering potential $V(t)$ up to first order in the adiabatic expansion as

$$\mathcal{S}(\varepsilon,t) = S_t(\varepsilon) + A_t(\varepsilon) + \dots\,. \tag{3.26}$$

Here, the frozen scattering matrix $S_t(\varepsilon)$ represents the zeroth order and the matrix

$$A_t(\varepsilon) = \sum_{\alpha}^{N} A_t^{\alpha}(\varepsilon)\dot{X}_{\alpha} \tag{3.27}$$

gives the first order correction term and is thus proportional to the velocity $\dot{\mathbf{X}}_t$. We dub this matrix A-matrix hereafter. We note that all quantities appearing on the right-hand side of Eq. (3.26) depend parametrically on time via the classical degree of freedom $\mathbf{X}_t$. In the following we give an explicit expression for the A-matrix in terms of the frozen scattering states. As the derivation is a bit lengthy we first present the result,

$$A_t^{\alpha,nk}(\varepsilon) = \frac{1}{2}\left\langle \partial_\varepsilon \psi_n^{\mathbf{X}_t -}(\varepsilon)\right| \partial_\alpha V_t \left|\psi_k^{\mathbf{X}_t +}(\varepsilon)\right\rangle - \frac{1}{2}\left\langle \psi_n^{\mathbf{X}_t -}(\varepsilon)\right| \partial_\alpha V_t \left|\partial_\varepsilon \psi_k^{\mathbf{X}_t +}(\varepsilon)\right\rangle, \tag{3.28}$$

where we defined $\partial_\alpha = \partial/\partial X_\alpha$ and $|\partial_\varepsilon \psi_k^{\mathbf{X}_t +}(\varepsilon)\rangle = \partial_\varepsilon |\psi_k^{\mathbf{X}_t +}(\varepsilon)\rangle$. We note that expressions of the A-matrix in terms of Green functions have been obtained in the literature in Refs. [Bode et al., 2011, Bode et al., 2012b, Vavilov et al., 2001] or alternatively by a first-order expansion of the exact solution of the time-dependent system [Moskalets and Büttiker, 2004,Moskalets and Büttiker, 2005]. By Eq. (3.28), however, the A-matrix is now directly expressed in terms of the frozen scattering states and can thus be systematically – as the scattering matrix itself, cf. Eq. (2.20) – obtained from the solution of the stationary scattering problem. Equation (3.28) is of crucial importance for the derivation of the adiabatic reaction forces which is performed below.

Aiming at deriving Eq. (3.28) we make use of the adiabatic expansion of the Schrödinger equation for the scattering states in Eq. (3.21). This expansion enables an adiabatic expansion of the full scattering matrix defined in Eq. (3.22). We choose t_0 to be the central time t by relying on the previously shown independence of t_0. We then expand the Wigner transform in Eq. (3.25) to first order in the

adiabatic parameter using of Eq. (3.21) as

$$\begin{aligned}\mathcal{S}(\varepsilon,t) &= \int \frac{\mathrm{d}\tilde{\varepsilon}}{2\pi}\mathrm{e}^{-i\tilde{\varepsilon}t}\langle\Psi^-(\varepsilon+\frac{\tilde{\varepsilon}}{2},t)|\Psi^+(\varepsilon-\frac{\tilde{\varepsilon}}{2},t)\rangle \\ &= \int \frac{\mathrm{d}\tilde{\varepsilon}}{2\pi}\langle\psi^{\mathbf{X}_t-}(\varepsilon+\frac{\tilde{\varepsilon}}{2})\,|\psi^{\mathbf{X}_t+}(\varepsilon-\frac{\tilde{\varepsilon}}{2})\rangle \\ &- i\int \frac{\mathrm{d}\tilde{\varepsilon}}{2\pi}\langle\psi^{\mathbf{X}_t-}(\varepsilon+\frac{\tilde{\varepsilon}}{2})\,|[G_t^R(\varepsilon-\frac{\tilde{\varepsilon}}{2})]^2\dot{V}_t\,|\psi^{\mathbf{X}_t+}(\varepsilon-\frac{\tilde{\varepsilon}}{2})\rangle \\ &+ i\int \frac{\mathrm{d}\tilde{\varepsilon}}{2\pi}\,\langle\psi^{\mathbf{X}_t-}(\varepsilon+\frac{\tilde{\varepsilon}}{2})\,|\dot{V}_t[G_t^R(\varepsilon+\frac{\tilde{\varepsilon}}{2})]^2\,|\psi^{\mathbf{X}_t+}(\varepsilon-\frac{\tilde{\varepsilon}}{2})\rangle \\ &+\ldots\end{aligned} \tag{3.29}$$

Applying the Green functions onto the scattering states gives $G_t^R(\varepsilon\pm\tilde{\varepsilon}/2)|\psi^{\mathbf{X}_t+}(\varepsilon_\mp)\rangle = (\pm\tilde{\varepsilon}+i\eta)^{-1}|\psi^{\mathbf{X}_t+}(\varepsilon_\mp)\rangle$. Then by using the identity $[(\tilde{\varepsilon}+i\eta)^{-2}-(-\tilde{\varepsilon}+i\eta)^{-2}] = 2\pi i\,\partial_{\tilde{\varepsilon}}\delta(\tilde{\varepsilon})$ we find

$$\mathcal{S}(\varepsilon,t) = S_t(\varepsilon) - \int \mathrm{d}\tilde{\varepsilon}\,[\partial_{\tilde{\varepsilon}}\delta(\tilde{\varepsilon})]\,\langle\psi^{\mathbf{X}_t-}(\varepsilon+\frac{\tilde{\varepsilon}}{2})\,|\dot{V}_t\,|\psi^{\mathbf{X}_t+}(\varepsilon-\frac{\tilde{\varepsilon}}{2})\rangle+\ldots \tag{3.30}$$

An integration by parts finally yields

$$\mathcal{S}(\varepsilon,t) = S_t(\varepsilon) + \frac{1}{2}\langle\partial_\varepsilon\psi^{\mathbf{X}_t-}(\varepsilon)\;|\dot{V}_t\,|\psi^{\mathbf{X}_t+}(\varepsilon)\rangle - \frac{1}{2}\langle\psi^{\mathbf{X}_t-}(\varepsilon)\;|\dot{V}_t\,|\partial_\varepsilon\psi^{\mathbf{X}_t+}(\varepsilon)\rangle+\ldots \tag{3.31}$$

which is the desired expression for the A-matrix in Eq. (3.28).

3.2.3. Some useful identities

In the remainder of this section we briefly derive some identities for the frozen scattering states, the frozen scattering matrix and the A-matrix, respectively, which will be useful in the derivation of the adiabatic reaction forces. We begin with the fact that we can evaluate the time derivative of the frozen scattering state explicitly by taking the time derivative of the Lippmann-Schwinger equation (3.12). With the aid of the relation $\partial_t G_t^{R/A} = G_t^{R/A}\,\partial_t V_t\,G_t^{R/A}$ we deduce that [Entin-Wohlman et al., 2002]

$$\partial_t|\psi^{\mathbf{X}_t\pm}(\varepsilon)\rangle = G_t^{R/A}(\varepsilon)\dot{V}_t\,|\psi^{\mathbf{X}_t\pm}(\varepsilon)\rangle\,. \tag{3.32}$$

Next we make use of the fact the frozen S-matrix is related to the frozen T-matrix via Eqs. (2.26) and (2.28). Taking the time derivative of Eq. (2.26) with the aid of Eq. (3.32) and the Lippmann-Schwinger equation (3.12) we then conclude

$$\partial_t S_t^{nk}(\varepsilon) = -i\,\langle\psi_n^{\mathbf{X}_t-}(\varepsilon)|\,\dot{V}_t\,|\psi_k^{\mathbf{X}_t+}(\varepsilon)\rangle\,. \tag{3.33}$$

We can use this identity to show that

$$\partial_\varepsilon \langle \psi^{\mathbf{X}_t -}(\varepsilon) \,|\, \dot{V}_t \,|\psi^{\mathbf{X}_t +}(\varepsilon)\rangle = i \partial_\varepsilon \partial_t S_t(\varepsilon)\,. \tag{3.34}$$

This gives the alternative expression for the A-matrix

$$A_t(\varepsilon) = -\langle \psi^{\mathbf{X}_t -}(\varepsilon) \,|\, \dot{V}_t \,|\partial_\varepsilon \psi^{\mathbf{X}_t +}(\varepsilon)\rangle + \frac{i}{2}\partial_\varepsilon \partial_t S_t(\varepsilon) \tag{3.35}$$

compared to the expression given in Eq. (3.28). Finally, we present a relation between the frozen scattering matrix and the A-matrix [Moskalets and Büttiker, 2004, Moskalets and Büttiker, 2005, Bode et al., 2011, Bode et al., 2012b], which is a consequence of the unitarity of the full scattering matrix. From Eq. (3.35) we get

$$\begin{aligned}
&S_t^\dagger(\varepsilon)\, A_t(\varepsilon) + A_t^\dagger(\varepsilon)\, S_t(\varepsilon) \\
&= -\partial_\varepsilon \langle \psi^{\mathbf{X}_t +}(\varepsilon)|\, \dot{V}_t \,|\psi^{\mathbf{X}_t +}(\varepsilon)\rangle + \frac{i}{2}\left[S_t^\dagger(\varepsilon)\, \partial_\varepsilon \partial_t S_t(\varepsilon) - \partial_\varepsilon \partial_t S_t^\dagger(\varepsilon)\, S_t(\varepsilon)\right] \\
&= -\frac{i}{2}\partial_\varepsilon \left[S_t^\dagger(\varepsilon)\, \partial_t S_t(\varepsilon) - \partial_t S_t^\dagger(\varepsilon)\, S_t(\varepsilon)\right] + \frac{i}{2}\left[S_t^\dagger(\varepsilon)\, \partial_\varepsilon \partial_t S_t(\varepsilon) - \partial_\varepsilon \partial_t S_t^\dagger(\varepsilon)\, S_t(\varepsilon)\right] \\
&= \frac{i}{2}\left[\partial_t S_t^\dagger(\varepsilon)\, \partial_\varepsilon S_t(\varepsilon) - \partial_\varepsilon S_t^\dagger(\varepsilon)\, \partial_t S_t(\varepsilon)\right]\,.
\end{aligned} \tag{3.36}$$

With these equations we are now ready to address the derivation of the adiabatic reaction forces purely within the framework of scattering theory.

3.3. Derivation of the adiabatic reaction forces

In this section, we derive the adiabatic reaction forces with the aid of the above formulas for the adiabatic expansion of the scattering states. We consider slowly varying degrees of freedom $\mathbf{X}_t$ and calculate the reaction forces to linear order in the adiabatic parameter. Important is our assumption of a non-interacting quantum environment, which enables a treatment within the Landauer-Büttiker approach and hence scattering theory. To this end, we introduce the creation and annihilation operators $a_n^\dagger(\varepsilon, t)$ and $a_n(\varepsilon, t)$ which create and annihilate, respectively, the time-dependent retarded scattering states $|\Psi_n^+(\varepsilon, t)\rangle$. The scattering states form a complete set of basis states since time evolution is unitary. In the following, we work in the Schrödinger picture so that the creation and annihilation operators have the time argument t appearing as a label to clarify which states are created or

annihilated. With these operators we can express the non-interacting many-body Hamiltonian $\mathcal{H}_t$ as

$$\mathcal{H}_t = \int \frac{\mathrm{d}\varepsilon}{2\pi} \int \frac{\mathrm{d}\varepsilon'}{2\pi} \sum_{mk} [H_t]_{mk}\, a_m^\dagger(\varepsilon, t) a_k(\varepsilon', t) \tag{3.37}$$

in terms of the single-particle Hamiltonian $H_t = H_0 + V_t$. In the Schrödinger picture, the operator of the total force, which is exerted by the out-of-equilibrium quantum environment on the classical parameter $\mathbf{X}_t$, is defined as

$$\hat{\mathcal{F}}_{\mathbf{X}} = -\nabla \mathcal{H} \tag{3.38}$$

where $\nabla(\ldots) = \partial_{\mathbf{X}_t}(\ldots)$ is taken with respect to the classical degrees of freedom. For any given trajectory $\mathbf{X}_t$ we can then determine the average force on the classical system by tracing out the quantum environment, that is

$$\mathcal{F}(t) = \mathcal{F}[\mathbf{X}_t] = \langle \hat{\mathcal{F}}_{\mathbf{X}_t} \rangle \,. \tag{3.39}$$

Here we have used the notation $\langle \ldots \rangle = \mathrm{Tr}\{\rho(t) \ldots\}$ which indicates the quantum-statistical average for a given $\mathbf{X}_t$ with $\rho(t)$ being the many-body density matrix of the quantum system evaluated at time t. We note that the average force given by Eq. (3.39) is a *functional* of the trajectory of the classical parameter. Its time dependence is thus expressed via $\mathbf{X}_t$ and its time derivatives $\dot{\mathbf{X}}_t$, $\ddot{\mathbf{X}}_t$, $\dot{\mathbf{X}}_t^2 \ldots$ As we assume a slow varying $\mathbf{X}_t$ we in fact expand in powers of derivatives of the classical degree of freedom and keep only linear order terms, i.e terms proportional to the velocity $\dot{\mathbf{X}}_t$.

By taking the quantum-statistical average in Eq. (3.39), the force $\mathcal{F}(t)$ contains only the average forces, which appear on the right-hand side of the Langevin equation (3.1). The Langevin equation also includes fluctuating forces $\boldsymbol{\xi}(t)$, which describe both Johnson-Nyquist noise and shot noise [Blanter and Büttiker, 2000, Nazarov and Blanter, 2010]. These fluctuating forces will be treated later. At this point, we stress that the force $\mathcal{F}(t)$ is an expectation value evaluated for a given $\mathbf{X}_t$. By this, no memory effects of the quantum environment are included and the Langevin equation (3.1) is given in the Markovian limit. In fact, the Langevin equation (3.1) implicitly contains a classical averaging over timescales, which are short compared to the timescale of the dynamics of the classical system and long compared to the timescale of the quantum environment. Within an out-of-equilibrium Born-Oppenheimer approximation [Bode et al., 2011, Bode et al., 2012b] the force is then represented by the above (average) quantum expectation value for a given $\mathbf{X}_t$.

We continue with the evaluation of the average force $\mathcal{F}(t)$. We readily observe that the expectation value $\langle a_m^\dagger(\varepsilon, t) a_k(\varepsilon', t) \rangle$ is independent of the time t. This

can be seen by realising that the density matrix $\rho(t)$ as well as the scattering states $|\psi_n^+(\varepsilon,t)\rangle$ evolved from the unperturbed states by a unitary time evolution. Following the Landauer-Büttiker theory of mesoscopic conductors we can then write

$$\left\langle a_m^\dagger(\varepsilon,t)a_k(\varepsilon',t)\right\rangle = f_k(\varepsilon)\delta_{km}2\pi\delta(\varepsilon-\varepsilon')\,, \tag{3.40}$$

where $f_k(\varepsilon)$ gives the distribution function of lead and channel m at energy ε. For an electronic quantum environment $f_k(\varepsilon)$ is the Fermi-distribution function, while for a bosonic environment $f_k(\varepsilon)$ represents the Bose-Einstein distribution. Similar to Eq. (3.37) the force operator is a one-particle operator which can be written as

$$\nabla\mathcal{H}_t = \int\frac{\mathrm{d}\varepsilon}{2\pi}\int\frac{\mathrm{d}\varepsilon'}{2\pi}\sum_{mk}\left[\nabla H_t\right]_{mk} a_m^\dagger(\varepsilon,t)a_k(\varepsilon',t)\,. \tag{3.41}$$

Taking the quantum-statistical average then results in the following expression for the average force

$$\mathcal{F} = -\int\frac{\mathrm{d}\varepsilon}{2\pi}\sum_k f_k(\varepsilon)\,\langle\psi_k^+(\varepsilon,t)|\,\nabla H_t\,|\psi_k^+(\varepsilon,t)\rangle\,. \tag{3.42}$$

We are now ready to determine the adiabatic reaction forces which appear in the Langevin equation since Eq. (3.42) expresses the average force in terms the full *time-dependent* scattering states. With the aid of the adiabatic expansion of these states as shown in Eq. (3.21) we can express the average force to linear order in the adiabatic parameter as

$$\begin{aligned}
\mathcal{F}[\mathbf{X}_t] = &-\int\frac{\mathrm{d}\varepsilon}{2\pi}\sum_k f_k(\varepsilon)\,\langle\psi_k^{\mathbf{X}_t+}(\varepsilon)|\,\nabla V_t\,|\psi_k^{\mathbf{X}_t+}(\varepsilon)\rangle\\
&-i\int\frac{\mathrm{d}\varepsilon}{2\pi}\sum_k f_k(\varepsilon)\,\langle\psi_k^{\mathbf{X}_t+}(\varepsilon)|\,\partial_t V_t\left(G_t^A\right)^2\,\nabla V_t\,|\psi_k^{\mathbf{X}_t+}(\varepsilon)\rangle\\
&+i\int\frac{\mathrm{d}\varepsilon}{2\pi}\sum_k f_k(\varepsilon)\,\langle\psi_k^{\mathbf{X}_t+}(\varepsilon)|\,\nabla V_t\,\left(G_t^R\right)^2\,\partial_t V_t\,|\psi_k^{\mathbf{X}_t+}(\varepsilon)\rangle\\
&+\ldots
\end{aligned} \tag{3.43}$$

Here we have made use of the fact that the Hamiltonian depends on the classical degree of freedom via the scattering potential so that $\nabla H_t = \nabla V_t$. From Eq. (3.43) we can read off the reaction forces. The Born-Oppenheimer force corresponds to the first line of the right-hand side of Eq. (3.43) as it depends on the instantaneous position $\mathbf{X}_t$ of the classical parameter. The first-order correction term which is proportional to $\dot{\mathbf{X}}_t$, that is the second and the third line of Eq. (3.43), give rise to the friction force and the Lorentz-like force. Both terms are combined as $-\boldsymbol{\gamma}\cdot\dot{\mathbf{X}}_t$ in the Langevin equation (3.1). We give expressions of the reaction forces in terms of the scattering matrix and the A-matrix in Secs. 3.3.1 and 3.3.2.

Next we address the stochastic force. To this end, we change from the Schrödinger picture to the Heisenberg picture, hence we deal with time-dependent operators so that $\hat{\mathcal{F}}_{\mathbf{X}}(t)$ depends explicitly on time. At the quantum-mechanical level we then define the fluctuations of the force via the Heisenberg stochastic force operator as

$$\hat{\xi}(t) \equiv \hat{\mathcal{F}}_{\mathbf{X}_t}(t) - \mathcal{F}(t). \tag{3.44}$$

The origin of the fluctuating nature of the force is twofold. On the one hand, fluctuations are a consequence of finite temperature effects, on the other hand scattering of quantum particles is a probabilistic process which results in non-equilibrium noise. We are interested in the noise correlator

$$D_{\alpha\beta}(t,t') = \left\{ \langle \hat{\xi}_\alpha(t) \hat{\xi}_\beta(t') \rangle \right\}_s , \tag{3.45}$$

which is symmetric with respect to the classical components α and β. The symmetrisation with respect to the components is indicated by the brackets $\{\ldots\}_s$. As we assume that $\mathbf{X}_t$ varies slowly compared to the characteristic timescales of the quantum system, we assume $D_{\alpha\beta}(t,t')$ to be local in time on scales which appear in the Langevin equation, i.e.

$$D_{\alpha\beta}(t,t') \simeq D_{\alpha\beta}(t)\delta(t-t') . \tag{3.46}$$

In order to take the fluctuations into account and to have the fluctuation-dissipation theorem satisfied, the stochastic force $\boldsymbol{\xi}(t)$ is included in the later description of the adiabatic reaction forces. The fluctuating force enters in the Langevin equation (3.1) with $\overline{\xi_\alpha(t)\xi_\beta(t')} = D_{\alpha\beta}(t)\delta(t-t')$. Here, the overline represents the classical averaging which is implicitly assumed in the Langevin equation. Aiming at evaluating the correlator $D_{\alpha\beta}(t)$, we perform a time average over the fast timescale, that is the relative time $\tau = t - t'$ in Eq. (3.45),

$$D_{\alpha\beta}\left(\mathbf{X}_t\right) = \int \mathrm{d}\tau D_{\alpha\beta}\left(t + \frac{\tau}{2}, t - \frac{\tau}{2}\right) . \tag{3.47}$$

We note that the fluctuation-dissipation theorem is already fulfilled in the limit of a frozen classical parameter $\mathbf{X}_t$ [Bode et al., 2011, Bode et al., 2012b]. Hence we evaluate Eq. (3.47) in the fully adiabatic limit and consider the zeroth order with a static Hamiltonian which depends on time via the classical degree of freedom $\mathbf{X}_\tau$. We can thus use the frozen retarded scattering states as they represent a complete basis. To this end, we introduce the creation and annihilation operators of the frozen retarded scattering states, $a_m^{\mathbf{X}_t\dagger}(\varepsilon)$ and $a_m^{\mathbf{X}_t}(\varepsilon)$, which create and annihilate the states $|\Psi_m^{\mathbf{X}_t}(\varepsilon)\rangle$ at time t which are eigenstates of the Hamiltonian H_t. This allows us to write

$$\hat{\mathcal{F}}_{\mathbf{X}_t} = -\int \frac{\mathrm{d}\varepsilon}{2\pi} \int \frac{\mathrm{d}\varepsilon'}{2\pi} \sum_{km} a_m^{\mathbf{X}_t\dagger}(\varepsilon) \, \left[\partial_\alpha H_t\right]_{mk} \, a_k^{\mathbf{X}_t}(\varepsilon') \tag{3.48}$$

for the force operator in the Schrödinger picture. The superscript, $\mathbf{X}_t$, of the creation and annihilation operators stresses the adiabatic limit. A transformation to the Schrödinger picture is readily done to zeroth order in the adiabatic parameter by substituting $a_k^{\mathbf{X}_t}(\varepsilon) \to a_k^{\mathbf{X}_t}(\varepsilon, t+\tau) = \mathrm{e}^{-i\,\varepsilon\,\tau} a_k^{\mathbf{X}_t}(\varepsilon)$ in the above expression where we set the reference time to change between the different representation pictures as t. For an evaluation of the noise correlator we then make use of the relation [Büttiker, 1992]

$$\begin{aligned}&\langle a_m^{\mathbf{X}_t\dagger}(\varepsilon_1) a_n^{\mathbf{X}_t}(\varepsilon_2) a_k^{\mathbf{X}_t\dagger}(\varepsilon_3) a_l^{\mathbf{X}_t}(\varepsilon_4)\rangle - \langle a_m^{\mathbf{X}_t\dagger}(\varepsilon_1) a_n^{\mathbf{X}_t}(\varepsilon_2)\rangle \langle a_k^{\mathbf{X}_t\dagger}(\varepsilon_3) a_l^{\mathbf{X}_t}(\varepsilon_4)\rangle \\ &\quad = (2\pi)^2 f_m(\varepsilon_1)\left[1 \mp f_k(\varepsilon_2)\right] \delta_{ml}\,\delta_{nk}\,\delta(\varepsilon_1-\varepsilon_4)\,\delta(\varepsilon_2-\varepsilon_3)\,.\end{aligned} \tag{3.49}$$

At this point we emphasise that this expression is valid for both a fermionic $(-)$ as well as a bosonic $(+)$ quantum environment. Making use of Eq. (3.49) we can express the averaged noise correlator in Eq. (3.47) as

$$\begin{aligned}D_{\alpha\beta}\left(\mathbf{X}_t\right) = \int \frac{\mathrm{d}\varepsilon}{2\pi} f_m(\varepsilon)\,\left[1 \mp f_k(\varepsilon)\right]\,\Big\{&\big\langle \psi_m^{\mathbf{X}_t+}(\varepsilon)\big|\partial_\alpha H_t\big|\psi_k^{\mathbf{X}_t+}(\varepsilon)\big\rangle \\ &\times \big\langle \psi_k^{\mathbf{X}_t+}(\varepsilon)\big|\partial_\beta H_t\big|\psi_m^{\mathbf{X}_t+}(\varepsilon)\big\rangle\Big\}_s\,.\end{aligned} \tag{3.50}$$

Below we now use the above derived expressions in Eqs. (3.43) and (3.50) for the adiabatic reaction forces, that is the Born-Oppenheimer force, the friction force, the Lorentz-like force and the noise correlator of the stochastic force, to express these forces in terms of the frozen scattering matrix and its first adiabatic correction, the A-matrix.

3.3.1. Born-Oppenheimer force

We read off the expression of the mean force (Born-Oppenheimer force) from the first line of Eq. (3.43) corresponding to the term which depends on the instantaneous $\mathbf{X}_t$ and is independent of the velocity of the classical particle. We find

$$F_\alpha = -\int \frac{\mathrm{d}\varepsilon}{2\pi} \sum_n f_n(\varepsilon)\,\langle \psi_n^{\mathbf{X}_t+}(\varepsilon)|\,\partial_\alpha V_t\,|\psi_n^{\mathbf{X}_t+}(\varepsilon)\rangle\,. \tag{3.51}$$

We can bring this expression into a form which contains the scattering matrix. By inserting a complete set $\mathbb{1} = \int \frac{\mathrm{d}\varepsilon}{2\pi} \sum_k |\psi_k^{\mathbf{X}_t-}(\varepsilon)\rangle\langle\psi_k^{\mathbf{X}_t-}(\varepsilon)|$ of advanced scattering states, cf. Eq. (2.16), we get

$$F_\alpha = -\int \frac{\mathrm{d}\varepsilon}{2\pi} \int \frac{\mathrm{d}\varepsilon'}{2\pi} \sum_{nm} f_n(\varepsilon)\,\langle \psi_n^{\mathbf{X}_t+}(\varepsilon)|\psi_m^{\mathbf{X}_t-}(\varepsilon')\rangle\,\langle \psi_m^{\mathbf{X}_t-}(\varepsilon')|\,\partial_\alpha V_t\,|\psi_n^{\mathbf{X}_t+}(\varepsilon)\rangle\,. \tag{3.52}$$

We identify the scattering matrix by comparing to Eq. (3.24). Moreover, we identify the derivative of the scattering matrix with respect to the classical degree of freedom. Indeed, due to the parametric time-dependence of the frozen S-matrix via the classical parameter we deduce that

$$\partial_\alpha S_{nk}(\varepsilon) = -i \left\langle \psi_n^{\mathbf{X}_t -}(\varepsilon) \right| \partial_\alpha V \left| \psi_k^{\mathbf{X}_t +}(\varepsilon) \right\rangle \tag{3.53}$$

by referring to Eq. (3.33). Altogether we conclude that

$$F_\alpha = \int \frac{\mathrm{d}\varepsilon}{2\pi i} \sum_{nm} f_n(\varepsilon) S_t^{mn\dagger}(\varepsilon) \partial_\alpha S_t^{mn}(\varepsilon) \,. \tag{3.54}$$

We can equivalently write this in matrix notation, which gives the result

$$F_\alpha(\mathbf{X}_t) = \int \frac{\mathrm{d}\varepsilon}{2\pi i} \sum_{n} f_n(\varepsilon) \mathrm{tr} \left\{ \Pi_n S_t^\dagger(\varepsilon) \partial_\alpha S_t(\varepsilon) \right\} \,, \tag{3.55}$$

where Π_n is a projector onto lead n and the lower-case trace, $\mathrm{tr}\{\ldots\}$, is over the channel space. We note that Eq. (3.55) agrees with the expression for the mean force obtained in Ref. [Bode et al., 2011] where the adiabatic reaction forces on a nanoelectromechanical system are studied by using the non-equilibrium Keldysh Green function approach.

We conclude this section by illustrating that the expression for the Born-Oppenheimer force obtained here is closely related to the Friedel sum rule [Friedel, 1952]. We begin by observing that for a discrete energy spectrum with energy levels $E_t^i = E^i(\mathbf{X}_t)$ we can express the equilibrium Born-Oppenheimer force as, cf. Eq. (3.51) as well as Ref. [Berry and Robbins, 1993],

$$F_\alpha(\mathbf{X}_t) = -\sum_i f\left(E_t^i\right) \partial_\alpha E_t^i \,. \tag{3.56}$$

We note that equilibrium means that all leads posses the same chemical potential $\mu_k = \mu$ and hence the index on the distribution function $f_n(\varepsilon)$ can be dropped. Next, we take the infinite volume limit which can be taken by replacing $E_t^i \to \int \mathrm{d}\varepsilon \, \varepsilon \, \delta(\varepsilon - E_t^i)$ in Eq. (3.56) and expressing the number of states up to energy ε by $N(\varepsilon, \mathbf{X}_t) = \int_{-\infty}^{\varepsilon} \mathrm{d}\varepsilon' \nu(\varepsilon', \mathbf{X}_t)$. Here, we have introduced the density of states ν and have made use of the relation $\partial_\alpha \Theta\left(\varepsilon - E_t^i\right) = -\delta\left(\varepsilon - E_t^i\right) \partial_\alpha E_t^i$. In the infinite volume limit the mean force can then be written as

$$F_\alpha(\mathbf{X}_t) = \int \mathrm{d}\varepsilon \, f(\varepsilon) \partial_\alpha N(\varepsilon, \mathbf{X}_t) \,. \tag{3.57}$$

The spatial derivative of the number of states is called emissivity [Büttiker et al., 1994] which is a known quantity in the context of adiabatic quantum pumping [Brouwer, 1998]. The Friedel sum rule [Friedel, 1952] relates $N(\varepsilon, \mathbf{X}_t)$ to the

frozen scattering matrix [Langer and Ambegaokar, 1961]

$$N(\varepsilon, \mathbf{X}_t) = \frac{1}{2\pi i} \mathrm{tr} \left\{ \ln S_t(\varepsilon) \right\} , \tag{3.58}$$

so that its spatial derivative reads

$$\partial_\alpha N(\varepsilon, \mathbf{X}_t) = \frac{1}{2\pi i} \mathrm{tr} \left\{ S_t^\dagger(\varepsilon) \partial_\alpha S_t(\varepsilon) \right\} . \tag{3.59}$$

This readily reproduces the expression of the Born-Oppenheimer force obtained in Eq. (3.55) in terms of the S-matrix in equilibrium.

3.3.2. Friction and Lorentz-like force

Both the friction tensor and the geometric Lorentz-like force, which are contained in the tensor $\boldsymbol{\gamma}$, are given by the second and third line of the right-hand side of Eq. (3.43). They constitute the adiabatic correction to the mean force. Since $\partial_t(\ldots) = \sum_\alpha \partial_\alpha(\ldots)\, \dot{X}_\alpha$, we read off

$$\begin{aligned} \gamma_{\alpha\beta} = i \int \frac{\mathrm{d}\varepsilon}{2\pi} \sum_k f_k(\varepsilon) \, \langle \psi_k^{\mathbf{X}_t +}(\varepsilon)| \left[\partial_\beta V_t \left(G_t^A(\varepsilon) \right)^2 \partial_\alpha V_t - \partial_\alpha V_t \left(G_t^R(\varepsilon) \right)^2 \partial_\beta V_t \right] \\ \times |\psi_k^{\mathbf{X}_t +}(\varepsilon)\rangle \, . \end{aligned} \tag{3.60}$$

We begin with the symmetric part of the tensor $\boldsymbol{\gamma}$, that is $\gamma^s_{\alpha\beta} = 1/2 \, (\gamma_{\alpha\beta} + \gamma_{\beta\alpha})$, which has the meaning of a friction tensor in the Langevin equation of the classical degree of freedom. By definition, we have

$$\begin{aligned} \gamma^s_{\alpha\beta} = i \int \frac{\mathrm{d}\varepsilon}{2\pi} \sum_k f_k(\varepsilon) \left\{ \langle \psi_k^{\mathbf{X}_t +}(\varepsilon)| \left[\partial_\beta V_t \left(G_t^A(\varepsilon) \right)^2 \partial_\alpha V_t - \partial_\alpha V_t \left(G_t^R(\varepsilon) \right)^2 \partial_\beta V_t \right] \right. \\ \left. \times |\psi_k^{\mathbf{X}_t +}(\varepsilon)\rangle \right\}_s \end{aligned} \tag{3.61}$$

from Eq. (3.60). Symmetrically exchanging the indices α and β as well as using the relation $\left(G_t^A\right)^2 - \left(G_t^R\right)^2 = -\partial_\varepsilon (G_t^A - G_t^R) = -2\pi i \partial_\varepsilon \delta(\varepsilon - H_t)$, we can rewrite Eq. (3.61) after performing an integration by parts as

$$\begin{aligned} \gamma^s_{\alpha\beta} = & \int \mathrm{d}\varepsilon \left[-\partial_\varepsilon f_k(\varepsilon) \right] \, \langle \psi_k^{\mathbf{X}_t +}(\varepsilon)| \, \partial_\alpha V_t \, \delta(\varepsilon - H_t) \, \partial_\beta V_t \, |\psi_k^{\mathbf{X}_t +}(\varepsilon)\rangle_s \\ & - \int \mathrm{d}\varepsilon f_k(\varepsilon) \langle \partial_\varepsilon \psi_k^{\mathbf{X}_t +}(\varepsilon)| \, \partial_\alpha V_t \, \delta(\varepsilon - H_t) \, \partial_\beta V_t \, |\psi_k^{\mathbf{X}_t +}(\varepsilon)\rangle_s \\ & - \int \mathrm{d}\varepsilon f_k(\varepsilon) \, \langle \psi_k^{\mathbf{X}_t +}(\varepsilon)| \, \partial_\alpha V_t \, \delta(\varepsilon - H_t) \, \partial_\beta V_t \, |\partial_\varepsilon \psi_k^{\mathbf{X}_t +}(\varepsilon)\rangle_s \, . \end{aligned} \tag{3.62}$$

We insert a complete set of advanced scattering states between the partial derivative of the scattering potential and the delta distribution in each of the three terms on the right-hand side. This yields

$$\begin{aligned}\gamma^s_{\alpha\beta} = &-\int \frac{\mathrm{d}\varepsilon}{2\pi}\partial_\varepsilon f_k(\varepsilon)\left\{\langle\psi_k^{\mathbf{X}_t+}(\varepsilon)|\,\partial_\alpha V_t\,|\psi_l^{\mathbf{X}_t-}(\varepsilon)\rangle\langle\psi_l^{\mathbf{X}_t-}(\varepsilon)|\,\partial_\beta V_t\,|\psi_k^{\mathbf{X}_t+}(\varepsilon)\rangle\right\}_s \\ &-\int \frac{\mathrm{d}\varepsilon}{2\pi} f_k(\varepsilon)\left\{\langle\partial_\varepsilon\psi_k^{\mathbf{X}_t+}(\varepsilon)|\,\partial_\alpha V_t\,|\psi_l^{\mathbf{X}_t-}(\varepsilon)\rangle\langle\psi_l^{\mathbf{X}_t-}(\varepsilon)|\,\partial_\beta V_t\,|\psi_k^{\mathbf{X}_t+}(\varepsilon)\rangle\right\}_s \\ &-\int \frac{\mathrm{d}\varepsilon}{2\pi} f_k(\varepsilon)\left\{\langle\psi_k^{\mathbf{X}_t+}(\varepsilon)|\,\partial_\alpha V_t\,|\psi_l^{\mathbf{X}_t-}(\varepsilon)\rangle\langle\psi_l^{\mathbf{X}_t-}(\varepsilon)|\,\partial_\beta V_t\,|\partial_\varepsilon\psi_k^{\mathbf{X}_t+}(\varepsilon)\rangle\right\}_s .\end{aligned} \tag{3.63}$$

We readily identify both the S-matrix, cf. Eq. (3.24) and Eq. (3.53), and the A-matrix, cf. Eq. (3.28) and Eq. (3.35), respectively, appearing in the above expression. This leads to the result

$$\begin{aligned}\gamma^s_{\alpha\beta}(\mathbf{X}_t) = &\int \frac{\mathrm{d}\varepsilon}{4\pi}\sum_n[-\partial_\varepsilon f_n(\varepsilon)]\mathrm{tr}\left\{\Pi_n\partial_\alpha S_t^\dagger(\varepsilon)\partial_\beta S_t(\varepsilon)\right\}_s \\ &+\int \frac{\mathrm{d}\varepsilon}{2\pi i}\sum_n f_n(\varepsilon)\mathrm{tr}\left\{\Pi_n\left[\partial_\alpha S_t^\dagger(\varepsilon)A_t^\beta(\varepsilon) - A_t^{\beta\dagger}(\varepsilon)\partial_\alpha S_t(\varepsilon)\right]\right\}_s .\end{aligned} \tag{3.64}$$

This expression coincides with the one obtained in Ref. [Bode et al., 2011]. The approach presented here enables a direct comparison to the calculation in Ref. [Berry and Robbins, 1993] where the friction tensor vanishes for a closed quantum system. With the above calculation we conclude that for an infinite quantum system with a continuous energy spectrum the classical degree of freedom indeed experiences a friction force proportional to the velocity.

We now turn to the geometric Lorentz-like force. We indicate antisymmetrisation with respect to the spatial indices α and β by the brackets $\{\ldots\}_a$. Then the antisymmetric part $\gamma^a_{\alpha\beta} = 1/2\,(\gamma_{\alpha\beta} - \gamma_{\beta\alpha})$ reads

$$\begin{aligned}\gamma^a_{\alpha\beta} = i\int \frac{\mathrm{d}\varepsilon}{2\pi}\sum_k f_k(\varepsilon)\,&\left\{\langle\psi_k^{\mathbf{X}_t+}(\varepsilon)|\left[\partial_\beta V_t\left(G_t^A(\varepsilon)\right)^2\partial_\alpha V_t - \partial_\alpha V_t\left(G_t^R(\varepsilon)\right)^2\partial_\beta V_t\right]\right. \\ &\left.\times|\psi_k^{\mathbf{X}_t+}(\varepsilon)\rangle\right\}_a ,\end{aligned} \tag{3.65}$$

which follows from the expression in Eq. (3.60). We can identify the A-matrix appearing in this expression by referring to Eq. (3.35). Making use of $[G_t^R(\varepsilon)]^2 = -\partial_\varepsilon G_t^R(\varepsilon)$ we show that

$$\left\{\partial_\alpha A_t^\beta(\varepsilon)\right\}_a = \left\{\langle\psi^{\mathbf{X}_t-}(\varepsilon)|\,\partial_\beta V_t\left(G_t^R(\varepsilon)\right)^2\partial_\alpha V_t\,|\psi^{\mathbf{X}_t+}(\varepsilon)\rangle\right\}_a , \tag{3.66}$$

and analogously for an expression in terms of the advanced Green function. We conclude for the antisymmetric part of the tensor $\boldsymbol{\gamma}$ that

$$\gamma^a_{\alpha\beta}(\mathbf{X}_t) = \int \frac{\mathrm{d}\varepsilon}{2\pi i} \sum_n f_n(\varepsilon)\, \mathrm{tr}\left\{\Pi_n \left[S_t^\dagger(\varepsilon)\partial_\beta A_t^\alpha(\varepsilon) - \partial_\beta A_t^{\alpha\dagger}(\varepsilon) S_t(\varepsilon)\right]\right\}_a \tag{3.67}$$

by performing similar steps as above.

The above obtained expression of the antisymmetric tensor $\gamma^a_{\alpha\beta}$ coincides with the expression in Ref. [Bode et al., 2011]. We remark that as opposed to Ref. [Lü et al., 2010], the Lorentz-like force does not diverge in all of the above expressions, as we necessarily deal with a finite dwell time.

3.3.3. Fluctuating force

We continue with the noise correlator of the stochastic force in Eq. (3.50). Inserting twice a complete set of advanced scattering states and comparing to Eqs. (3.24) and (3.53) we conclude

$$D_{\alpha\beta} = \int \frac{\mathrm{d}\varepsilon}{2\pi} f_n(\varepsilon)\, [1 \mp f_m(\varepsilon)] \left\{\partial_\alpha S_t^{nk\dagger}(\varepsilon)\, S_t^{km}(\varepsilon)\, S_t^{ml\dagger}(\varepsilon)\, \partial_\beta S_t^{ln}(\varepsilon)\right\}_s . \tag{3.68}$$

Similar to the friction tensor and the Lorentz-like force, we write this in matrix notation as

$$D_{\alpha\beta}(\mathbf{X}_t) = \sum_{nm} \int \frac{\mathrm{d}\varepsilon}{2\pi}\, f_n(\varepsilon)\, [1 \mp f_m(\varepsilon)]\, \mathrm{tr}\left\{\Pi_n \left[S_t^\dagger(\varepsilon)\, \partial_\alpha S_t(\varepsilon)\right]^\dagger \Pi_m\, S_t^\dagger(\varepsilon)\, \partial_\beta S_t(\varepsilon)\right\}_s . \tag{3.69}$$

This expression coincides with the result in Ref. [Bode et al., 2011], where a fermionic quantum environment is considered. From Eq. (3.69) we deduce that a similar result holds for a bosonic quantum system by replacing the Fermi distribution function by the Bose-Einstein distribution and changing a sign.

3.4. Application: quantum dot attached to leads

The above expressions of the Born-Oppenheimer force, the friction force, the Lorentz-like force and the noise correlator have been obtained in Refs. [Bode et al., 2011, Bode et al., 2012b] by using Keldysh Green functions. In this work a nanoelectromechanical mechanical system is considered which is attached to leads and couples to

the "heavy" classical degree of freedom $\mathbf{X}_t$ via electron-phonon coupling. The classical degree of freedom corresponds to a mechanical vibrational mode of the system and the forces acting on the classical parameter are induced by a current which runs through the system. In this section we show how the use of scattering theory is related to this work. Accordingly, we consider the Hamiltonian [Bode et al., 2011, Bode et al., 2012b]

$$\mathcal{H}_{\mathbf{X}_t} = \mathcal{H}_{\mathbf{X}} + \mathcal{H}_L + \mathcal{H}_D + \mathcal{H}_T \tag{3.70}$$

where the different terms are specified as

$$\mathcal{H}_{\mathbf{X}} = \frac{P^2}{2M} + U(\mathbf{X}_t) \tag{3.71}$$

$$\mathcal{H}_L = \int \frac{\mathrm{d}\varepsilon}{2\pi} \sum_{\eta} (\varepsilon - \mu_\eta)\, c_\eta^\dagger(\varepsilon) c_\eta(\varepsilon) \tag{3.72}$$

$$\mathcal{H}_D = \sum_{mm'} d_m^\dagger \left[h_0(\mathbf{X}_t)\right]_{mm'} d_{m'} \tag{3.73}$$

$$\mathcal{H}_T = \int \frac{\mathrm{d}\varepsilon}{\sqrt{2\pi}} \sum_{\eta m} \left(c_\eta^\dagger(\varepsilon) W_{\eta m}(\varepsilon) d_m + h.c. \right) . \tag{3.74}$$

Here, the operators $c_\eta^\dagger(\varepsilon)$ and $c_\eta(\varepsilon)$ create and annihilate, respectively, the free electronic states $|\phi_\eta(\varepsilon)\rangle$, which are approaching the scattering region from lead $\eta = L, R$ with chemical potential $\mu_L \geq \mu_R$. $\mathcal{H}_{\mathbf{X}}$ describes the evolution of the mode $\mathbf{X}_t$ in the potential $U(\mathbf{X}_t)$, with mass M and frequency ω_0. The Hamiltonian H_D models the system's Hamiltonian with states $|m\rangle$, created and annihilated, respectively, by the operators $d_m^\dagger$ and d_m. Furthermore, H_T represents tunnelling between the leads and the system with tunnelling amplitudes $W_{\eta m}(\varepsilon) = \langle \phi_\eta(\varepsilon)|W|m\rangle/\sqrt{2\pi}$. The mechanical degree of freedom couples to the electrons in the dot which is assumed to be instantaneous and described by the matrix $h_0(\mathbf{X}_t)$.

Our aim is to define a scattering problem from the electronic part of the Hamiltonian in Eq. (3.70) and to find an explicit expression of the A-matrix in terms of Green functions. We start by observing that the free Hamiltonian $\mathcal{H}_0$ in the above notation is given by the lead Hamiltonian $\mathcal{H}_L$. The scattering potential is given by the dot and the coupling to the leads so that we can write $V_t = \Pi_D W^\dagger \Pi_L + \Pi_L W \Pi_D + \Pi_D H_D \Pi_D$ with the projector onto the lead space, Π_L, and the projector onto dot space, Π_D. We note that the Hilbert space is a direct product of dot and leads spaces so that $\Pi_L \cdot \Pi_D = \Pi_D \cdot \Pi_L = 0$. With this we can define the Lippmann-Schwinger equation, cf. Eq. (3.12), which defines the scattering process as

$$|\psi_\eta^{\mathbf{X}_t +}(\varepsilon)\rangle = \Pi_L\, |\phi_\eta(\varepsilon)\rangle + G_t^R(\varepsilon) V_t\, \Pi_L\, |\phi_\eta(\varepsilon)\rangle\,, \tag{3.75}$$

where the Green function $G_t^R(\varepsilon) = (\varepsilon - H_t + i\eta)^{-1}$ is the adiabatic Green function of the full Hamiltonian, i.e. the dot and the leads. We project Eq. (3.75) onto the dot

space and define the adiabatic Green function of the dot as $G_D^R(\varepsilon) = \Pi_D\, G_t^R(\varepsilon)\, \Pi_D$. This gives

$$\begin{aligned} \Pi_D \left|\psi_\eta^{\mathbf{X}_t+}(\varepsilon)\right\rangle &= \Pi_D\, G_t^R(\varepsilon)\, \Pi_D\, W^\dagger\, \Pi_L \left|\phi_\eta(\varepsilon)\right\rangle \\ &= G_D^R(\varepsilon)\, W^\dagger \left|\phi_\eta(\varepsilon)\right\rangle . \end{aligned} \tag{3.76}$$

The reason for projecting the Lippmann-Schwinger equation onto the dot space is that the coupling to the mechanical degree of freedom is only via the dot Hamiltonian. This means that $\partial_t V_t = \Pi_D \partial_t H_D \Pi_D$ which implies by referring to the definition of the A-matrix in Eq. (3.28) that

$$\begin{aligned} A_t^{\eta\alpha}(\varepsilon) = \frac{1}{2}\Big(&\langle \partial_\varepsilon \psi_\eta^{\mathbf{X}_t-}(\varepsilon)| \Pi_D \partial_t H_D\, \Pi_D \left|\psi_\alpha^{\mathbf{X}_t+}(\varepsilon)\right\rangle \\ &- \langle \psi_\eta^{\mathbf{X}_t-}(\varepsilon)|\, \Pi_D\, \partial_t H_D\, \Pi_D \left|\partial_\varepsilon \psi_\alpha^{\mathbf{X}_t+}(\varepsilon)\right\rangle \Big) . \end{aligned} \tag{3.77}$$

With the aid of Eq. (3.76) we then deduce

$$\begin{aligned} A_t^{\eta\alpha}(\varepsilon) = \pi \sum_{klmn} \Big\{ &\partial_\varepsilon \left(W_{\eta k}(\varepsilon) \left[G_D^R(\varepsilon)\right]_{kl} \right) \left[\partial_t h_{lm}\right] \left[G_D^R(\varepsilon)\right]_{mn} W_{n\alpha}^\dagger(\varepsilon) \\ &- W_{\eta k}(\varepsilon) \left[G_D^R(\varepsilon)\right]_{kl} \left[\partial_t h_{lm}\right] \partial_\varepsilon \left(\left[G_D^R(\varepsilon)\right]_{mn} W_{n\alpha}^\dagger(\varepsilon) \right) \Big\} , \end{aligned} \tag{3.78}$$

which coincides with the expression obtained for the A-matrix in Refs. [Bode et al., 2011, Bode et al., 2012b].

3.5. Conclusion

Nanoelectromechanical systems are a paradigm for systems in which a fast quantum fermionic environment couples to slow classical coordinates. Aiming at controlling these systems, an understanding of the forces induced by the environment on the classical degrees of freedom is of crucial importance. In this chapter we have phrased such an interaction generally by considering a classical parameter coupled to an open quantum environment which can be both fermionic or bosonic. The setup thus applies to a wide range of systems, ranging from nanoelectromechanical to optomechanical and to cold-atom systems. Motivated by the fact that nanoelectromechanical systems constitute open systems, we have considered a quantum environment with a continuous energy spectrum. This has naturally led to the appearance of additional reaction forces such as dissipation and noise as opposed to the

case of a closed quantum environment with a discrete energy-level spectrum [Berry and Robbins, 1993].

Since transport in nanoelectromechanical systems is predominantly described by the Landauer-Büttiker theory we have used scattering theory as a natural tool for describing the environment-induced reaction forces. Out-of-equilibrium situations have been taken into account by adjusting the chemical potential of the respective scattering channels differently. We note however that scattering theory assumes a non-interacting (many-body) model, so that we stress that all the above results hold for the non-interacting case only.

Recently, the adiabatic-reaction forces have been expressed in terms of the scattering matrix and its first adiabatic correction in Refs. [Bode et al., 2011, Bode et al., 2012b] in the context of nanoelectromechanical systems. Their derivation is based on the usage of Keldysh Green functions. Here we have presented a rederivation of these results, which solely relies on the methods of scattering theory, and thus is much more direct. Due to the generality of our results the derivation furthermore allows for a comparison with earlier results on adiabatic reaction forces for closed quantum systems. While the adiabatic condition for closed quantum systems implies that the typical frequency of the classical degree of freedom Ω is much smaller than the energy-level spacing of the quantum system, this is obviously violated for an open system with a continuous energy spectrum. As it has turned out, adiabaticity requires the frequency Ω to be much smaller than the inverse dwell time, which naturally distinguishes the two characteristics timescales of the quantum and the classical system from each other.

Finally, as a consequence of the adiabatic expansion in the framework of the scattering theory, we have obtained an explicit expression of the first adiabatic correction of the scattering matrix, the A-matrix, in terms of the adiabatic scattering states. This is not only of theoretical importance, but also strongly simplifies direct calculations of concrete applications.

4. Relation between the Anderson orthogonality catastrophe and the adiabatic reaction forces

The present chapter is devoted to the Anderson orthogonality catastrophe of a quantum fermionic system and its relation to the adiabatic reaction forces, which appear in the Langevin equation (3.1). They describe the motion of a nanoelectromechanical system – or, more generally, a heavy particle – moving in a quantum environment out of equilibrium. Our basic motivation stems from the seminal work in Ref. [Schönhammer, 1991] where for a free electron gas in equilibrium a direct relation between the orthogonality exponent and the dissipation has been obtained in the limit of small variations of the classical system. Our main aim is a generalisation of this work to out-of-equilibrium situations.

We use the framework of scattering theory to connect the orthogonality catastrophe to the adiabatic reaction forces. By this, we can rely on the previously obtained expressions of the reaction forces in chapter 3. In equilibrium, the orthogonality exponent was expressed in Ref. [Yamada and Yosida, 1982] in terms of the scattering matrix for finite systems. This relation constitutes the starting point in Ref. [Schönhammer, 1991] for identifying a relation to dissipation in the limit of small distance, i.e. small variations in the coordinates of the heavy particle. In the present chapter, we generalise these ideas to infinite systems and finite times by studying the Loschmidt echo and the fidelity amplitude, which represent dynamical measures of the orthogonality catastrophe.

We detail the close relation of the orthogonality catastrophe to the Loschmidt echo and the fidelity amplitude later in this chapter. Both the orthogonality catastrophe and the fidelity amplitude have been studied in many different contexts. Famous is the so-called impurity problem which describes the effect on a fermionic system when a local perturbation is suddenly changed. In this context, the Fermi-edge or X-ray singularity constitutes a paradigm of the impurity problem where a power-law divergence of the spectral function of the Fermi system is seen at the frequency

threshold [Mahan, 1967, Nozières and de Dominicis, 1969]. Other examples include cold-atom systems with time-dependent impurities [Knap et al., 2012], the one-channel Kondo problem [Yuval and Anderson, 1970] and Luttinger liquids [Schotte and Schotte, 1969, Ogawa et al., 1992, Kane et al., 1994] including their extensions [Imambekov et al., 2012]. The Fermi-edge singularity is studied in out-of-equilibrium situations with the aid of diagrammatic techniques [Ng, 1995, Ng, 1996] and using functional determinants [Abanin and Levitov, 2004, Abanin and Levitov, 2005] as well as scattering matrices at zero temperature [Muzykantskii et al., 2003]. Moreover, a generic spin-fermion model is discussed in Ref. [Segal et al., 2007] and temperature effects in Refs. [Dóra et al., 2011, Sindona et al., 2013]. Examples with interacting particles can be found in Refs. [Dóra et al., 2013, Sachdeva et al., 2014].

In this work, we discuss the relation between the fidelity amplitude and the adiabatic reaction forces in the regime of small displacements of the classical system by relying on the expressions of the adiabatic reaction forces in terms of both scattering theory [Thomas et al., 2012] and Green functions [Bode et al., 2011, Bode et al., 2012b]. We begin in Sec. 4.1 by defining the fidelity amplitude and the Loschmidt echo for nanoelectromechanical systems and summarise their relation to the orthogonality catastrophe. Thereafter we consider the regime of small displacements of the classical system in Sec. 4.2. Before treating out-of-equilibrium situations in Sec. 4.3, we review some aspects on the equilibrium case in Sec. 4.4. To illustrate our findings we apply our results in Sec. 4.7 to a simple model which is a single level coupling to one vibrational mode. Finally, we conclude in Sec. 4.8.

This chapter is based on the unpublished joint work with T. Karzig, S. Viola Kusminskiy and F. von Oppen to which we refer as Ref. [Thomas et al., 2015].

4.1. Definition for nanoelectromechanical systems

The fidelity amplitude, $\mathcal{A}(\tau)$, is defined as the overlap of two quantum many-body states, which evolve in time from the same initial state according to different many-body Hamiltonians. For an initial quantum statistical mixture, this definition can be generalised to

$$\mathcal{A}(\tau) = \langle\, e^{i\mathcal{H}_i\tau}\, e^{-i\mathcal{H}_f\tau}\,\rangle\,, \tag{4.1}$$

where the brackets $\langle \ldots \rangle$ denote the quantum statistical expectation value with respect to the (initial) Hamiltonian, $\mathcal{H}_i$. The (final) Hamiltonian, $\mathcal{H}_f$, characterises the perturbed Hamiltonian. Equivalently, the fidelity amplitude can be interpreted

as a quantity which measures how closely a quantum system returns to the initial state when forward and backward evolutions are governed by different Hamiltonians. The name fidelity amplitude originates from its applications to quantum information theory. The Loschmidt echo is defined as the absolute square value of the fidelity amplitude, i.e.

$$\mathcal{L}(\tau) = |\mathcal{A}(t)|^2 \,. \tag{4.2}$$

The Loschmidt echo and the fidelity are good measures of the Anderson orthogonality catastrophe. This connection is well known in the literature and we illuminate it in the following.

In the same year in which P. W. Anderson's seminal paper on the orthogonality catastrophe [Anderson, 1967] appeared, it was shown that the emission and the absorption spectral functions of a fermionic system diverge at the frequency threshold as a power law [Mahan, 1967]. This divergence is referred to as the X-ray or Fermi edge singularity. Two years later, the Fermi edge singularity and the orthogonality catastrophe were shown in Ref. [Nozières and de Dominicis, 1969] to be competing effects by analysing the creation and annihilation of a hole deep in the Fermi sea. In this context, the creation of a localised core hole can be modelled as a sudden switching on of a perturbation of the Hamiltonian. In particular, P. Noziéres and C. de Dominicis showed that the Green function of a tunnelling electron, which describes the Fermi edge singularity, can be decomposed into two terms. The first term describes the single-particle scattering by a time-dependent potential and produces a divergence in the X-ray absorption spectral function to the creation of excitons when the core hole is created. The second term, on the other hand, describes the orthogonality effect, meaning the response of the Fermi sea to the creation of the core hole. It tends to suppress the divergence of the absorption spectral function with a power-law exponent given by the Anderson orthogonality exponent [Rivier and Simanek, 1971]. In this context, the response of the Fermi sea is described in terms of the core hole propagator. It is evaluated by calculating the ground-state overlap of the many-body fermionic states where one state evolves in time with respect to the unperturbed Hamiltonian (without the core hole), and the other state evolves with respect to the perturbed Hamiltonian (with the created hole). Hence it is given by a fidelity amplitude of the form given in Eq. (4.1) where the Hamiltonians $\mathcal{H}_i$ and $\mathcal{H}_f$ describe the system in the presence and absence of the hole, respectively.

The interpretation of the fidelity amplitude in the context of nanoelectromechanical systems is illustrated in Fig. 1.7 and Fig. 4.1. When the classical system moves, the scattering potential, felt by the quantum environment, changes. Hence the displacements, $\mathbf{X}$ and $\mathbf{X} + \delta\mathbf{X}$, induce the different Hamiltonians, $\mathcal{H}_i = \mathcal{H}_0 + \mathcal{V}_{\mathbf{X}}$

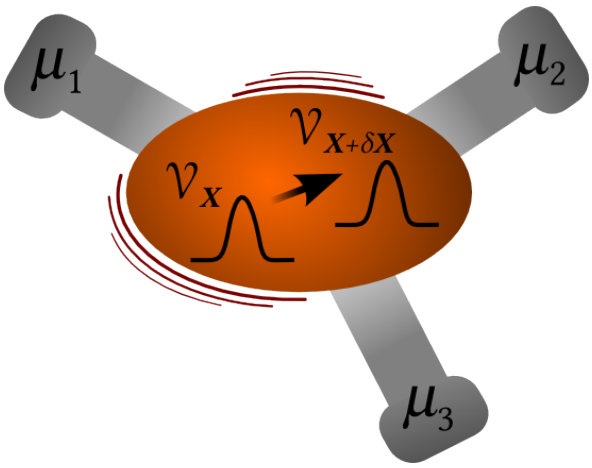

Figure 4.1.: Sketch of a scattering region coupled to a classical degree of freedom. A change of the position of the scatterer from $\mathbf{X}$ to $\mathbf{X}+\delta\mathbf{X}$ is associated with a different scattering potential $\mathcal{V}$ felt by the electrons travelling through the system.

and $\mathcal{H}_f = \mathcal{H}_0 + \mathcal{V}_{\mathbf{X}+\delta\mathbf{X}}$.

In Eq. (4.1) the change of the Hamiltonian from $\mathcal{H}_i$ to $\mathcal{H}_f$ happens instantaneously, that is on a timescale much smaller than other timescales of the problem. We generalise the expression in Eq. (4.1) to include different ways of changing between the initial and the final Hamiltonian. This generalisation provides more insight into the dynamics of the coupled system-environment set-up and explains that *adiabatic* quantities, such as the friction force, appear in a quantity which describes the *sudden* change of the classical parameter, as we deduce later. Accordingly, we allow for continuously changing the displacement of the classical system and consider the Hamiltonian

$$\mathcal{H}(t) = \mathcal{H}_0 + \mathcal{V}_{\mathbf{X}} + g(t)\,\delta\mathcal{H}_{\mathbf{X}} \tag{4.3}$$

with $\delta\mathcal{H}_{\mathbf{X}} = \mathcal{V}_{\mathbf{X}+\delta\mathcal{X}} - \mathcal{V}_{\mathbf{X}}$. This Hamiltonian is assumed to describe a non-interacting fermionic environment, but is otherwise arbitrary. The function $g(t)$ introduced in Eq. (4.3) determines the quench protocol. It controls how rapidly the nanoelectromechanical system changes its displacement. Initially at $t = 0$ we assume the classical system to be at the position $\mathbf{X}$ which is associated with the Hamiltonian $\mathcal{H}_0 + \mathcal{V}_{\mathbf{X}}$ so that $g(0) = 0$. We further consider the quench to stop at time τ which means that we impose $g(\tau) = 1$. For a time-dependent Hamiltonian as in Eq. (4.3), the fidelity amplitude generalises to

$$\mathcal{A}(\tau) = \langle\, U_0^\dagger(\tau, 0)\, U(\tau, 0)\,\rangle\,, \tag{4.4}$$

where U_0 denotes the time-evolution operator of the initial Hamiltonian $\mathcal{H}_0 + \mathcal{V}_{\mathbf{X}}$ and U describes the time-evolution with respect to the time-dependent Hamiltonian $\mathcal{H}(t)$. Equation (4.4) gives the most general expression of the fidelity amplitude.

In this work, we are particularly interested in the following two different quench protocols: (i) a *sudden* quench with $g(t) = 1$ for $t > 0$, for which the fidelity amplitude in Eq. (4.4) reduces to Eq. (4.1), and (ii) an *adiabatic* quench protocol, where we assume a smoothly varying displacement with linearly increasing $g(t) = t/\tau$. Later we show that the results in equilibrium do not depend on the particular form of the adiabatic quench protocol. The results in out-of-equilibrium situations, that is in the presence of an applied bias voltage, on the other hand can depend on the precise form of $g(t)$.

4.2. Perturbative expansion in small distances

We treat the fidelity amplitude and the Loschmidt echo in the regime of small displacements $\delta\mathbf{X}$ of the classical system. This allows for a perturbative treatment. To do so, we introduce the interaction picture with respect to the initial Hamiltonian $\mathcal{H}_i$. We realise that the term within the quantum statistical expectation value in Eq. (4.4) is the time-evolution operator in the interaction picture. This means that we can express the fidelity amplitude as

$$\mathcal{A}(\tau) = \langle\, T\, \exp\Big(-i \int_0^\tau \mathrm{d}t\, g(t)\, \delta\hat{\mathcal{H}}_{\mathbf{X}}(t) \Big) \,\rangle\,, \tag{4.5}$$

where the time dependence is given by $\delta\hat{\mathcal{H}}_{\mathbf{X}}(t) \equiv e^{i\mathcal{H}_i t}\delta\mathcal{H}_i e^{-i\mathcal{H}_{\mathbf{X}} t}$ and T denotes the time-ordering operator. We use Eq. (4.5) to perform a perturbative expansion for small variations of the local potential via the classical parameter $\delta\mathbf{X}$, so that we consider

$$\delta\mathcal{H}_{\mathbf{X}} = \sum_\alpha \partial_\alpha \mathcal{V}_{\mathbf{X}} \delta X_\alpha = \sum_\alpha \partial_\alpha \mathcal{H}_{\mathbf{X}} \delta X_\alpha\,. \tag{4.6}$$

As in the previous chapter, we denote the components of the classical degree of freedom by α and β. To first non-vanishing order in both, the real and the imaginary

part, we get from Eq. (4.4) for small $\delta\mathbf{X}$

$$\begin{aligned}\ln \mathcal{A}(\tau) = &-i \int_0^\tau \mathrm{d}t\, g(t)\, \langle \delta\hat{\mathcal{H}}_{\mathbf{X}}(t)\rangle \\ &- \frac{1}{2}\int_0^\tau \mathrm{d}t \int_0^\tau \mathrm{d}t' \sum_{\alpha\beta} g(t)\, g(t')\, D_{\alpha\beta}(t,t')\cdot \delta X_\alpha\, \delta X_\beta\,,\end{aligned} \tag{4.7}$$

where the first term is purely real and the second term purely imaginary. In the above equation we have identified the noise correlator $D_{\alpha\beta}(t,t') = \langle \delta\hat{\mathcal{H}}_{\mathbf{X}}(t)\, \delta\hat{\mathcal{H}}_{\mathbf{X}}(t')\rangle - \langle \delta\hat{\mathcal{H}}_{\mathbf{X}}(t)\rangle\langle \delta\hat{\mathcal{H}}_{\mathbf{X}}(t')\rangle$ which is equivalent to the noise correlator defined in Eq. (3.45) in the previous chapter. We note that only the symmetric part of the noise correlator is relevant due to the summation over the indices α and β. As the first term in Eq. (4.7) is purely real, it gives rise to an overall phase of the fidelity amplitude. The expression of this phase is readily identified to be identical to the expression for the infinitesimal amount of work performed by the Born-Oppenheimer force. This is revealed by a comparison to the expression of the Born-Oppenheimer force in terms of scattering states, cf. Eqs. (3.51) to (3.55). The identification of this infinitesimal work entering as a phase in the fidelity amplitude is consistent with the acquired dynamical phase of the eigenstate of the system by changing the Hamiltonian by $\delta\mathcal{H}_{\mathbf{X}}$. Hence we can write

$$\mathcal{A}_P(\tau) = e^{i\frac{\tau}{\lambda_P}\mathbf{F}(\mathbf{X})\cdot\delta\mathbf{X}} |\mathcal{A}_P(\tau)| \tag{4.8}$$

for both, the sudden ($P = S$) and the adiabatic ($P = A$) quench scenario. As $\lambda_A = 2\,\lambda_S$, cf. Table 4.1, the phase of the sudden quench fidelity amplitude is half the phase of the adiabatic fidelity amplitude.

In the following we restrict our analysis to the Loschmidt echo, which by Eq. (4.2) is defined as the absolute square value of the fidelity amplitude. We introduce the matrix notation $\sum_{\alpha\beta}(\ldots)_{\alpha\beta}\,\delta X_\alpha \delta X_\beta = \delta\mathbf{X}^\dagger\cdot(\ldots)\cdot\delta\mathbf{X}$ and deduce from Eq. (4.7) that the Loschmidt echo for small displacements $\delta\mathbf{X}$ reads

$$\ln \mathcal{L}(\tau) = -\int_0^\tau \mathrm{d}t \int_0^\tau \mathrm{d}t'\, g(t)\, g(t')\, \delta\mathbf{X}^\dagger\cdot\mathbf{D}(t,t')\cdot\delta\mathbf{X}\,. \tag{4.9}$$

The Loschmidt echo is thus purely given by the integrated noise correlator $\mathbf{D}(t,t')$. The function $g(t)$ describing the quench protocol enters as a weighting factor. For Gaussian white noise, which is treated in the previous chapter, cf. Eq. (3.46), and which is delta-correlated in time, we readily deduce from Eq. (4.9) an exponential decay of the Loschmidt echo. The strength of the decay is determined by $\delta\mathbf{X}^\dagger\cdot\mathbf{D}(\mathbf{X})\cdot\delta\mathbf{X}$, where the precise exponent depends on $g(t)$.

In this chapter we consider the case where the correlator $D_{\alpha\beta}(t,t')$ depends on the difference $t-t'$ in the time arguments. This is valid for stationary states. We introduce the Fourier transform

$$\tilde{\mathbf{D}}(\omega) = \int_{-\infty}^{\infty} \mathrm{d}\Delta t\, e^{i\omega\,\Delta t}\, \mathbf{D}(\Delta t)\,, \tag{4.10}$$

which immediately yields

$$\ln \mathcal{L}(\tau) = -\int_0^{\infty} \frac{\mathrm{d}\omega}{\pi} \left| \int_0^{\tau} \mathrm{d}t\, g(t)\, e^{i\omega t} \right|^2 \delta\mathbf{X}^{\dagger} \cdot \mathbf{D}(\omega) \cdot \delta\mathbf{X} \tag{4.11}$$

with the symmetric noise correlator, $\mathbf{D}(\omega) = [\tilde{\mathbf{D}}(\omega) + \tilde{\mathbf{D}}(-\omega)]/2$. By specifying the quench protocol, the above time integration can be performed. For the sudden and the adiabatic (linear) quench we then obtain

$$\ln \mathcal{L}_P(\tau) = -\int_0^{\infty} \frac{\mathrm{d}\omega}{\pi}\, B_P(\omega,\tau)\, \delta\mathbf{X}^{\dagger} \cdot \mathbf{D}(\omega) \cdot \delta\mathbf{X}\,, \tag{4.12}$$

where we have introduced the function $B_P(\omega,\tau)$ as

$$B_S(\omega,\tau) = 2\,\frac{1-\cos(\omega\,\tau)}{\omega^2} \tag{4.13}$$

$$B_A(\omega,\tau) = \frac{2\,[1-\cos(\omega\,\tau) - \omega\tau\sin(\omega\tau)] + \omega^2\tau^2}{\tau^2\omega^4} \tag{4.14}$$

for the respective quench dynamics. We note that the upper cut-off of the frequency integral in Eq. (4.11) is given by the inverse dwell time. In the following analysis we consider the limit of large times $\tau \gg \tau_D$, where the function $B_P(\omega,\tau)$ is sharply peaked at small frequencies $\omega = 0$. This behaviour enables a perturbative treatment of the noise correlator $\mathbf{D}(\omega)$ for small frequencies with respect to the inverse dwell time. The relation between ω and the temperature T determines whether the noise is quantum or classical as we detail below.

We note that the above obtained relations of the Loschmidt echo and the fidelity amplitude in terms of the correlator of the fluctuating force are generally valid for small displacements $\delta\mathbf{X}$. In particular this means, that they also apply to situations where the fermionic environment is driven out of equilibrium by applying a bias voltage. Before addressing the out-of-equilibrium case, however, we first treat the equilibrium situation in which fluctuations are determined by the fluctuation-dissipation theorem.

4.3. Equilibrium

In equilibrium, all leads possess the same chemical potential, which we denote by μ. In Ref. [Schönhammer, 1991] it was shown for finite systems in equilibrium that the Anderson orthogonality exponent is directly proportional to the friction tensor induced by the (non-interacting) fermionic environment. For the Loschmidt echo as a dynamical quantity of the Anderson orthogonality this corresponds to the infinite time limit $\tau \to \infty$. In the following we generalise the result of Ref. [Schönhammer, 1991] to open quantum systems which have a continuous energy spectrum and determine the behaviour of the Loschmidt echo for finite times τ larger than the dwell time.

In equilibrium, the correlator of the fluctuating force and the friction tensor[1] are generally related via the fluctuation-dissipation theorem

$$\mathbf{D}(\omega) = \omega \coth\left(\frac{\beta\omega}{2}\right) \boldsymbol{\gamma}^{eq}(\omega) \tag{4.15}$$

with inverse temperature $\beta = 1/T$. We begin with the case of zero temperature and describe the effect of finite temperature later in Sec. 4.3.2. At zero temperature, that is to lowest order in $\beta\omega \gg 1$, we deduce from the fluctuation-dissipation theorem that $\mathbf{D}(\omega) = |\omega|\, \boldsymbol{\gamma}^{eq}(\omega)$. Inserting this into Eq. (4.12) yields

$$\ln \mathcal{L}_P(\tau) = -\frac{1}{\pi} \int_0^{1/\tau_D} \omega \,\mathrm{d}\omega\, B_P(\omega, \tau)\, \delta\mathbf{X}^\dagger \cdot \boldsymbol{\gamma}^{eq} \cdot \delta\mathbf{X} \tag{4.16}$$

to leading order in τ/τ_D, where the friction tensor $\boldsymbol{\gamma}^{eq}$ is taken at zero frequency. Evaluating the above energy integral readily gives

$$\ln \mathcal{L}_P(\tau) = -\frac{\alpha_P}{\pi}\left[\ln\left(\frac{\tau}{\tau_D}\right) + \gamma_e\right] \delta\mathbf{X}^\dagger \cdot \boldsymbol{\gamma}^{eq} \cdot \delta\mathbf{X} \tag{4.17}$$

with Euler-Mascheroni constant $\gamma_e = 0.5772$. The constant α_P takes a protocol-dependent value. It takes the values $\alpha_S = 2$ and $\alpha_A = 1$ for the respective quench protocol. In the following analysis further constants occur, which depend on the precise form of $g(t)$. We summarise the protocol-dependent parameters in Table 4.1.

By referring to Eq. (4.17) we conclude, that to leading order in τ/τ_D the Loschmidt echo decays as a power law in time for both quench scenarios. This reflects the

[1] For notational simplicity, we omit the superscript s of the friction coefficient, which has been used in the previous chapter. For the same reason, we drop the notation, which stresses the explicit dependence on $\mathbf{X}$.

Table 4.1.: Protocol-dependent constants which are used throughout the chapter. The constant α_P is universal and independent of the precise adiabatic quench protocol. The other constants are only valid for the linear quench scenario, i.e. $g(t) = t/\tau$.

Symbol	Sudden quench ($P = S$)	Adiabatic quench ($P = A$)
α_P	2	1
β_P	1	3
δ_P	2	1/2
λ_P	1	2

Anderson orthogonality catastrophe [Anderson, 1967]. In particular, we note that the Loschmidt echo of the slow quench gives the orthogonality exponent. This can be understood by referring to the definition of the Loschmidt echo in Eqs. (4.2) and (4.4). In the infinite-time limit, the quantum many-body states, which appear in the expectation value, adiabatically evolve to the many-body eigenstates of the initial and the final Hamiltonian due to the respective evolution operator U_0 and U. By this, the adiabatic Loschmidt echo is the squared overlap of the quantum many-body states of the initial and the final Hamiltonian, which explicitly shows the relation to the orthogonality catastrophe [Dóra et al., 2013]. We note that for a finite system the limit of infinite times can be taken by replacing τ/τ_D by the size of the system (up to prefactors, which are not dimensionless) [Münder et al., 2012]. This yields the usual power-law decay with system size [Anderson, 1967].

As expected, the power-law decay of the Loschmidt echo in Eq. (4.17) is directly proportional to the dissipation, which is in agreement with the known results in the literature [Schönhammer, 1991]. The proportionality factor, however, depends on the quench protocol. The coefficient α_P takes the values $\alpha_S = 2$ and $\alpha_A = 1$, as summarised in Table 4.1, so that we deduce the relation

$$\mathcal{L}_S(\tau) = \mathcal{L}_A(\tau)^2 \,. \tag{4.18}$$

This relation between the adiabatic and the sudden quench Loschmidt echo was also recently found in Refs. [Dóra et al., 2013, Sachdeva et al., 2014] for a Luttinger Liquid for finite systems and infinite times τ. For our system, we show that this relation is independent of the assumption that $g(t)$ increases linearly in time.

4.3.1. Adiabatic Protocols

The relation between the Loschmidt echo of the sudden and the adiabatic quench as given in Eq. (4.18) is valid for any adiabatic quenching protocol with a function $g(t)$ with $g(0) = 0$ and $g(\tau) = 1$, which increases as a power law on a timescale much larger than the dwell time. We prove this in particular for $g(t) = (t/\tau)^n$ where $n \geq 1$ is a positive integer and show that Eq. (4.17) holds with $\alpha_P = 1$. For this particular form of $g(t)$ the Loschmidt echo reads

$$\ln \mathcal{L}_A(\tau) = -\frac{1}{\pi} \int_0^{1/\tau_D} \mathrm{d}\omega\, \omega \left| \int_0^\tau \mathrm{d}t \left(\frac{t}{\tau}\right)^n e^{i\omega t} \right|^2 \delta\mathbf{X}^\dagger \cdot \boldsymbol{\gamma}^{eq} \cdot \delta\mathbf{X}\,, \tag{4.19}$$

which follows from Eq. (4.11) using the zero-temperature fluctuation-dissipation theorem $\mathbf{D}(\omega) = |\omega|\, \boldsymbol{\gamma}^{eq}(\omega)$. We can split the above integral into the regions $\omega \leq 1/\tau$ and $\omega \geq 1/\tau$. The first part contributes a constant to the Loschmidt echo, where the precise value depends on the choice of n, and thus becomes irrelevant to leading order in $\tau/\tau_D \gg 1$. Keeping only the remaining term, the Loschmidt echo is given by

$$\ln \mathcal{L}_A(\tau) = -\frac{1}{\pi} \int_{1/\tau}^{1/\tau_D} \mathrm{d}\omega\, \omega \left| \int_0^\tau \mathrm{d}t \left(\frac{t}{\tau}\right)^n e^{i\omega t} \right|^2 \delta\mathbf{X}^\dagger \cdot \boldsymbol{\gamma}^{eq} \cdot \delta\mathbf{X}\,. \tag{4.20}$$

The above time integral can be performed by integrating by parts. To leading order in $\tau/\tau_D \gg 1$ we find

$$\int_0^\tau \mathrm{d}t \left(\frac{t}{\tau}\right)^n e^{i\omega t} = \frac{e^{i\omega\tau}}{i\omega}\,. \tag{4.21}$$

Substituting this into Eq. (4.19) and integrating over frequencies yields

$$\ln \mathcal{L}_A(\tau) = -\frac{1}{\pi} \ln\left(\frac{\tau}{\tau_D}\right) \delta\mathbf{X}^\dagger \cdot \boldsymbol{\gamma}^{eq} \cdot \delta\mathbf{X} + \text{const.} \tag{4.22}$$

for all $g(t) = \left(\frac{t}{\tau}\right)^n$. We deduce for the large time decay of the Loschmidt echo the desired power law as in Eq. (4.17). This readily gives Eq. (4.18) which is thus valid for a wide range of protocols.

4.3.2. Finite temperature

Assuming a noise correlator which is delta-correlated in time, cf. Eq. (3.46), yields an exponential decay of the Loschmidt echo for the sudden and adiabatic quench

scenarios. The result in Eq. (4.17) is a power-law decay of the Loschmidt echo which is thus inconsistent with assuming white noise. Thus, the power-law decay shows the breakdown of the description in terms of a semiclassical, Markovian Langevin equation, cf. Eq. (3.1). The Markovian approximation becomes invalid since the system loses its memory as a power law and not exponentially. The reason for the power-law decay of the Loschmidt echo in equilibrium and at zero temperature is that the classical noise correlator vanishes in this limit. In the following we show that both, finite temperatures and finite bias voltage, induce an additional exponential decay on top of the power-law decay. We treat both cases separately in the following and begin in this section by considering finite temperatures in the absence of a bias voltage.

We start by considering the regime of small temperatures $0 < T \ll \omega$. From the fluctuation-dissipation theorem in Eq. (4.15) we determine the finite temperature correction term to the noise correlator as $\mathbf{D}(\omega) = |\omega| \left[1 + 2\,\exp(-\beta\omega)\right] \boldsymbol{\gamma}^{eq}(\omega)$. To leading order in τ/τ_D we deduce

$$\ln \mathcal{L}_P(\tau) = -\frac{1}{\pi} \int_0^{1/\tau_D} \mathrm{d}\omega\, \omega\, B_P(\omega,\tau)\, \left(1 + 2\, e^{-\beta\omega}\right)\, \delta\mathbf{X}^\dagger \cdot \boldsymbol{\gamma}^{eq} \cdot \delta\mathbf{X}\,. \tag{4.23}$$

We can evaluate the above energy integral to quadratic order in τ/β and to lowest order in τ_D/β. We obtain

$$\ln \mathcal{L}_P(\tau) = -\frac{\alpha_P}{\pi}\, \left[\ln\left|\frac{\tau}{\tau_D}\right| + \gamma_e + \frac{\alpha_P}{2}\,\frac{\tau^2}{\beta^2}\right]\, \delta\mathbf{X}^\dagger \cdot \boldsymbol{\gamma}^{eq} \cdot \delta\mathbf{X}\,. \tag{4.24}$$

We conclude that small finite temperatures induce a Gaussian decay of the Loschmidt echo in addition to the power law.

The regime of large temperatures $T \gg \omega$ corresponds to the classical regime. In the classical limit, the noise correlator in Eq. (4.15) becomes $\mathbf{D}(\omega) = 2\,T\,\boldsymbol{\gamma}^{eq}(\omega)$, cf. Sec. 3.3.3, which is the classical fluctuation-dissipation theorem. Inserting the classical noise correlator into Eq. (4.12) and performing the frequency integral yields

$$\ln \mathcal{L}_P(\tau) = -\frac{2\tau}{\beta\beta_P} \delta\mathbf{X}^\dagger \cdot \boldsymbol{\gamma}^{eq} \cdot \delta\mathbf{X} \tag{4.25}$$

to lowest order in τ/τ_D, where $\beta_S = 1$ and $\beta_A = 3$ depends on the protocol, cf. Table 4.1. Indeed, the Loschmidt echo decays exponentially for both quenching protocols in the classical limit at large $T \gg \omega$.

4.4. Out of equilibrium

We now turn to the analysis of a fermionic environment driven out of equilibrium by a bias voltage. This means that we consider different chemical potentials in the leads. For clarity, we restrict the analysis to the case of two leads with chemical potentials $\mu_L = \mu + \Delta\mu/2$ and $\mu_R = \mu - \Delta\mu/2$. Without loss of generality we consider positive $\Delta\mu > 0$. We then determine the decay of the Loschmidt echo up to linear response in the bias voltage in the exponent, that is we consider linear order terms in $\Delta\mu\tau_D \ll 1$.

Essential for the behaviour of the Loschmidt echo is the form of the noise correlator, cf. Eq. (4.12). Both, with the aid of scattering theory and using non-equilibrium Green functions, we find an expression of the noise correlator in terms of the friction tensor valid to linear order in the bias voltage. We postpone the derivation to Sec. 4.5 and Sec. 4.6, respectively. Here, we present the result, that is

$$\begin{aligned}\mathbf{D}(\omega) = {} & \omega \coth\left(\frac{\beta\omega}{2}\right)\left(\boldsymbol{\gamma}^{eq} - \frac{\mathbf{D}_{[0,\Delta\mu]}}{\Delta\mu}\right) \\ & + \frac{1}{2}\left((\omega+\Delta\mu)\coth\left(\frac{\beta(\omega+\Delta\mu)}{2}\right) + (\omega-\Delta\mu)\coth\left(\frac{\beta(\omega-\Delta\mu)}{2}\right)\right)\frac{\mathbf{D}_{[0,\Delta\mu]}}{\Delta\mu} \\ & + \frac{\omega}{2}\left((\omega+\Delta\mu)\coth\left(\frac{\beta(\omega+\Delta\mu)}{2}\right) - (\omega-\Delta\mu)\coth\left(\frac{\beta(\omega-\Delta\mu)}{2}\right)\right)\frac{\boldsymbol{\gamma}^{neq}}{\Delta\mu}\,.\end{aligned} \tag{4.26}$$

As in chapter 3 the friction tensor $\boldsymbol{\gamma} = \boldsymbol{\gamma}^{eq} + \boldsymbol{\gamma}^{neq}$ is split into the pure out-of-equilibrium contribution, $\boldsymbol{\gamma}^{neq}$ [cf. Eq. (3.4)], which vanishes in equilibrium, and the remaining part, $\boldsymbol{\gamma}^{eq}$ [cf. Eq. (3.3)], which however also contains a part stemming from out-of-equilibrium conditions. The noise correlator generally depends on both bias voltage and temperature. At zero frequency we denote the correlator as $\mathbf{D}_{[T,\Delta\mu]}$. In particular, $\mathbf{D}_{[0,\Delta\mu]}$ describes the zero-frequency correlator at zero temperature, We note that as Eq. (4.26) is valid to linear response in the bias voltage, the friction tensor is evaluated to linear response as $\boldsymbol{\gamma}^{eq} = \boldsymbol{\gamma}_0^{eq} + \boldsymbol{\gamma}_1^{eq}$ and $\boldsymbol{\gamma}^{neq} = \boldsymbol{\gamma}_1^{neq}$, where the index denotes the order in the bias voltage. Moreover, we notice that Eq. (4.26) reduces to the equilibrium case in Eq. (4.15) for $\Delta\mu = 0$.

In the following, we focus on the zero temperature limit. More precisely, this means that we consider the limit $T \ll \omega$ as well as $T \ll \Delta\mu$ to be sensitive to out-of-

equilibrium effects. In this regime Eq. (4.26) becomes

$$\begin{aligned}\mathbf{D}(\omega) = |\omega| \left(\boldsymbol{\gamma}^{eq} - \frac{\mathbf{D}_{[0,\Delta\mu]}}{\Delta\mu}\right) + \left(|\omega+\Delta\mu| + |\omega-\Delta\mu|\right) \frac{\mathbf{D}_{[0,\Delta\mu]}}{\Delta\mu} \\ + \omega \left(|\omega+\Delta\mu| - |\omega-\Delta\mu|\right) \frac{\boldsymbol{\gamma}^{neq}}{\Delta\mu}\,.\end{aligned} \tag{4.27}$$

In particular, this means that

$$\mathbf{D}(\omega) = \begin{cases} \mathbf{D}_{[0,\Delta\mu]} + |\omega| \left(\boldsymbol{\gamma}^{eq} - \frac{\mathbf{D}_{[0,\Delta\mu]}}{\Delta\mu}\right) + \frac{\omega^2}{2} \frac{\boldsymbol{\gamma}^{neq}}{\Delta\mu} & , \quad |\omega| < \Delta\mu \\ |\omega| \left(\boldsymbol{\gamma}^{eq} + \boldsymbol{\gamma}^{neq}\right) & , \quad |\omega| > \Delta\mu \end{cases}, \tag{4.28}$$

which will be of interest below. We can use the noise correlator in Eq. (4.27) and (4.28) to determine the behaviour of the Loschmidt echo in terms of the macroscopic coefficients appearing in the Langevin equation (3.1) for large times $\tau \gg \tau_D$. Inserting the expression of the noise correlator into Eq. (4.12) and performing the time integration yields

$$\begin{aligned}\ln \mathcal{L}_S(\tau) = &- \frac{1}{\pi}\int_0^{1/\tau_D} \mathrm{d}\omega\, \omega\, B_P(\omega,\tau)\, \delta\mathbf{X}^\dagger \cdot \left(\boldsymbol{\gamma}^{eq} + \boldsymbol{\gamma}^{neq}\right) \cdot \delta\mathbf{X} \\ &- \frac{1}{\pi}\int_0^{\Delta\mu} \mathrm{d}\omega\, B_P(\omega,\tau)\, \delta\mathbf{X}^\dagger \cdot \mathbf{D}_{[0,\Delta\mu]} \cdot \delta\mathbf{X} \\ &+ \frac{1}{\pi}\int_0^{\Delta\mu} \mathrm{d}\omega\, \omega\, B_P(\omega,\tau)\, \delta\mathbf{X}^\dagger \cdot \left(\frac{\mathbf{D}_{[0,\Delta\mu]}}{\Delta\mu} + \boldsymbol{\gamma}^{neq}\right) \cdot \delta\mathbf{X} \\ &- \frac{1}{\pi}\int_0^{\Delta\mu} \mathrm{d}\omega\, \omega^2\, B_P(\omega,\tau)\, \delta\mathbf{X}^\dagger \cdot \frac{\boldsymbol{\gamma}^{neq}}{\Delta\mu} \cdot \delta\mathbf{X}\,,\end{aligned} \tag{4.29}$$

where we have split the integral into a part where $\omega > \Delta\mu$ and a part where $\omega < \Delta\mu$. It is now instructive to consider the different regimes of large and small times τ relative to the inverse potential difference $1/\Delta\mu$ as these limits are analytically solvable. We call the regime of small $\Delta\mu\tau \ll 1$ short-time dynamics and the regime of large $\Delta\mu\tau \gg 1$ long-time dynamics. Note that in both cases we still consider large τ/τ_D.

4.4.1. Short-time dynamics

In the short-time limit, only the first integral in Eq. (4.29) survives to lowest order in $\Delta\mu\tau$ while the other terms give quadratic corrections. An integration analogous to the equilibrium case gives

$$\ln \mathcal{L}_P(\tau) = -\frac{\alpha_P}{\pi}\left[\gamma_e + \ln\left(\frac{\tau}{\tau_D}\right)\right] \delta\mathbf{X}^\dagger \cdot \left(\boldsymbol{\gamma}^{eq} + \boldsymbol{\gamma}^{neq}\right) \cdot \delta\mathbf{X}\,. \tag{4.30}$$

We thus find that the short-time dynamics of the Loschmidt echo is determined by the full friction tensor $\boldsymbol{\gamma} = \boldsymbol{\gamma}^{eq} + \boldsymbol{\gamma}^{neq}$ in linear response. The decay of the Loschmidt echo is, as in the equilibrium case, given by a power law. This is due to the fact that at short timescales $\Delta\mu\tau \ll 1$ the system is not sensitive to the bias voltage. Consequently, we recover the behaviour of the equilibrium case.

The power-law decay in Eq. (4.30) is valid within a certain time interval, which we characterise in the following. To this end, we define two timescales. First, we introduce the characteristic timescale, $\tau_{char} \sim \tau_D \exp[1/(\delta\mathbf{X}^\dagger \cdot \gamma \cdot \delta\mathbf{X})]$, which defines the validity of the perturbative approach of treating small $\delta\mathbf{X}$. Our results are thus valid for $\tau \gg \tau_{char}$. Moreover, we introduce a second timescale, $\tau_{cor} \sim \tau_D[|\ln(\Delta\mu\,\tau_D)|/(\Delta\mu\,\tau_D)]^{1/2}$. This timescale signals the onset of higher order corrections in $\Delta\mu\tau$, which are of quadratic order, compared to the logarithmic term $\propto \ln(\tau/\tau_D)$, which is responsible for the power-law decay. We conclude that Eq. (4.30) is valid for times τ_D, $\tau_{char} \ll \tau \ll \tau_{cor}$, where the power-law exponent is given by the full friction tensor. Since the short-time dynamics of the Loschmidt echo in this regime is essentially equivalent to the equilibrium case, we further conclude that the relation in Eq. (4.18) between the Loschmidt echo of the sudden quench and the Loschmidt echo of the adiabatic quench still holds in this limit.

4.4.2. Long-time dynamics

The long-time dynamics of the Loschmidt echo behaves quite differently from the equilibrium case since the system becomes sensitive to the imposed bias voltage. Analogous to the short-time dynamics, we use Eq. (4.29) to determine the behaviour of the Loschmidt echo. An evaluation of the energy integrals in the long-time limit $\Delta\mu\tau \gg 1$ yields

$$\begin{aligned}\ln \mathcal{L}_P(\tau) = &-\frac{\alpha_P}{\pi}\left[\gamma_e + \ln\left(\frac{\tau}{\tau_D}\right)\right]\delta\mathbf{X}^\dagger\cdot\boldsymbol{\gamma}\cdot\delta\mathbf{X}\\ &+\frac{\alpha_P}{\pi}\left[\gamma_e + \ln\left(\Delta\mu\tau\right)\right]\delta\mathbf{X}^\dagger\cdot\left(\frac{\mathbf{D}_{[0,\Delta\mu]}}{\Delta\mu}+\boldsymbol{\gamma}_1^{neq}\right)\cdot\delta\mathbf{X}\\ &-\frac{\tau}{\beta_P}\,\delta\mathbf{X}^\dagger\cdot\mathbf{D}_{[0,\Delta\mu]}\cdot\delta\mathbf{X}-\frac{\delta_P}{\pi}\,\delta\mathbf{X}^\dagger\cdot\boldsymbol{\gamma}_1^{neq}\cdot\delta\mathbf{X}\\ &+\frac{1}{\pi}\Big(\alpha_P-\frac{2}{\beta_P}\cos(\Delta\mu\,\tau)\Big)\,\delta\mathbf{X}^\dagger\cdot\frac{\mathbf{D}_{[0,\Delta\mu]}}{\Delta\mu}\cdot\delta\mathbf{X}\,.\end{aligned} \tag{4.31}$$

where $\delta_S = 2$ and $\delta_A = 1/2$ as written in Table 4.1. In the linear response regime for small bias voltages $\Delta\mu\tau_D \ll 1$ we can simplify this expression by writing the logarithmic term as $\ln(\tau/\tau_D) = \ln(\Delta\mu\,\tau/(\Delta\mu\,\tau_D))$. Since $\Delta\mu\,\tau_D\,\ln(\Delta\mu\,\tau_D)$ vanishes

for small $\Delta\mu\,\tau_D$, we can write the long-time dynamics of the Loschmidt echo in this regime as

$$\begin{aligned}\ln\mathcal{L}_P(\tau) = &-\frac{\tau}{\beta_P}\,\delta\mathbf{X}^\dagger\cdot\mathbf{D}_{[0,\Delta\mu]}\cdot\delta\mathbf{X} + \frac{1}{\pi}\Big(\alpha_P - \frac{2}{\beta_P}\,\cos(\Delta\mu\,\tau)\Big)\,\delta\mathbf{X}^\dagger\cdot\frac{\mathbf{D}_{[0,\Delta\mu]}}{\Delta\mu}\cdot\delta\mathbf{X}\\ &-\frac{\alpha_P}{\pi}\Big[\gamma_e + \ln(\Delta\mu\tau)\Big]\delta\mathbf{X}^\dagger\cdot\left(\boldsymbol{\gamma}^{eq} - \frac{\mathbf{D}_{[0,\Delta\mu]}}{\Delta\mu}\right)\cdot\delta\mathbf{X}\\ &+\frac{\alpha_P}{\pi}\,\ln(\Delta\mu\,\tau_D)\,\delta\mathbf{X}^\dagger\cdot\boldsymbol{\gamma}_0^{eq}\cdot\delta\mathbf{X} - \frac{\delta_P}{\pi}\,\delta\mathbf{X}^\dagger\cdot\boldsymbol{\gamma}_1^{neq}\cdot\delta\mathbf{X}\,.\end{aligned} \tag{4.32}$$

By neglecting irrelevant terms for large times $\Delta\mu\,\tau$ we can summarise the long-time dynamics as

$$\begin{aligned}\mathcal{L}_P(\tau)\propto\;&\exp\left(-\frac{\tau}{\beta_P}\delta\mathbf{X}^\dagger\cdot\mathbf{D}_{[0,\Delta\mu]}\cdot\delta\mathbf{X}\right)\,(\Delta\mu\,\tau)^{-\frac{\alpha_P}{\pi}\delta\mathbf{X}^\dagger\cdot\left[\boldsymbol{\gamma}^{eq}-\frac{\mathbf{D}_{[0,\Delta\mu]}}{\Delta\mu}\right]\cdot\delta\mathbf{X}}\\ &\times(\Delta\mu\,\tau_D)^{\frac{\alpha_P}{\pi}\delta\mathbf{X}^\dagger\cdot\boldsymbol{\gamma}^{eq}\cdot\delta\mathbf{X}}\,.\end{aligned} \tag{4.33}$$

Equation (4.33) indeed shows a power-law decay of the Loschmidt echo which is accompanied by an exponential suppression. The exponential decay, on the one hand, is characterised by the shot-noise fluctuations in the system with positive definite $\mathbf{D}_{[0,\Delta\mu]}$. This is in agreement with assuming white noise for the noise correlator to leading order. The power-law decay, on the other hand, characterises the next-order corrections to the white-noise contribution. The power-law exponent, $-\alpha_P/\pi\,\delta\mathbf{X}^\dagger\cdot[\boldsymbol{\gamma}^{eq} - \frac{\mathbf{D}_{[0,\Delta\mu]}}{\Delta\mu}]\cdot\delta\mathbf{X}$, is given by a competition between dissipation and fluctuations. This is a clear fingerprint of out-of-equilibrium situations. We note that fluctuations and dissipation are related as $\boldsymbol{\gamma}^{eq} = \mathbf{D}_{[T,0]}/(2\,T)$ in equilibrium so that the asymmetry between shot and Nyquist noise determines the sign of the power-law exponent in the linear-response regime. The exponent can indeed be of arbitrary sign, which is called "anti-orthogonality" in Ref. [Segal et al., 2007] when it is positive. The leading order contribution of the power-law exponent in $\Delta\mu\,\tau_D$, however, that is $-\alpha_P/\pi\,\delta\mathbf{X}^\dagger\cdot[\boldsymbol{\gamma}_0^{eq} - \frac{\mathbf{D}_{[0,\Delta\mu]}}{\Delta\mu}]\cdot\delta\mathbf{X}$, is restricted to positive values. The sign change occurs when the leading order term vanishes and the linear response correction term, given by $\boldsymbol{\gamma}_1^{eq}$, becomes the relevant contribution.

Due to the presence of the protocol-dependent prefactor β_P in Eq. (4.33), which determines the exponential decay of the Loschmidt echo, we conclude that the identity $\mathcal{L}_S(\tau) = \mathcal{L}_A(\tau)^2$, cf. Eq. (4.18), is no longer valid for the long-time dynamics in out-of-equilibrium situations. This departure can be attributed to the form of the function $g(t)$. By means of Eq. (4.9) we immediately obtain an exponential decay of the Loschmidt echo with an exponent $-\delta\mathbf{X}^\dagger\cdot\mathbf{D}_{[0,\Delta\mu]}\cdot\delta\mathbf{X}$ when assuming Gaussian

white noise for the sudden quench, while the exponent $-1/3\,\delta\mathbf{X}^\dagger \cdot \mathbf{D}_{[0,\Delta\mu]} \cdot \delta\mathbf{X}$ follows from the linear behaviour $g(t) = t/\tau$. A quench protocol where $g(t)$ grows as an arbitrary power law $g(t) = (t/\tau)^n$ with positive integer n changes this prefactor depending on the choice of n.

4.5. Derivation within scattering theory

In this section we present the derivation of Eq. (4.26) which gives the noise correlator in terms of the dissipation to linear response in the bias voltage and which determines the behaviour of the Loschmidt echo. We derive the expression of the noise correlator within the methods of scattering theory in this section and present an equivalent derivation in terms of non-equilibrium Green functions in Sec. 4.6.

We begin the derivation by expressing the coloured noise correlator $\mathbf{D}(t,t')$ defined in Eq. (3.45) in terms of single-particle scattering states. To this end, we express the non-interacting many-body Hamiltonian

$$\mathcal{H}_i = \int \frac{\mathrm{d}\varepsilon}{2\pi} \int \frac{\mathrm{d}\varepsilon'}{2\pi} \sum_{kn} [H_i]_{kn}(\varepsilon,\varepsilon') a_k^{\mathbf{X}\dagger}(\varepsilon) a_n^{\mathbf{X}}(\varepsilon')\,, \tag{4.34}$$

in terms of the *single-particle* Hamiltonian $H_i = H_0 + V_{\mathbf{X}}$. Analogously, we introduce the single-particle Hamiltonian $\delta H_X = \nabla V_{\mathbf{X}} \cdot \delta\mathbf{X}$. Similar to Eq. (3.37), the operators $a_m^{\mathbf{X}\dagger}(\varepsilon)$ and $a_m^{\mathbf{X}}(\varepsilon)$ create and annihilate the retarded *single-particle* scattering states $|\psi_m^{\mathbf{X}+}(\varepsilon)\rangle$ of the initial Hamiltonian H_i with combined channel and lead index m and energy ε. The corresponding advanced scattering states are indicated with the superscript "$-$" instead of the superscript "$+$". The scattering states obey the Lippman-Schwinger equation, cf. Eqs. (2.14) and (3.12), and the boundary conditions in Eq. (2.5) as well as the normalisation condition in Eq. (2.15). In the basis of the scattering states we denote the matrix elements of the operator $\nabla V_{\mathbf{X}}$ as

$$\partial_\alpha V_{\mathbf{X}}^{kn}(\varepsilon,\varepsilon') = \langle \psi_k^{\mathbf{X}+}(\varepsilon) | \partial_\alpha V_{\mathbf{X}} | \psi_n^{\mathbf{X}+}(\varepsilon') \rangle\,. \tag{4.35}$$

For notational reasons, we introduce the matrix elements

$$K_{kn}^{\alpha\beta}(\varepsilon,\varepsilon') = \left\{ \partial_\alpha V_{\mathbf{X}}^{kn}(\varepsilon,\varepsilon')\, \partial_\beta V_{\mathbf{X}}^{nk}(\varepsilon',\varepsilon) \right\}_s\,. \tag{4.36}$$

With these definitions we are now ready to express the explicit time-dependent noise correlator in Eq. (3.45) in terms of the single-particle scattering states via the function $K_{kn}^{\alpha\beta}(\varepsilon,\varepsilon')$. By calculating the quantum statistical expectation values [Büttiker, 1992] analogous to the derivation of Eq. (3.50), we get

$$\mathbf{D}(t,t') = \int \frac{\mathrm{d}\varepsilon}{2\pi} \int \frac{\mathrm{d}\varepsilon'}{2\pi} \sum_{kn} f_k(\varepsilon)\,[1 - f_n(\varepsilon')]\, e^{i(\varepsilon-\varepsilon')\,(t-t')}\, \mathbf{K}_{kn}(\varepsilon,\varepsilon')\,. \tag{4.37}$$

We continue in Fourier space. We define the Fourier transform of the noise correlator as

$$\tilde{\mathbf{D}}(\omega) = \int \frac{\mathrm{d}\varepsilon}{2\pi} \sum_{kn} f_k\Big(\varepsilon - \frac{\omega}{2}\Big) \Big(1 - f_n\Big(\varepsilon + \frac{\omega}{2}\Big)\Big) \, \mathbf{K}_{kn}\Big(\varepsilon - \frac{\omega}{2}, \varepsilon + \frac{\omega}{2}\Big) \,. \tag{4.38}$$

We make two observations. First, we stress that by referring to the definitions in Eqs. (4.35) and (4.36), the function $\mathbf{K}(\varepsilon, \varepsilon')$ is expressed in terms of scattering states, which are associated with an energy difference $\omega = \varepsilon - \varepsilon'$. We expect the overlaps in Eq. (4.35) to change on energy scales up to the inverse dwell time $1/\tau_D$. A description of the behaviour of the Loschmidt echo in terms of scattering states is valid for large times $\tau \gg \tau_D$. Accordingly, we focus on this limit and evaluate the function $\mathbf{K}_{kn}(\varepsilon - \omega/2, \varepsilon + \omega/2)$ to linear order in $\omega \ll 1/\tau_D$, which captures the long-time behaviour of the Loschmidt echo for $\tau \gg \tau_D$. We note that a description of the Loschmidt echo for microscopic timescales which are smaller than the dwell time is beyond the scope of this chapter.

The second observation deals with the product of the Fermi functions, i.e. $f_k(\varepsilon)\,[1 - f_n(\varepsilon')]$, in the expression of the noise correlator. Here, the out-of-equilibrium conditions enter. We note that the form of the product limits the average energy $\bar{\varepsilon} = (\varepsilon + \varepsilon')/2$ to a region of the order $\Delta\mu_{kn} = \mu_k - \mu_n$ around the averaged chemical potential $\overline{\mu}_{kn} = (\mu_k + \mu_n)/2$. In order to still find an analytical expression, we thus consider the linear response regime of small $\Delta\mu_{kn}\,\tau_D \ll 1$. This allows for an expansion of the function $\mathbf{K}_{kn}(\varepsilon, \varepsilon')$ around $\overline{\mu}_{kn}$ for small deviation $\bar{\varepsilon}$.

With these two observations we can make analytical progress to lowest order in $\tau_D/\tau \ll 1$ and to linear response in $\Delta\mu_{kn}\,\tau_D \ll 1$. An expansion of the function $\mathbf{K}_{kn}(\varepsilon - \omega/2, \varepsilon + \omega/2)$ in Eq. (4.38) with respect to these regimes yields

$$\begin{aligned} \tilde{\mathbf{D}}(\omega) = \int \frac{\mathrm{d}\varepsilon}{2\pi} \sum_{kn} & f_k\Big(\varepsilon - \frac{\omega}{2}\Big) \Big(1 - f_n\Big(\varepsilon + \frac{\omega}{2}\Big)\Big) \\ & \times \left\{\mathbf{K}_{kn}(\overline{\mu}_{kn}) + 2(\varepsilon - \overline{\mu}_{kn})\, \partial^s \mathbf{K}_{kn}(\mu) - \omega\, \partial^a \mathbf{K}_{kn}(\mu)\right\}_s \,. \end{aligned} \tag{4.39}$$

For notational reasons we have introduced the function $\mathbf{K}_{kn}(\varepsilon) = \mathbf{K}_{kn}(\varepsilon, \varepsilon)$ as well as the abbreviations

$$\partial^{s/a} \mathbf{K}_{kn}(\varepsilon) = \frac{1}{2} \left(\partial_\varepsilon \pm \partial_{\varepsilon'}\right) \mathbf{K}_{kn}(\varepsilon, \varepsilon') \Big|_{\varepsilon' = \varepsilon} \tag{4.40}$$

for the symmetric and antisymmetric energy derivatives of the function $\mathbf{K}_{kn}(\varepsilon, \varepsilon')$. The energy integral in Eq. (4.38) can now be analytically performed. We find

$$\tilde{\mathbf{D}}(\omega) = \frac{1}{2\pi} \sum_{kn} \frac{\omega + \Delta\mu_{kn}}{e^{\beta(\omega + \Delta\mu_{kn})} - 1} \, e^{\beta(\omega + \Delta\mu_{kn})} \left(\mathbf{K}_{kn}(\overline{\mu}_{kn}) - \omega\, \partial^a \mathbf{K}_{kn}(\overline{\mu}_{kn})\right) \,. \tag{4.41}$$

In order to be consistent with the linear response regime in $\Delta\mu_{kn}\,\tau_D \ll 1$, the functions $\mathbf{K}_{kn}(\overline{\mu}_{kn})$ and $\partial^a\mathbf{K}_{kn}(\overline{\mu}_{kn})$ needs to be expanded to first order in $\Delta\mu_{kn}\,\tau_D$. In accordance with the previous section, we write the expression in Eq. (4.39) explicitly for two leads with $\mu_L = \mu + \Delta\mu/2$ and $\mu_R = \mu - \Delta\mu/2$ and $\Delta\mu > 0$. This means that the linear response regime requires the replacements

$$\mathbf{K}_{LL}(\mu_L) = \mathbf{K}_{LL}(\mu) + \Delta\mu\,\partial^s\mathbf{K}_{LL}(\mu)\,, \tag{4.42}$$

$$\mathbf{K}_{RR}(\mu_R) = \mathbf{K}_{RR}(\mu) - \Delta\mu\,\partial^s\mathbf{K}_{RR}(\mu)\,, \tag{4.43}$$

$$\partial^a\mathbf{K}_{kn}(\overline{\mu}_{kn}) = \partial^a\mathbf{K}_{kn}(\mu) \tag{4.44}$$

in Eq. (4.41). We note that energy derivatives of the function $\mathbf{K}_{kn}$ are of the order of the Wigner time delay, which is estimated to be of the order of the dwell time. Hence this expansion is indeed valid to linear order in $\Delta\mu\,\tau_D$. Moreover, we observe the relations $\mathbf{K}_{RL}(\mu) = \mathbf{K}_{LR}(\mu)$ and $\partial^a\mathbf{K}_{RL}(\mu) = -\partial^a\mathbf{K}_{LR}(\mu)$ which follows immediately from the definition in Eqs. (4.35) and (4.36). With these considerations we conclude that the symmetric noise correlator $\mathbf{D}(\omega) = [\tilde{\mathbf{D}}(\omega) + \tilde{\mathbf{D}}(-\omega)]/2$ can be written as

$$\begin{aligned}
\mathbf{D}(\omega) = {}& \frac{1}{4\pi}\,\omega\,\coth\left(\frac{\beta\omega}{2}\right)\Big[\mathbf{K}_{LL}(\mu) + \mathbf{K}_{RR}(\mu) + \Delta\mu\Big(\partial^s\mathbf{K}_{LL}(\mu) - \partial^s\mathbf{K}_{RR}(\mu)\Big)\Big] \\
& + \frac{1}{4\pi}\left((\omega+\Delta\mu)\,\coth\left(\frac{\beta(\omega+\Delta\mu)}{2}\right) + (\omega-\Delta\mu)\,\coth\left(\frac{\beta(\omega-\Delta\mu)}{2}\right)\right)\mathbf{K}_{LR}(\mu) \\
& + \frac{\omega}{4\pi}\left((\omega-\Delta\mu)\,\coth\left(\frac{\beta(\omega-\Delta\mu)}{2}\right) - (\omega+\Delta\mu)\,\coth\left(\frac{\beta(\omega+\Delta\mu)}{2}\right)\right)\partial^a\mathbf{K}_{LR}(\mu)
\end{aligned} \tag{4.45}$$

since $\coth x = (e^{2x}+1)/(e^{2x}-1)$. The coefficient in the above equation can be related to different terms describing the fluctuations and the dissipation of a heavy particle in a quantum environment. In appendix A we show that

$$\frac{1}{4\pi}\sum_{kn}\mathbf{K}_{kn}(\mu) = \boldsymbol{\gamma}_0^{eq}\,, \tag{4.46}$$

$$\frac{1}{2\pi}\mathbf{K}_{LR}(\mu) = \frac{1}{4\pi}\left(\mathbf{K}_{LR}(\mu) + \mathbf{K}_{RL}(\mu)\right) = \frac{\mathbf{D}_{[0,\Delta\mu]}}{\Delta\mu}\,, \tag{4.47}$$

$$\frac{\Delta\mu}{4\pi}\left(\partial^s\mathbf{K}_{LL}(\mu) + \partial^s\mathbf{K}_{RR}(\mu)\right) = \boldsymbol{\gamma}_1^{eq}\,, \tag{4.48}$$

$$\frac{\Delta\mu}{4\pi}\left(\partial^a\mathbf{K}_{RL}(\mu) - \partial^a\mathbf{K}_{LR}(\mu)\right) = \boldsymbol{\gamma}_1^{neq}\,. \tag{4.49}$$

With these identifications we immediately deduce from Eq. (4.45) the desired expression of the symmetrised noise correlator in Eq. (4.26).

4.6. Derivation within Green function formalism

Next, we present the derivation of the expression of the noise correlator in Eq. (4.26) within the methods of non-equilibrium Green functions. Since Eq. (4.26) is of crucial importance as it defines the decay of the Loschmidt echo and gives the connection to the adiabatic reaction forces, we present this alternative derivation here. Moreover, the formulation in terms of Green function allows for a more intuitive treatment of applications to specific models, which we illustrate in the next section. To this end, we write the initial Hamiltonian as

$$\mathcal{H}_i = \mathcal{H}_{\mathbf{X}} + \mathcal{H}_L + \mathcal{H}_D + \mathcal{H}_T \,, \tag{4.50}$$

similar to the Hamiltonian in Eq. (3.70). The particular terms are defined in Eqs. (3.71) to (3.74). Moreover, we define the *time-dependent* Green functions of the dot

$$(\mathcal{G}_D)^R_{mm'}(t,t') = -i\theta(t-t')\,\langle\{d_m(t), d^\dagger_{m'}(t')\}\rangle \,, \tag{4.51}$$
$$(\mathcal{G}_D)^A_{mm'}(t,t') = i\theta(t'-t)\,\langle\{d_m(t), d^\dagger_{m'}(t')\}\rangle \,, \tag{4.52}$$
$$(\mathcal{G}_D)^>_{mm'}(t,t') = -i\,\langle d_m(t)\, d^\dagger_{m'}(t')\rangle \,, \tag{4.53}$$
$$(\mathcal{G}_D)^<_{mm'}(t,t') = i\,\langle d^\dagger_{m'}(t')\, d_m(t)\rangle \,, \tag{4.54}$$

where the notation $\{\ldots,\ldots\}$ denotes the anti-commutator and the expectation values are taken with respect to the Hamiltonian $\mathcal{H}_i$. Our aim is to find an expression for the noise correlator defined in Eq. (3.45) in terms of Green functions in Fourier space. We note that for stationary states the above Green functions depend on the time difference $t-t'$. With the above definitions we can then write the noise correlator in time space as [Bode et al., 2012b]

$$\begin{aligned} D_{\alpha\beta}(t-t') &= \mathrm{tr}\Big\{\Lambda_\alpha\, \mathcal{G}^>_D(t-t')\,\Lambda_\beta\, \mathcal{G}^<_D(t'-t)\Big\}_s \\ &= \int \frac{\mathrm{d}\varepsilon}{2\pi}\int \frac{\mathrm{d}\varepsilon'}{2\pi}\, e^{i(\varepsilon-\varepsilon')(t-t')}\,\mathrm{tr}\Big\{\Lambda_\alpha\, \mathcal{G}^>_D(\varepsilon)\,\Lambda_\beta\, \mathcal{G}^<_D(\varepsilon')\Big\}_s \end{aligned} \tag{4.55}$$

with $\Lambda_\alpha = \partial_\alpha h_0$. The functions $\mathcal{G}^>_D(\varepsilon)$ and $\mathcal{G}^<_D(\varepsilon')$ represent the Fourier transforms of the corresponding time-dependent Green function of the dot. From Eq. (4.55) we find for the Fourier transform of the fluctuating force

$$\begin{aligned} \tilde{D}_{\alpha\beta}(\omega) &= \int \mathrm{d}\Delta t\, e^{i\omega\Delta t}\, D_{\alpha\beta}(\Delta t) \\ &= \int \frac{\mathrm{d}\varepsilon}{2\pi}\,\mathrm{tr}\Big\{\Lambda_\alpha\, \mathcal{G}^>_D\Big(\varepsilon-\frac{\omega}{2}\Big)\,\Lambda_\beta\, \mathcal{G}^<_D\Big(\varepsilon+\frac{\omega}{2}\Big)\Big\}_s \\ &= \int \frac{\mathrm{d}\varepsilon}{2\pi}\,\mathrm{tr}\Big\{\Lambda_\alpha\, G^>_D\Big(\varepsilon-\frac{\omega}{2}\Big)\,\Lambda_\beta\, G^<_D\Big(\varepsilon+\frac{\omega}{2}\Big)\Big\}_s \,. \end{aligned} \tag{4.56}$$

In the last step we have replaced the time-dependent Green functions by the frozen *adiabatic* Green functions [Bode et al., 2012b]. This replacement is justified as the fluctuation-dissipation theorem is already satisfied after this replacement, cf. chapter 3. The retarded and advanced frozen Green function can be expressed in terms of the respective retarded and advanced self-energies $\Sigma^{R/A}(\varepsilon) = \mp i \sum_k \Gamma_k(\varepsilon)$ with $\Gamma_k(\varepsilon) = W^\dagger(\varepsilon)\,\Pi_k\,W(\varepsilon)/2$ and projector $\Pi_k(\varepsilon) = |\phi_k(\varepsilon)\rangle\langle\phi_k(\varepsilon)|$ onto lead k. The coupling matrix W is defined via the tunnelling Hamiltonian in Eq. (3.74). We stress the appearance of the factor $1/\sqrt{2\pi}$ in the definition of the coupling matrix, that is $W_{km}(\varepsilon) = \langle\phi_k(\varepsilon)|\,W\,|m\rangle/\sqrt{2\pi}$, where m defines the dot level. In particular, we have [Jauho et al., 1994]

$$G_D^{R/A}(\varepsilon) = \frac{1}{\varepsilon - h_0(\mathbf{X}) - \Sigma^{R/A}}\,. \tag{4.57}$$

The frozen lesser and greater Green function, which appear in the expression of the noise correlator, can be related to the adiabatic retarded and advanced Green function with the aid of the Langreth rule [Jauho et al., 1994]

$$G_D^<(\varepsilon) = G_D^R(\varepsilon)\,\Sigma^<(\varepsilon)\,G_D^A(\varepsilon)\,, \tag{4.58}$$
$$G_D^>(\varepsilon) = G_D^R(\varepsilon)\,\Sigma^>(\varepsilon)\,G_D^A(\varepsilon)\,. \tag{4.59}$$

Here, we have introduced the lesser and greater self-energies

$$\Sigma^<(\varepsilon) = i\sum_k f_k(\varepsilon)\,W^\dagger(\varepsilon)\,\Pi_k(\varepsilon)\,W(\varepsilon) \tag{4.60}$$
$$\Sigma^>(\varepsilon) = -i\sum_k (1 - f_k(\varepsilon))\,W^\dagger(\varepsilon)\,\Pi_k(\varepsilon)\,W(\varepsilon)\,. \tag{4.61}$$

In order to simplify the notation we further define the function

$$\begin{aligned}\tilde{K}_{kn}^{\alpha\beta}(\varepsilon,\varepsilon') = \mathrm{tr}\Big\{&\Lambda_\alpha\,G_D^R(\varepsilon)\,W^\dagger(\varepsilon)\,\Pi_k(\varepsilon)\,W(\varepsilon)\,G_D^A(\varepsilon)\\ &\times\Lambda_\beta\,G_D^R(\varepsilon')\,W^\dagger(\varepsilon')\,\Pi_n(\varepsilon')\,W(\varepsilon')\,G_D^A(\varepsilon')\Big\}_s\,.\end{aligned} \tag{4.62}$$

We can now continue with the evaluation of noise correlator in Eq. (4.56). A substitution of the lesser and greater Green function in Eqs. (4.58) and (4.59) into the expression of the noise correlator in Fourier space, cf. Eq. (4.56), then gives

$$\tilde{\mathbf{D}}(\omega) = \int\frac{\mathrm{d}\varepsilon}{2\pi}\sum_{kn} f_k\Big(\varepsilon - \frac{\omega}{2}\Big)\,\Big(1 - f_n\Big(\varepsilon + \frac{\omega}{2}\Big)\Big)\,\tilde{\mathbf{K}}_{kn}\Big(\varepsilon - \frac{\omega}{2}, \varepsilon + \frac{\omega}{2}\Big)\,. \tag{4.63}$$

We thus find an analogous expression of the noise correlator compared to the previously found expression in Eq. (4.38), which has been derived within the methods of scattering theory. The only difference, however, is that the function $\mathbf{K}_{kn}^{\alpha\beta}(\varepsilon,\varepsilon')$

is replaced by the function $\tilde{\mathbf{K}}_{kn}^{\alpha\beta}(\varepsilon,\varepsilon')$. In order to evaluate the above expression of the noise correlator, we can follow the same steps as in the previous section. To leading order in $\tau_D/\tau \ll 1$ and linear order in $\Delta\mu_{kn}\,\tau_D \ll 1$, we can expand the function $\tilde{\mathbf{K}}_{kn}(\varepsilon-\frac{\omega}{2},\varepsilon+\frac{\omega}{2})$ in small ω and to first order in ε around $\varepsilon=\overline{\mu}_{kn}$. This yields an expression analogous to Eq. (4.45) where each function $\mathbf{K}_{kn}$ is replaced by $\tilde{\mathbf{K}}_{kn}$. Hence, for a derivation of the desired Eq. (4.26), we are left with identifying the friction coefficient and the zero-frequency noise correlator in terms of the function $\tilde{\mathbf{K}}$. Indeed, in appendix B we show that

$$\frac{1}{4\pi}\sum_{kn}\tilde{\mathbf{K}}_{kn}(\mu)=\boldsymbol{\gamma}_0^{eq} \tag{4.64}$$

$$\frac{1}{2\pi}\tilde{\mathbf{K}}_{LR}(\mu)=\frac{1}{4\pi}\left(\tilde{\mathbf{K}}_{LR}(\mu)+\tilde{\mathbf{K}}_{RL}(\mu)\right)=\frac{\mathbf{D}_{[0,\Delta\mu]}}{\Delta\mu} \tag{4.65}$$

$$\frac{\Delta\mu}{4\pi}\left(\partial^s\tilde{\mathbf{K}}_{LL}(\mu)+\partial^s\tilde{\mathbf{K}}_{RR}(\mu)\right)=\boldsymbol{\gamma}_1^{eq} \tag{4.66}$$

$$\frac{\Delta\mu}{4\pi}\left(\partial^a\tilde{\mathbf{K}}_{RL}(\mu)-\partial^a\tilde{\mathbf{K}}_{LR}(\mu)\right)=\boldsymbol{\gamma}_1^{neq} \tag{4.67}$$

to linear response in $\Delta\mu\tau_D$, which gives the connection to the adiabatic reaction forces appearing in the Langevin equation. Moreover, we explicitly show in appendix B the equivalence between the derivation in terms of Green functions and the derivation within the methods of scattering theory in this appendix.

4.7. Example: one-level model coupled to one vibrational mode

Now, we show how to apply the above formulas to a concrete example. We consider a one-level system which couples to one classical degree of freedom and is attached to two electron reservoirs. This model serves as a minimal model to illustrate the above results and their validity. In the context of nanoelectromechanical systems, this model can for instance describe a quantum dot confined on a nanotube which is in contact with two electronic leads. The classical coordinate corresponds to a one-dimensional vibrational mode of the tube in this picture. We focus on the analysis of the sudden quench Loschmidt echo, since the behaviour of the slow quench dynamics is qualitatively the same and differs only by the protocol-dependent constants listed in Table 4.1.

We denote the classical degree of freedom in one dimension by $X=X(t)$ and consider the Hamiltonian in Eq. (4.50) including the definitions in Eqs. (3.71) to (3.74).

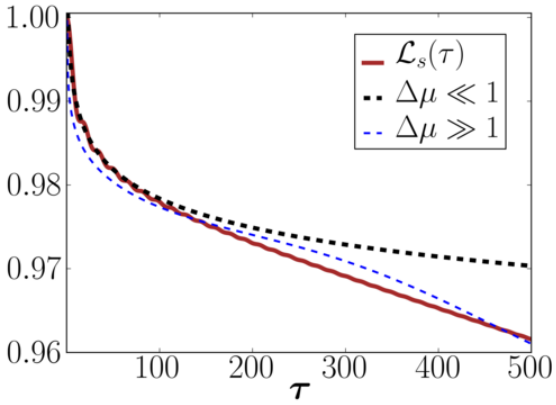

Figure 4.2.: Plot of the Loschmidt echo in linear response, i.e. Eq. (4.29), (solid red line) and comparison to the short-time dynamics in Eq. (4.30) (thick, dashed black line) and to the long-time dynamics in Eq. (4.31) (thin, dashed blue line). Parameters: $\Gamma_L = 0.3$, $\Gamma_R = 0.1$, $\tau_D = 1/(\Gamma_L+\Gamma_R) = 2.5$, $\Delta\mu = 0.1$, $\tau_{char} = 30.37$ (calculated), $\varepsilon_0 = 0$, $\delta X = 0.1$, $X = -0.3$. All distances are in units of $\lambda/(M\omega_0^2)$ and energies and inverse times are in units of $\lambda^2/(M\omega_0^2)$.

We stress that the dot's Hamiltonian $\mathcal{H}_D = h_0(X)\, d^\dagger\, d$ depends on the classical coordinate which expresses the coupling of the electrons in the dot to the classical degree of freedom. In this example we treat the case of a linear coupling so that

$$h_0(X_t) = \varepsilon_0 + \lambda\, X_t\,, \tag{4.68}$$

where λ defines the strength of the coupling. We introduce the tunnelling amplitudes, Γ_L and Γ_R, which describe electronic tunnelling between the dot and the left and right lead, respectively. In the wide-band approximation we can assume that the tunnelling amplitudes are independent of the energy so that the coupling matrix W is energy independent as well and reads

$$W = \begin{pmatrix} \sqrt{2\,\Gamma_L} \\ \sqrt{2\,\Gamma_R} \end{pmatrix}. \tag{4.69}$$

From the coupling matrix we can deduce the retarded and advanced self-energy as $\Sigma^{R/A} = \mp i(\Gamma_L + \Gamma_R)$. With the aid of Eq. (4.57), we then conclude that the retarded and advanced Green function can be written as

$$G_D^{R/A}(\varepsilon) = \frac{1}{\varepsilon - h_0(X) \pm i(\Gamma_L + \Gamma_R)}\,. \tag{4.70}$$

By referring to the Mahaux-Weidenmüller formula [Aleiner et al., 2002] we get an expression of the frozen scattering matrix from the retarded and advanced Green

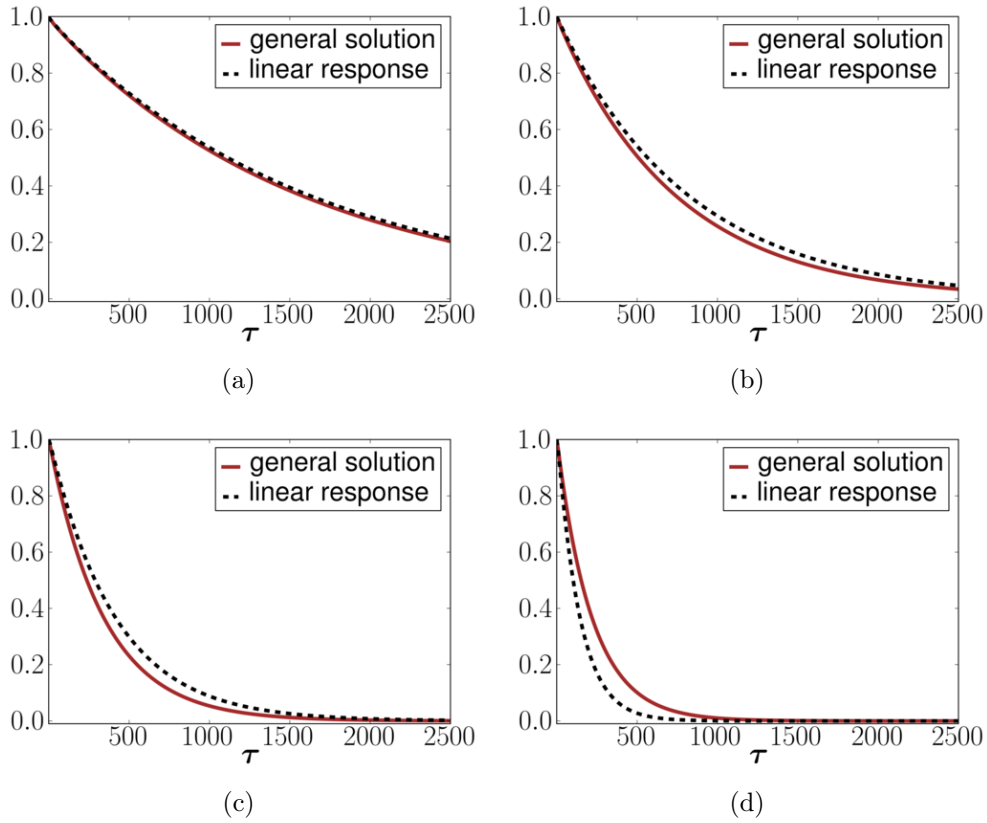

Figure 4.3.: Illustration of the validity of the linear response solution in Eq. (4.29) (dashed black line) by comparing to the general solution (solid red line). The general solution is obtained by a direct evaluation of the noise correlator in Eq. (4.38) or (4.63) for (a) $\Delta\mu = 0.2$, (b) $\Delta\mu = 0.4$, (c) $\Delta\mu = 0.8$ and (d) $\Delta\mu = 2.4$. Other parameters are the same as in Fig. 4.2.

function. We find

$$S_t(\varepsilon) = 1 - i\, W(\varepsilon)\, G_D^R(\varepsilon)\, W^\dagger(\varepsilon) \tag{4.71}$$

$$= \mathbb{1} - \frac{2i}{\varepsilon - \varepsilon_0 - \lambda X + i\,(\Gamma_L + \Gamma_R)} \begin{pmatrix} \Gamma_L & \sqrt{\Gamma_L \Gamma_R} \\ \sqrt{\Gamma_L \Gamma_R} & \Gamma_R \end{pmatrix}, \tag{4.72}$$

where we have dropped the index t of the frozen scattering matrix to simplify the notation. We note that the A-matrix vanishes for the case of a one-dimensional classical degree of freedom so that $\boldsymbol{\gamma}^{neq} = 0$ [Bode et al., 2012b]. Consequently, the behaviour of the Loschmidt echo is completely determined by the frozen scattering matrix, since the adiabatic reaction forces can be calculated from the S-matrix alone.

We illustrate the result of the Loschmidt echo in Eq. (4.29), which is valid to linear response in the bias voltage, in Fig. 4.2 as a function of time. A comparison to the short-time dynamics, cf. Eq. (4.30), and the long time dynamics, cf. Eq. (4.31), shows consistency in the respective limit. The dwell time in the present model is given by the inverse electronic tunnelling rates, that is $\tau_D = 1/(\Gamma_L + \Gamma_R)$. We stress that the use of scattering theory limits our results to timescales which are larger than the dwell time. We chose an asymmetric coupling $\Gamma_L \neq \Gamma_R$ to guarantee that $\boldsymbol{\gamma}_1^{eq}$ is non-zero.

The one-level model coupled to a one-dimensional classical degree of freedom allows for a comparison of the linear response solution in Eq. (4.29) and the general non-linear response solution, which is not restricted to small $\Delta\mu\,\tau_D$, at zero temperature. The general solution can be obtained by a direct calculation of the coloured noise correlator in Fourier space, that is Eq. (4.38) in terms of scattering states or Eq. (4.63) in terms of Green functions. The behaviour of the Loschmidt echo is then obtained by referring to Eq. (4.12). The matrix $\partial_X V_X(\varepsilon, \varepsilon')$ in Eq. (4.35), which is necessary to evaluate the coloured noise correlator, can be expressed in terms of the retarded Green function of the dot as

$$\partial_X V_X^{kn}(\varepsilon, \varepsilon') = \left[W \cdot G_D^R(\varepsilon)^\dagger\, \partial_X h_0(X)\, G_D^R(\varepsilon') \cdot W^\dagger\right]_{kn} , \tag{4.73}$$

where the product of the coupling matrices is an outer product. This can bee seen by recalling that $\partial_X V_X = \Pi_D\, \partial_X h_0(X)\, \Pi_D$ and by substituting Eq. (3.76) into Eq. (4.35). We note that Eq. (4.12) is general in the sense that it is neither restricted to to large times $\tau \gg \tau_D$ nor to the linear response regime $\Delta\mu\,\tau_D \ll 1$. We depict a comparison of the general solution and the linear response solution in Fig. 4.3 for different values of $\Delta\mu$ keeping the dwell time constant. Indeed, Fig. 4.3 shows that the linear response solution is consistent with the general solution for small $\Delta\mu\,\tau_D \ll 1$.

4.8. Conclusion

In this chapter we have expressed the decay of the fidelity amplitude and its absolute square value, the Loschmidt echo, as microscopic quantities in terms of the mesoscopic reaction forces, which describe the motion of a heavy particle in a quantum fermionic environment. Our results are valid for small changes of the position of the heavy particle. By the Anderson orthogonality it is known that small changes of the scattering potential felt by the fermionic environment, which are induced by small displacements of a classical particle, can have drastic consequences for large

quantum systems. For a finite system the Anderson orthogonality exponent has been related to the friction coefficient in equilibrium in the small-distance limit in Ref. [Schönhammer, 1991]. Motivated by nanoelectromechanical systems, we have generalised this relation to out-of-equilibrium situations which possess a continuous energy spectrum.

The fidelity amplitude and the Loschmidt echo are dynamical quantities of the Anderson orthogonality. Generally allowing for both, a slow and a sudden quench scenario, we have expressed their dependence on time in terms of the coloured noise correlator of the classical degree of freedom. At zero temperature without an applied bias voltage the fluctuation-dissipation theorem then predicts a power-law decay of the Loschmidt echo at times larger than the dwell time with an exponent controlled by the dissipation. The power-law behaviour reflects the Anderson orthogonality catastrophe. This behaviour is inconsistent with a noise correlator which is delta-correlated in time as white noise induces an exponential decay. In this sense, the power-law decay signals the breakdown of the semiclassical description in terms of the Langevin equation in the Markovian limit since the classical noise correlator is zero in equilibrium in the zero temperature limit.

Moreover, at times smaller than the inverse bias voltage, we have shown that the Loschmidt echo of the sudden quench scenario is the absolute square value of the Loschmidt echo characterising a slow quench. For finite quantum systems this relation has recently been derived in the infinite time limit within a Luttinger Liquid model in Refs. [Dóra et al., 2013, Sachdeva et al., 2014]. In this chapter, we have found this relation for non-interacting infinite systems and finite times.

At long times, which are larger than the inverse applied bias voltage, we have shown to linear order in the bias voltage that the power-law decay of the Loschmidt echo is exponentially suppressed with a strength controlled by the shot-noise fluctuations. This decay is in agreement with assuming white noise to leading order. The power-law behaviour characterises the next-order correction term to the white-noise contribution where have shown that the power-law exponent is determined by a competition between dissipation and fluctuations. Due to this competition the power-law exponent can change its sign when the system is driven out of equilibrium, a phenomenon called anti-orthogonality [Segal et al., 2007].

Small but finite temperatures imply a Gaussian behaviour of the Loschmidt echo. When the temperature is large and the classical limit is reached, we have recovered an exponential decay of the Loschmidt echo which stems from the classical version of the fluctuation-dissipation theorem. Finally, we have shown how to apply the derived expressions to a concrete example by considering a single level coupled to

one vibrational mode. This example describes for instance a quantum dot confined on a nanotube and thus illustrates the applicability to nanoelectromechanical systems.

5. Atomic-scale gate control of a single-molecule transistor by individual atoms

In this chapter we present a theoretical description and explanation of the experiment performed in Ref. [Martínez-Blanco et al., 2015]. The experiment deals with a system miniaturised to its ultimate limit, that is a transistor made up of a single organic molecule. The set-up is schematically depicted in Fig. 1.8 and consists of a single molecule on a semiconductor surface with adjacent STM tip. The source and drain electrodes are formed by the surface and the STM tip, respectively, and positively charged atoms on the surface in the vicinity of the molecule serve as a gate electrode by inducing a local electrostatic potential on the molecule. The current running through the system when applying a bias voltage between the surface and the tip is then controlled by repositioning the charges on the surface.

Three-terminal electronic devices on the molecular scale have recently been realised using electron-beam lithography [Park et al., 2000, Liang et al., 2002, Kubatkin et al., 2003, Yu and Natelson, 2004, Roch et al., 2008, Song et al., 2009, Leturcq et al., 2009] and gated break junctions [Champagne et al., 2005, Perrin et al., 2013] in the context of spin correlations [Liang et al., 2002, Roch et al., 2008], vibronic excitations [Park et al., 2002, Song et al., 2009, Leturcq et al., 2009] and Coulomb blockade [Park et al., 2002, Liang et al., 2002, Champagne et al., 2005, Leturcq et al., 2009, Perrin et al., 2013]. Atomic-scale gating however is not possible with these approaches. The experiment in Ref. [Martínez-Blanco et al., 2015] uses scanning tunnelling microscopy as a basic mechanism for gating on the atomic and molecular scale [Stroscio and Eigler, 1991] and thus provides a new technique towards engineering and controlling single-molecule electronic devices.

Concerning the theoretical description, this chapter is an example of the incoherent transport limit where transport is described by classical probabilities. Since decreasing the size of an electronic device towards the molecular scale means that the average level spacing of the system increases, we consider the limit where tun-

nelling rates are much smaller than both the level spacing and the temperature. Consequently, electrons tunnel sequentially through the device which is treated in analogy to a semiconductor quantum dot [Kouwenhoven et al., 2001]. This is opposed to the mesoscopic systems described in the previous chapters where we assume coherent transport.

The present chapter is based on Ref. [Martínez-Blanco et al., 2015]. The experiment was performed by J. Martínez-Blanco, C. Nacci and S. Fölsch. M. Thomas, E. Locane, F. von Oppen and P. Brouwer provided the theoretical description and modelling.[1] Experimental data, which is used in this chapter, has been provided by S. Fölsch and J. Martínez-Blanco.

5.1. Experimental set-up and observations

The main ingredients of the molecular transistor in Ref. [Martínez-Blanco et al., 2015] constitute the planar π-conjugated molecules free-base phthalocyanine (H_2Pc) and copper phthalocyanine (CuPc) whose structure is shown in Fig. 5.1(a). The molecules are adsorbed on an indium arsenide InAs(111)A-(2×2) surface where the centre of the molecule is positioned above an indium (In) vacancy site, cf. Fig. 5.1(b). By construction, the InAs surface contains a low coverage of approximately 0.005 monolayers of additional native donor-type In adatoms which are positively charged. Since van der Waals interactions dominate the surface binding with no charge transfer between the surface and the molecule, both the molecule and the In adatoms are weakly bound to the In vacancies and can thus be repositioned by attractive force interactions with the STM tip. This allows for controlling the induced electrostatic potential, ϕ, of the molecule by changing the distance between molecule and charged In adatoms. The experimental set-up thus describes a three-terminal molecular transistor where the STM tip and the surface act as electrodes and the In adatoms serve as an analogue of a gate electrode.

The principal operating mechanism of the molecular transistor is illustrated in Figs. 5.1(c) and (d). Figure 5.1(c) shows topography images of two collected trimers of In adatoms and the H_2Pc molecule in a distant position (right panel) and in a position between the trimers (left panel). The reduced apparent height of the molecule in the centre of the trimers as compared to the remote position indicates that the molecule is charged when the molecule is in close vicinity of the trimers.

[1] Using density functional theory S. C. Erwin predicted the molecular orientations for the different charge states.

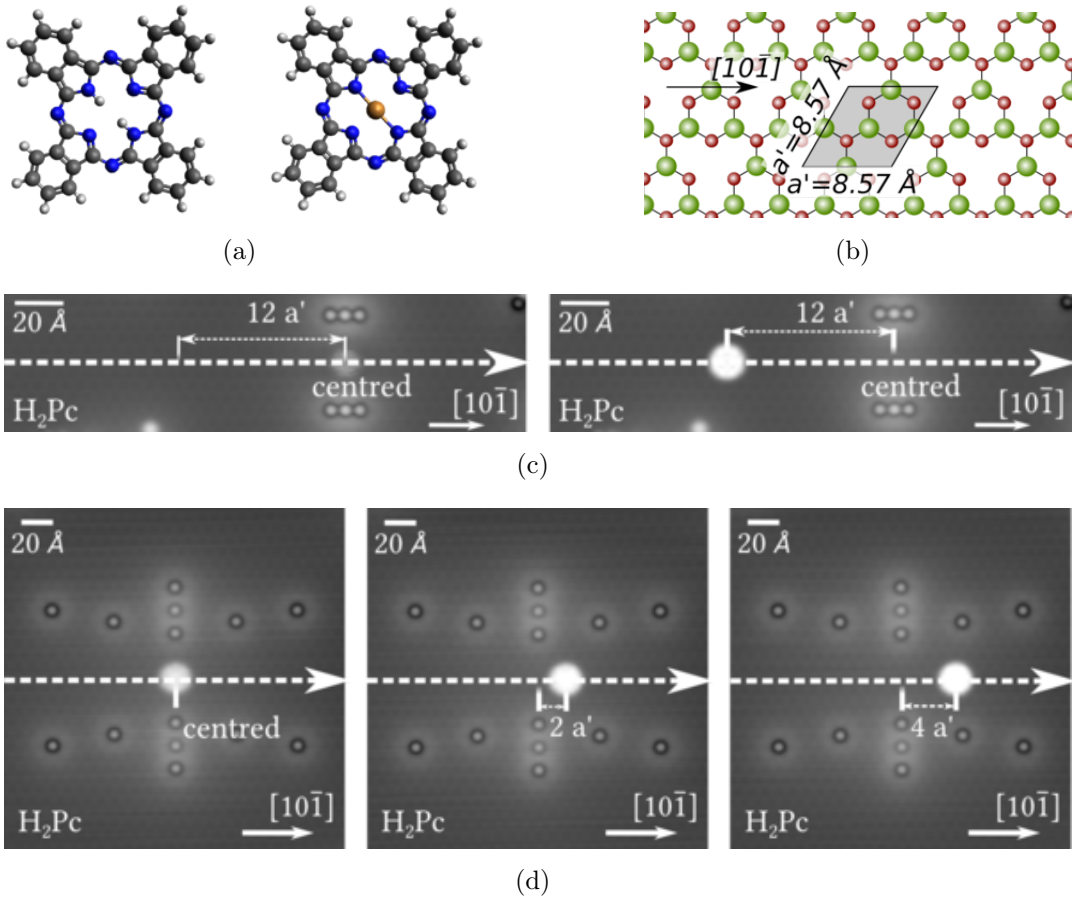

Figure 5.1.: (a) Molecular structure of free-base phthalocyanine (left) and copper phthalocyanine (right) with hydrogen (light grey), carbon (dark grey), nitrogen (blue), copper (brown). (b) Structure of the InAs(111)A-(2×2) surface. The indium atoms (green) form the topmost layer and the arsenic atoms (red) the second layer. The lattice constant of the (2×2) In-vacancy reconstruction is $a' = 8.57$ Å. (c,d) STM topography image of the set-up. (c) The H_2Pc molecule (large white circle) is positioned in the centre of the two trimers of In adatoms (left panel) and moved along the dashed arrow to a distance of $12a'$ away from the centred position (right panel). The apparent height of the molecule is 2.2 Å in the position away from the centre and 0.9 Å in between the trimers. This indicates the charged state of the molecule in the centred position. The STM images were taken at 50 pA and 0.5 V. (d) The H_2Pc molecule is moved along the dashed arrow in between In adatoms forming a corral. The molecule is positioned in the centre (left panel), and $2a'$ (middle panel) and $4a'$ (right panel) away from it. The values of the induced potential in (d) correspond to the values of ϕ in Fig. 5.2. These STM topography images were taken at 100 pA and 0.65 V.

In fact, moving the molecule towards the In adatoms shifts the lowest unoccupied molecular orbital (LUMO) of the phthalocyanine molecule below the Fermi energy, which eventually charges the molecule. This increases the local work function and thus the local tunnelling barrier so that a charged molecule is seen with a reduced apparent height [Swart et al., 2011, Fernández-Torrente et al., 2012].

In order to get a more fine-tuned stepwise increase of the local induced potential ϕ, which enables further insights into the process of charging the molecule, different assemblies of indium adatoms have been constructed. Figure 5.1(d) shows a corral assembly which induces an electrostatic potential which is highest at the centre of the corral and decreases approximately linearly with increasing distance along the dashed arrow drawn in Fig. 5.1(d). This figure shows three different positions of the H_2Pc molecule, which gives rise to three different gating potentials ϕ. The resulting current I at these gatings as a function of the applied bias voltage, V_b, is depicted in Figs. 5.2(a)-(c) by keeping the STM tip fixed above the molecule. With increasing potential ϕ a switch between two I-V_b curves with different slopes is clearly visible in all graphs where at intermediate ϕ the transition reveals a hysteretic behaviour. The different curves indicate the different charge states of the molecule. In particular, the steeper slope corresponds to the neutral state since a higher potential charges the molecule negatively. A similar characteristic behaviour of the hysteresis has been observed in the context of bistable switching of phthalocyanine molecules on layers of sodium chloride which are grown on copper substrates [Swart et al., 2011]. In the present experiment, however, the hysteresis is only observed at low bias voltages, while at higher bias voltages a dynamical crossover between the neutral and the charged state is observed. The CuPc molecule shows analogous behaviour. There, the crossover is observed at a gating potential which is approximately 45 mV larger as compared to the H_2Pc molecule. For both molecules the coercivity, that is the width of the hysteresis, varies when changing the ramping speed of the bias voltage. Figure 5.2(d) shows this dependence, where the error bars result from statistical fluctuations of subsequent measurements of the coercivity.

Figure 5.3 depicts STM images for parameters where the molecule is bistable. Different ground-state conformations are observed for the respective charge states of the molecule. In principle, the three equivalent conformers, $\{M^0\}$, of the neutral H_2Pc molecule are observed for which the molecular lobes are parallel or perpendicular to any of the three $\langle 110 \rangle$ in-plane directions [Nacci et al., 2012]. At higher potential ϕ, when the H_2Pc molecule is negatively charged, STM images reveal six equivalent conformational states, $\{M^-\}$. Figure 5.3 shows one conformation corresponding to the neutral molecule and two conformers corresponding to the negative charge state. The topography images indicate that the transition between the two different conformational states is given by an in-plane rotation of the molecule in-

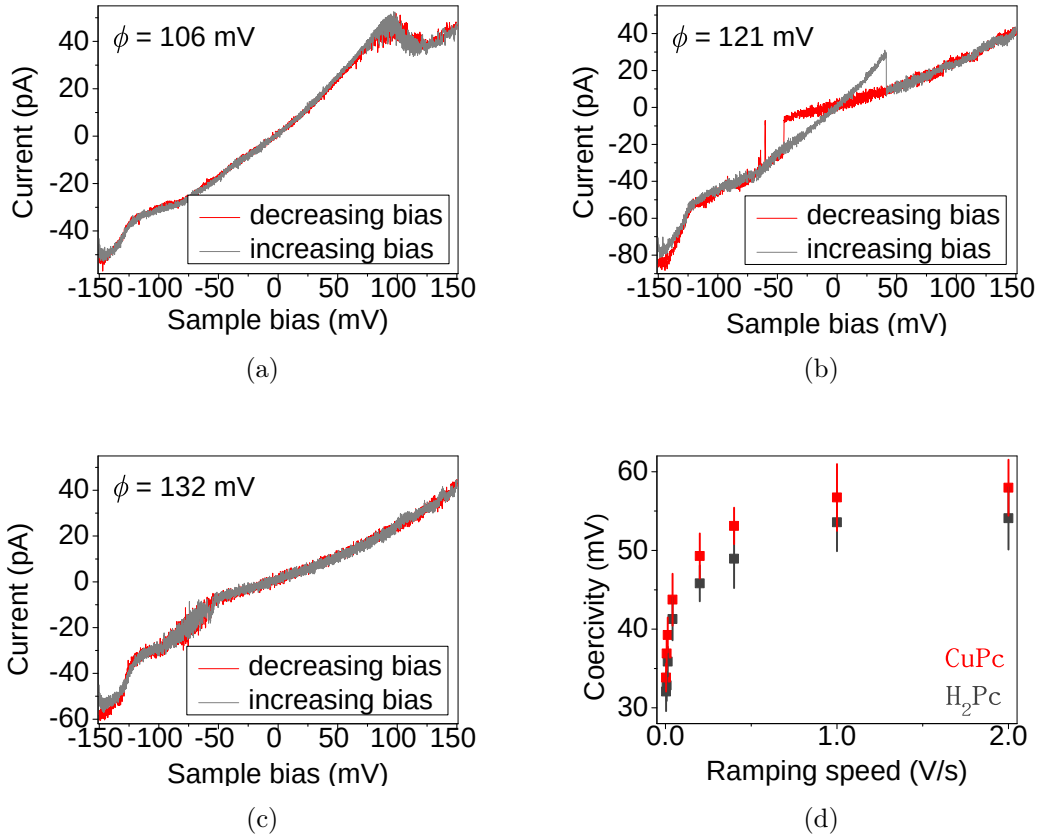

Figure 5.2.: Current as a function of bias voltage (I-V_b curves) at constant (a) $\phi = 106\,\mathrm{mV}$, (b) $\phi = 121\,\mathrm{mV}$ and (c) $\phi = 132\,\mathrm{mV}$ corresponding to the positions shown in Fig. 5.1(d). The STM tip is held fixed above the H_2Pc molecule. At intermediate ϕ the current switches between two different curves in form of a hysteresis. The hysteresis is quenched and the crossover is shifted to different biases at higher and lower ϕ. At a bias voltage of approximately $-125\,\mathrm{mV}$ a kink in all figures indicates an InAs surface state [Fölsch et al., 2014] which is confined by the charged indium adatoms. (d) Coercivity as a function of ramping speed for the H_2Pc molecule (dark grey) and the CuPc molecule (red) at constant $\phi = 125\,\mathrm{mV}$ and $\phi = 170\,\mathrm{mV}$, respectively.

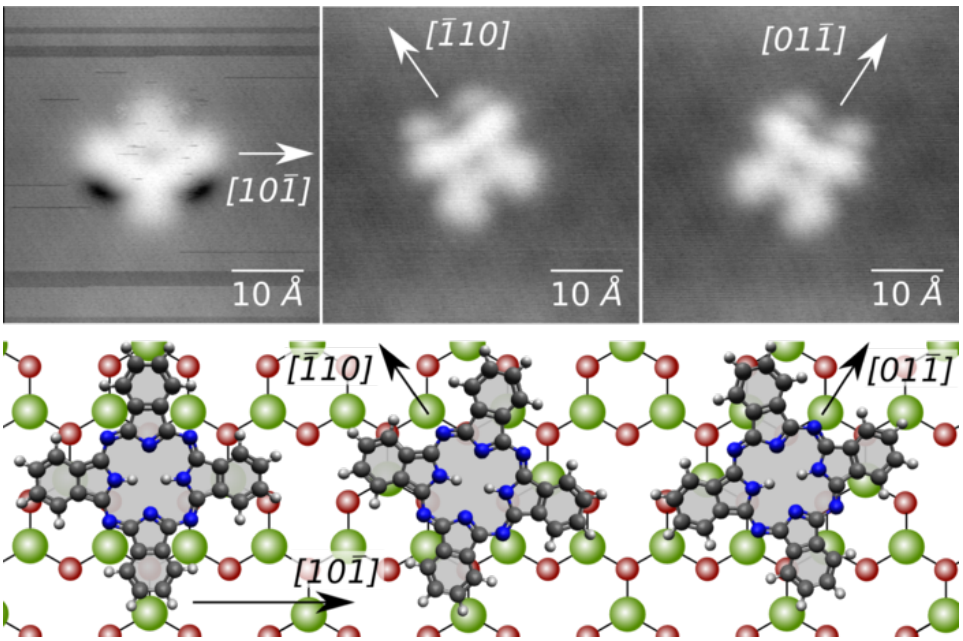

Figure 5.3.: Upper panels: STM images of the H_2Pc molecule on the InAs(111)A-(2×2) surface at 50 pA and −60 mV. The negatively charged molecule (middle and right panel) is rotated by ±15° and a slightly tilted and shifted compared to the neutral molecule (left panel). The horizontal stripes in the left STM image are due to a charging of the molecule while the image was taken. The CuPc molecule show an analogous behaviour. Lower panel: Sketch of the molecular conformations corresponding to the above STM images. Only the in-plane rotations are depicted.

cluding a tilt or a slow shift of the molecule in the lateral direction [Schuler et al., 2013]. For the CuPc molecule analogous conformers are observed.

The observed current through the molecule dramatically depends on the induced electrostatic potential. Figure 5.4(a) depicts the measured I-V_b curves in form of a diagram for a larger range of ϕ with fixed STM tip above a single CuPc molecule. In agreement with the description of sequential tunnelling through a single level attached to two leads [Nazarov and Blanter, 2010], a conductance gap is observed for each ϕ which decreases when the gate voltage shifts the level closer to the Fermi energy. The deduced normalised conductance map in Fig. 5.4(b) elucidates this behaviour. The strong peaks in the normalised conductance as a function of V_b and ϕ correspond to the values where the LUMO enters the conduction window and thus indicates when the sequential tunnelling sets in. Remarkably, however, the normalised conductance map shows a pronounced gap of approximately 600 mV

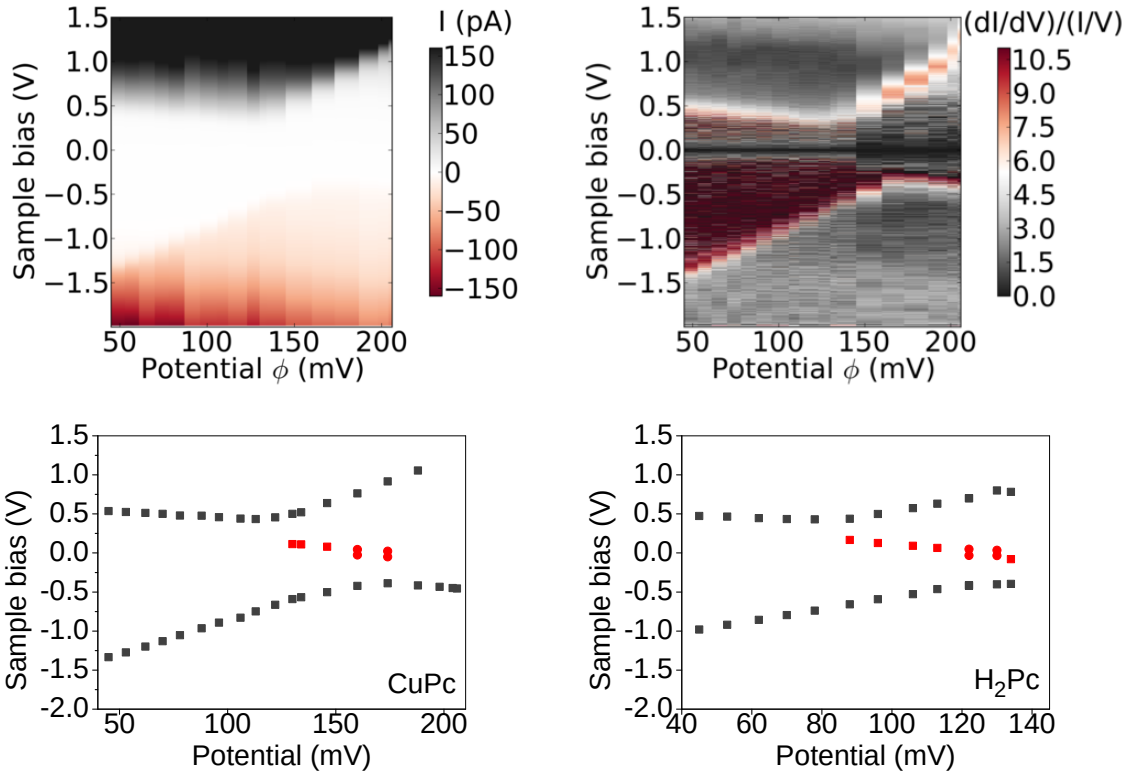

Figure 5.4.: (a) Current I as a function of the gating potential ϕ and the sample bias V_b for the CuPc molecule. The STM tip is held fixed above the molecule. (b) Normalised differential conductance calculated from Fig. (a). (c) The peaks extracted from the differential conductance in Fig. (b) together with the observed crossover in the conductance in Fig. 5.2. (d) Same as Fig. (c) for the H_2Pc molecule.

instead of an expected charge degeneracy point. Moreover, the observed crossover in the conductance and the hysteresis, cf. Fig. 5.2, are observed within this gap as depicted in Fig. 5.4(c). The H_2Pc molecule shows similar features as summarised in Fig. 5.4(d). In the next chapter we present an explanation of these observations within a rate equation approach describing the coupled evolution of the electronic and conformational dynamics of the molecule.

5.2. Theoretical model and explanations

The general observations of the experiment can be explained within a schematic model which describes sequential tunnelling through a single level. This level is formed by the phthalocyanine molecule which is modelled as a semiconductor quantum dot [2] and is attached to the STM tip and the InAs(111)A-(2×2) surface both acting as electron reservoirs. Inspired by the above experimental observations, we assume that the neutral and the negatively charged molecule possess different ground state conformations. Generally the molecule can exist in the two conformations denoted by $\kappa = M^0, M^-$ irrespective of the charge state, where the conformation M^0 corresponds to the ground state of the neutral molecule and the conformation M^- to the ground state of the negatively charged molecule. We assume that transitions between these conformations are thermally induced, and current-induced switching of the conformational state is strongly suppressed by Franck-Condon physics. We will see in the following that these assumptions naturally lead to a pronounced gap in the differential conductance map as observed in Fig. 5.4.

We begin with defining the Hamiltonian of the set-up. Depending on the conformational state κ, electron transport is described by the tunnelling Hamiltonian

$$H^{(\kappa)} = H^{(\kappa)}_{\mathrm{mol}} + H_s + H_t + H^{(\kappa)}_{\mathrm{mol}-s} + H^{(\kappa)}_{\mathrm{mol}-t}\,, \tag{5.1}$$

where the individual terms are introduced in the following. The first term in Eq. (5.1) describes the phthalocyanine molecule, which we model by discrete energy levels

$$H^{(\kappa)}_{\mathrm{mol}} = \sum_{\nu_D} \varepsilon^{(\kappa)}_{\nu_D}\, c^\dagger_{\nu_D}\, c_{\nu_D} + U(\hat{N}_c)\,. \tag{5.2}$$

Here, $\varepsilon^{(\kappa)}_{\nu_D}$ is the energy of the ν_D-th level in the molecule [created (annihilated) by $c^\dagger_{\nu_D}$ (c_{ν_D})] in conformation κ. The term $U(\hat{N}_c)$ in Eq. (5.2) accounts for the electron-electron interactions in the molecule, where $\hat{N}_c$ gives the charge state of the molecule. In the constant interaction model the electron-electron interaction is given by the electrostatic energy $E_C \hat{N}_c\,(\hat{N}_c - 1)$ with charging energy $E_C = e^2/(2C_\Sigma)$ where $C_\Sigma = C_t + C_s + C_g$ is the sum of tip, gate and substrate capacitances, cf. Fig. 5.5(a). We include the effect of the bias voltage V_b and the induced local potential ϕ on the molecule into the definition of $U(\hat{N}_c)$, which is changing the

[2] We call the quantum dot in the limit of small temperatures relative to the level spacing "semiconductor" quantum dot. This highlights the similarity to a semiconductor, where only a small fraction of the total number of electrons contributes to the electric current [Kouwenhoven et al., 2001].

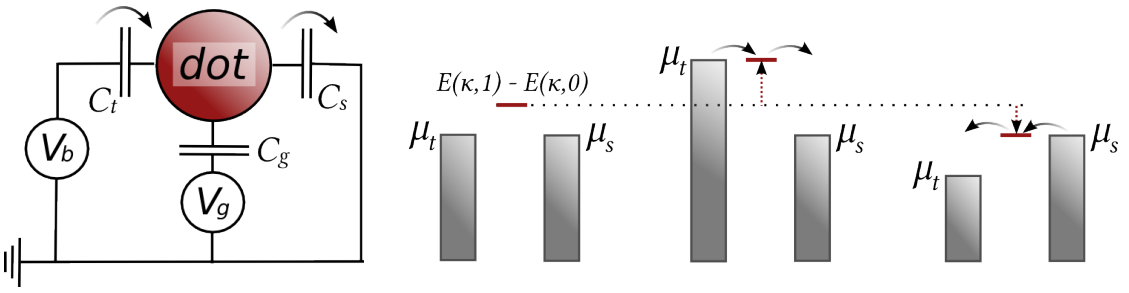

(a) (b)

Figure 5.5.: (a) Schematic switching circuit of the set-up, cf. Fig. 1.8. The charged indium adatoms induce a local potential $\phi = C_g/C_\Sigma\, V_g$ on the molecule with $C_\Sigma = C_t + C_s + C_g$. The coupling between tip and molecule is described by the level arm factor $\alpha = C_t/C_\Sigma$. (b) Sequential tunnelling through the LUMO at positive and negative bias voltages.

effective energy levels of the molecule. Hence $U(\hat{N}_c)$ reads

$$U(\hat{N}_c) = E_C\, \hat{N}_c\, (\hat{N}_c - 1) + e\, \hat{N}_c\, \phi + e\, \alpha\, \hat{N}_c\, V_b\,. \tag{5.3}$$

The so-called lever arm factor, $\alpha = C_t/C_\Sigma$, characterises the coupling between the molecule and the STM tip and takes a value between zero and one. The closer α is to one, the stronger is the coupling.

We model the tip (subscript t) and the substrate (subscript s) as electronic reservoirs kept at fixed chemical potential μ_t and μ_s, respectively. Electrons with energy ε and channel index ν_t or ν_s in the respective lead are created (annihilated) by the operators $c^\dagger_{\nu_s/\nu_t}(\varepsilon)$ $[c_{\nu_s/\nu_t}(\varepsilon)]$. Hence

$$H_j = \int \frac{\mathrm{d}\varepsilon}{2\pi} \sum_{\nu_j} (\varepsilon - \mu_j)\, c^\dagger_{\nu_j}(\varepsilon)\, c_{\nu_j}(\varepsilon) \tag{5.4}$$

where $j = t, s$. The leads are assumed to be metallic where the electrons are regarded as non-interacting and they hence possess a continuous energy spectrum. Tunnelling to/from the tip and the substrate is described by

$$H^{(\kappa)}_{\mathrm{mol}-t} = \int \frac{\mathrm{d}\varepsilon}{2\pi} \sum_{\nu_t} \left(t^{(\kappa,t)}_{\nu_t}\, c^\dagger_{\nu_t}(\varepsilon)\, c_\kappa + t^{(\kappa,t)\,*}_{\nu_t}\, c^\dagger_\kappa\, c_{\nu_t}(\varepsilon) \right)\,, \tag{5.5}$$

$$H^{(\kappa)}_{\mathrm{mol}-s} = \int \frac{\mathrm{d}\varepsilon}{2\pi} \sum_{\nu_s} \left(t^{(\kappa,s)}_{\nu_s}\, c^\dagger_{\nu_s}(\varepsilon)\, c_\kappa + t^{(\kappa,s)\,*}_{\nu_s}\, c^\dagger_\kappa\, c_{\nu_s}(\varepsilon) \right)\,, \tag{5.6}$$

where $c^\dagger_\kappa$ occupies the lowest unoccupied molecular orbit (LUMO) in conformation κ. We assume tunnelling only through the LUMO as we consider a strong effective dependence of the energy levels on the bias voltage, cf. Fig. 5.5(b).

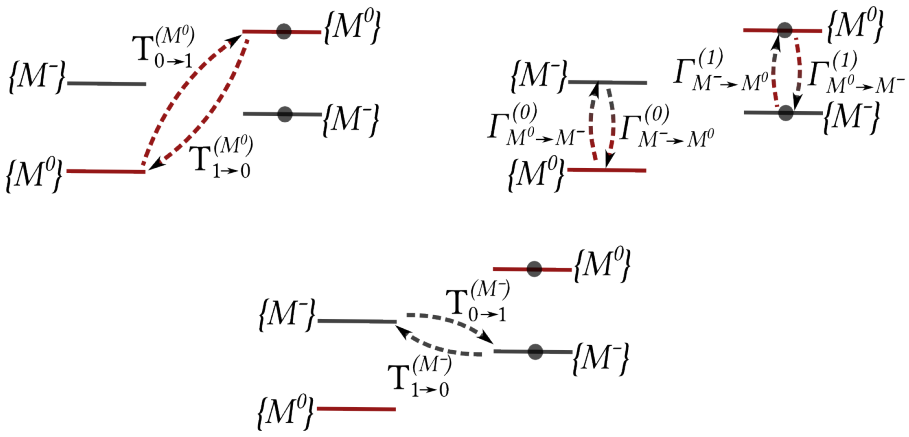

Figure 5.6.: Definitions of the rates appearing in the master equation.

Motivated by the experiment, we can restrict our model to the cases $N_C = 0, 1$ as the molecule is either in the neutral or negatively charged state. Denoting the charge state by 0 and 1, this leads to the effective four states $|M^0, 0\rangle$, $|M^0, 1\rangle$, $|M^-, 0\rangle$, and $|M^-, 1\rangle$ relevant for our description. While $|M^0, 0\rangle$ and $|M^-, 1\rangle$ are the ground states of the neutral and charged molecule, respectively, the corresponding excited states are $|M^-, 0\rangle$ and $|M^-, 1\rangle$. We introduce the effective energies, $E(\kappa, 0)$ and $E(\kappa, 1)$, associated with these states. Using Eqs. (5.2) and (5.3) we can write

$$E(M^0, 0) = \varepsilon_0^{(M^0)} \tag{5.7}$$

$$E(M^0, 1) = \varepsilon_1^{(M^0)} + e\,\phi + e\,\alpha\,V_b \tag{5.8}$$

$$E(M^-, 0) = \varepsilon_0^{(M^-)} \tag{5.9}$$

$$E(M^-, 1) = \varepsilon_1^{(M^-)} + e\,\phi + e\,\alpha\,V_b\,. \tag{5.10}$$

We note that the many-body energy $\varepsilon_0^{(\kappa)}$ consists of a sum of the energies $\varepsilon_{\nu_D}^{(\kappa)}$ in Eq. (5.2) up to the highest occupied orbital level of the isolated molecule and the many-body energy $\varepsilon_1^{(\kappa)}$ consists of the sum up to the lowest unoccupied level of the isolated molecule.

Our main assumption is that the neutral and the negatively charged molecules have different ground-state conformations. This means that we assume

$$\varepsilon_0^{(M^0)} < \varepsilon_0^{(M^-)} \quad \text{and} \quad \varepsilon_1^{(M^-)} < \varepsilon_1^{(M^0)}\,. \tag{5.11}$$

We consider the sequential tunnelling regime, which assumes that tunnelling rates are much smaller than both temperature and level spacing of the molecule. We thus consider the limit of incoherent transport and describe the system by the

occupation probabilities $P(M^0,0)$, $P(M^0,1)$, $P(M^-,0)$ and $P(M^-,1)$ of the four states of the molecule. The Pauli master equation describes the time dependence of these probabilities and reads

$$\frac{dP(M^0,0)}{dt} = \Gamma^{(0)}_{M^-\to M^0} P(M^-,0) + T^{(M^0)}_{1\to 0} P(M^0,1) - [\Gamma^{(0)}_{M^0\to M^-} + T^{(M^0)}_{0\to 1}] P(M^0,0)\,, \tag{5.12}$$

$$\frac{dP(M^-,0)}{dt} = \Gamma^{(0)}_{M^0\to M^-} P(M^0,0) + T^{(M^-)}_{1\to 0} P(M^-,1) - [\Gamma^{(0)}_{M^-\to M^0} + T^{(M^-)}_{0\to 1}] P(M^-,0)\,, \tag{5.13}$$

$$\frac{dP(M^0,1)}{dt} = \Gamma^{(1)}_{M^-\to M^0} P(M^-,1) + T^{(M^0)}_{0\to 1} P(M^0,0) - [\Gamma^{(1)}_{M^0\to M^-} + T^{(M^0)}_{1\to 0}] P(M^0,1)\,, \tag{5.14}$$

$$\frac{dP(M^-,1)}{dt} = \Gamma^{(1)}_{M^0\to M^-} P(M^0,1) + T^{(M^-)}_{0\to 1} P(M^-,0) - [\Gamma^{(1)}_{M^-\to M^0} + T^{(M^-)}_{1\to 0}] P(M^-,1)\,. \tag{5.15}$$

This should be combined with the normalisation condition $P(M^0,0) + P(M^0,1) + P(M^-,0) + P(M^-,1) = 1$. The rates appearing in the master equation, which are denoted by T, describe the electronic tunnelling rates between the charge states of the molecule. The charge state is indicated by the superscript. The conformational transition rates on the other hand are denoted by Γ where the superscript labels the conformation. In the rate equations (5.12) to (5.15) we have neglected tunnelling-induced switching rates which are strongly suppressed due to Franck-Condon physics. The rates are illustrated in Fig. 5.6 and specified below.

We calculate the tunnelling rates to linear order in the tunnelling Hamiltonian, cf. Eqs. (5.5) and (5.6), with the aid of Fermi's golden rule. For the electronic rates this leads to

$$T^{(\kappa)}_{0\to 1} = t^{(\kappa)}_{\mathrm{s}} n_{\mathrm{F}}[E(\kappa,1) - E(\kappa,0)]| + t^{(\kappa)}_{\mathrm{t}} n_{\mathrm{F}}[E(\kappa,1) - eV_{\mathrm{b}} - E(\kappa,0)]\,, \tag{5.16}$$

$$T^{(\kappa)}_{1\to 0} = t^{(\kappa)}_{\mathrm{s}} n_{\mathrm{F}}[E(\kappa,0) - E(\kappa,1)]| + t^{(\kappa)}_{\mathrm{t}} n_{\mathrm{F}}[E(\kappa,0) + eV_{\mathrm{b}} - E(\kappa,1)] \tag{5.17}$$

with Fermi distribution function $n_{\mathrm{F}}(\varepsilon) = 1/(e^{\varepsilon/k_{\mathrm{B}}T}+1)$. The electronic rates consist of two terms. The term proportional to $t^{(\kappa)}_{\mathrm{t}}$ describes electronic tunnelling from or to the tip and the term proportional to $t^{(\kappa)}_{\mathrm{s}}$ tunnelling from or to the substrate. Note that $n_{\mathrm{F}}(-\varepsilon) = 1 - n_{\mathrm{F}}(\varepsilon)$.

We assume that the transitions between the two conformations are thermally induced [Danilov et al., 2006]. A calculation of the conformational switching rates is done in analogy to the case of the electronic rates by replacing the coupling to the electronic reservoirs by a coupling to a (bosonic) thermal bath. The Fermi distribution function is then replaced by the Planck function, $n_{\mathrm{P}}(\varepsilon) = 1/(e^{\varepsilon/k_{\mathrm{B}}T} - 1)$,

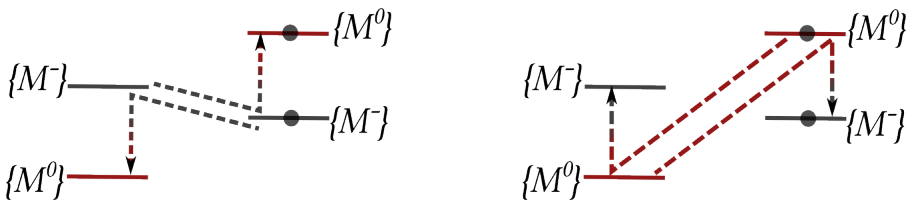

Figure 5.7.: Two-step transitions. Left: The rate A_0 which describes the switch $M^- \to M^0$. Right: The rate A_- describing the switch $M^0 \to M^-$.

and anti-commutation relations by commutation relations. Using Fermi's golden rule, we find that

$$\Gamma^{(N_C)}_{M^0 \to M^-} = \gamma^{(N_C)} \left| n_{\mathrm{P}}[E(M^-, N_C) - E(M^0, N_C)] \right|, \tag{5.18}$$

$$\Gamma^{(N_C)}_{M^- \to M^0} = \gamma^{(N_C)} \left| n_{\mathrm{P}}[E(M^0, N_C) - E(M^-, N_C)] \right| \tag{5.19}$$

with $N_C = 0, 1$. The rate $\gamma^{(N_C)}$ is independent of the potential and temperature.

For the investigated molecules in the experiment the electronic tunnelling rates are much larger than the conformational switching rates. We can find a closed-form solution of the master equation (5.12)-(5.15) to linear order in this ratio. We begin with the zeroth order solution

$$P(\kappa, 0) = \frac{T^{(\kappa)}_{1\to 0}}{T^{(\kappa)}_{1\to 0} + T^{(\kappa)}_{0\to 1}} P(\kappa)\,, \tag{5.20}$$

$$P(\kappa, 1) = \frac{T^{(\kappa)}_{0\to 1}}{T^{(\kappa)}_{1\to 0} + T^{(\kappa)}_{0\to 1}} P(\kappa)\,, \tag{5.21}$$

which results from neglecting all conformational rates Γ in the master equation. Here, $P(\kappa) = P(\kappa, 0) + P(\kappa, 1)$ describes the probability of finding the molecule in the conformational state κ regardless of the charge state. In order to find the solution valid to first order in the conformational tunnelling rates, we insert the solution in Eqs. (5.20) and (5.21) into the rate equations (5.12)-(5.15). This yields

$$\frac{dP(M^{(0)})}{dt} = A_0\, P(M^-) - A_-\, P(M^0)\,, \tag{5.22}$$

$$\frac{dP(M^{(-)})}{dt} = A_-\, P(M^0) - A_0\, P(M^-)\,, \tag{5.23}$$

where we have introduced the notation

$$A_0 = \frac{T^{(M^-)}_{1\to 0}\Gamma^{(0)}_{M^-\to M^0} + T^{(M^-)}_{0\to 1}\Gamma^{(1)}_{M^-\to M^0}}{T^{(M^-)}_{1\to 0} + T^{(M^-)}_{0\to 1}}\,, \tag{5.24}$$

$$A_- = \frac{T^{(M^0)}_{1\to 0}\Gamma^{(0)}_{M^0\to M^-} + T^{(M^0)}_{0\to 1}\Gamma^{(1)}_{M^0\to M^-}}{T^{(M^0)}_{1\to 0} + T^{(M^0)}_{0\to 1}}\,. \tag{5.25}$$

The rates A_0 and A_- describe the switching between the molecular conformations as two-step transitions as sketched in Fig. 5.7. We are interested in the stationary solution of Eqs. (5.22)-(5.23) which we denote as $\overline{P}(M^0)$ and $\overline{P}(M^-)$. Together with the normalisation condition $\overline{P}(M^0) + \overline{P}(M^-) = 1$ we find

$$\overline{P}(M^0) = \frac{A_0}{A_- + A_0}\,, \tag{5.26}$$

$$\overline{P}(M^-) = \frac{A_-}{A_- + A_0}\,. \tag{5.27}$$

We use the stationary solution of the master equation to calculate the stationary electronic current through the molecule as

$$I = e\left(T_{0\to1}^{(M^0)}\,\overline{P}(M^0,0) + T_{0\to1}^{(M^-)}\,\overline{P}(M^-,0) - T_{1\to0}^{(M^0)}\,\overline{P}(M^0,1) - T_{1\to0}^{(M^-)}\,\overline{P}(M^-,1)\right). \tag{5.28}$$

The resulting current diagram as a function of the induced local potential ϕ and the bias voltage V_b is depicted in Fig. 5.8(a) for the parameters $T = 30\,\mathrm{K}$, $C_t = 10^{-15}\,\mathrm{F}$, $C_s = 10^{-17}\,\mathrm{F}$, $C_g = 1.9\cdot10^{-16}\,\mathrm{F}$, $\varepsilon(M^0,0) = 420\,\mathrm{meV}$, $\varepsilon(M^0,1) = 650\,\mathrm{meV}$, $\varepsilon(M^-,0) = 530\,\mathrm{meV}$, $\varepsilon(M^-,1) = 545\,\mathrm{meV}$, $t_s^{(M^0)} = t_s^{(M^-)} = 10^{11}\,\mathrm{s}^{-1}$, $t_t^{(M^0)} = t_t^{(M^-)} = 3\cdot10^9\,\mathrm{s}^{-1}$, $\gamma^{(0)} = \gamma^{(1)} = 10^7\,\mathrm{s}^{-1}$. Strikingly, the current shows a pronounced gap of zero current at all ϕ in agreement with the experimental observations. The additional black lines in Fig. 5.8(a) which distinguish the regions of zero and nonzero current can be read off from the electronic transition rates in Eqs. (5.16) and (5.17). They are given by

$$E(\kappa,1) - E(\kappa,0) = 0\,, \tag{5.29}$$

$$E(\kappa,1) - E(\kappa,0) - eV_\mathrm{b} = 0\,. \tag{5.30}$$

While the first equation characterises the transition line where an electron enters (leaves) the molecule from (into) the substrate, the second equation describes the transition for tunnelling processes from (into) the tip.

The gap in the current–voltage diagram is highlighted schematically in Fig. 5.8(b) and can be understood as follows. We first note that by the assumption that the neutral and the negative molecules possess different ground-state energies, both conformations have different charge degeneracy points. In particular, assuming Eqs. (5.11) means that the charge degeneracy point of the conformation M^0 is shifted to larger ϕ as compared to the charge degeneracy point of the conformation M^-. This gives rise to different regions in the current–voltage diagram, which we label by I-IX in Fig. 5.8(b). These regions differ by the conformations that are

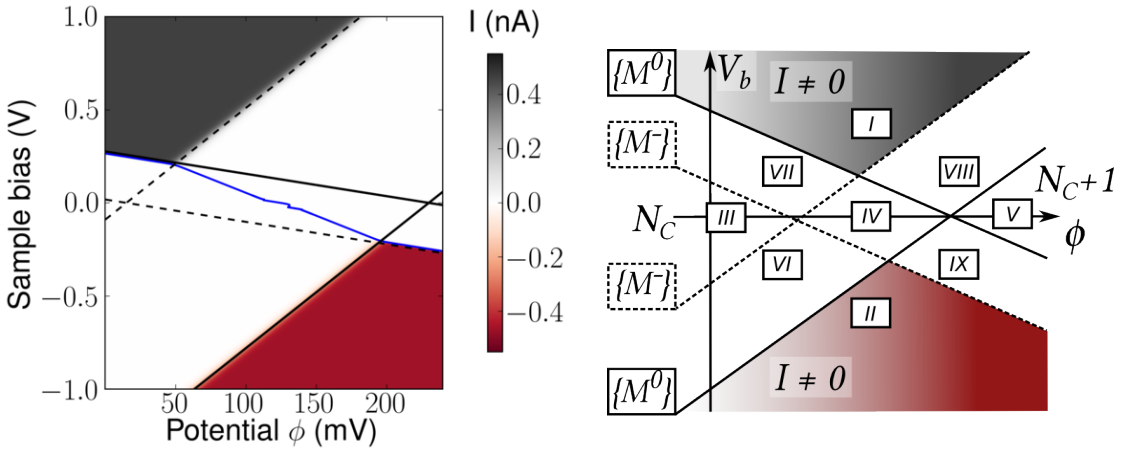

(a) (b)

Figure 5.8.: Current I as a function of ϕ and V_b and stability diagram. (a) Calculated current using Eq. (5.28) and (b) sketch of the current diagram. The black lines correspond to Eqs. (5.29) and (5.30) with $\kappa = M^0$ (solid black line) and $\kappa = M^-$ (dashed black line). The blue line represents the switching line which is calculated from Eq. (5.31). The observed crossover in the conductance and the hysteresis is along this switching line in region IV.

favoured and hence define the observed current. Irrespective of the conformational state, the molecule is in the conducting regime in regions I and II and in the blocked regime in regions III-V. The situation is more subtle in the regions VI-IX. Here the current is blocked for one conformation while the molecule is conducting in the other conformation. As tunnelling-induced conformational transitions are strongly suppressed by Franck-Condon physics, the conformation M^0 is stable in regions VI and VII and the conformation M^- is stable in regions VIII and IX. This means that the current is blocked in all the regions VI-IX and we find a conductance gap at all ϕ.

In the experiment, a small co-tunnelling [Nazarov and Blanter, 2010] current is observed in the region IV of Fig. 5.8(b), which depends on the molecular conformation, cf. Figs. 5.2 and 5.4. The above description which calculates the electronic transition rates by using Fermi's golden rule, however, predicts a vanishing current in this region and is valid to linear order in the tunnelling Hamiltonian, cf. Eqs. (5.5) and (5.6). A description of co-tunnelling includes higher order correction terms in the tunnelling Hamiltonian. The resulting co-tunnelling current in region IV is determined by the time-averaged co-tunnelling current for the conformations M^0 and M^-, weighted by the probabilities to find the

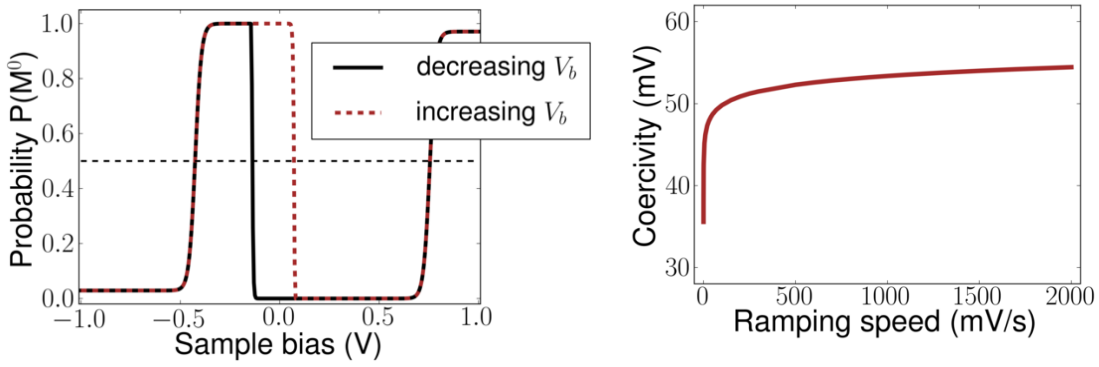

(a) (b)

Figure 5.9.: (a) Non-stationary solution $P(M^0)$ of the master equation with linearly varying bias voltage at fixed $\phi = 150\,\mathrm{mV}$ and constant ramping speed $500\,\mathrm{mV/s}$. The coercivity is defined as the half-distance between the solution with increasing (red dashed line) and decreasing (black solid line) bias voltage at probability $P(M^0) = 1/2$. (b) Calculated coercivity as a function of ramping speed at $\phi = 150\,\mathrm{mV}$. Other parameters in both plots are the same as in Fig. 5.8(a).

molecule in the respective conformations, that is $\overline{P}(M^0) = \overline{P}(M^0, 0) + \overline{P}(M^0, 1)$ and $\overline{P}(M^-) = \overline{P}(M^-, 0) + \overline{P}(M^-, 1)$.

The crossover of the conductance between two different values and the hysteretic behaviour presented in Figs. 5.2 and 5.4 are observed within this region IV and are seen because of co-tunnelling effects. These features can also be explained within the present model. To this end, we use the stationary solution of the master equation to determine the transition line

$$\overline{P}(M^0) = \overline{P}(M^-) = \frac{1}{2}\,, \tag{5.31}$$

where the switch between the conformations M^0 and M^- takes place. This switching line splits region IV in the current–voltage diagram into two regions with different molecular conformations. As each conformation gives rise to a different co-tunnelling conductance, the crossover between the two different conductances is along this line shown as the blue line in Fig. 5.8(a). Since the conformational switching rates are slow compared to the electronic tunnelling rates, hysteretic behaviour is observed when sweeping the bias voltage across this line. Figures 5.4(c) and (d) show that the hysteresis is most pronounced at small biases. This is due to the fact that the corresponding switching rates between the conformations, cf. Eqs. (5.24) and (5.25), depend on the bias voltage via the Fermi function. At low

bias voltages the switching rates are small so that finite ramping speeds of the bias induce hysteresis. As the switching rate increases exponentially with increasing bias voltage, hysteresis is only observed at low biases.

We can determine the coercivity, that is the half-width of the hysteresis, by numerically solving the time dependent master equation (5.12)-(5.15) for linearly increasing or decreasing bias voltage at constant ϕ. A typical solution is shown in Fig. 5.9(a) for the same parameters as in Fig. 5.8(a) but at fixed $\phi = 150\,\mathrm{mV}$. Clearly the conformational state at small bias voltages is seen to depend on how the bias voltage is swept. While an increasing bias voltage favours the conformation M^0 at small bias voltages, decreasing the bias voltage on the other hand results in the favoured conformation M^- for values around zero bias. The coercivity is then extracted by taking the difference of the solutions for gradually increasing and decreasing the bias voltage at probability one half and dividing by two. The resulting coercivity as a function of ramping speed is depicted in Fig. 5.9(b). We find good qualitative agreement with the experimental observations.

5.3. Conclusion

Single-molecule transistors play an important role in the process of miniaturising electric circuits towards the ultimate limit, i.e. circuits with elements made up of single atoms or molecules. A realisation of a single-molecule transistor is presented in Ref. [Martínez-Blanco et al., 2015] where the transistor is formed by the H_2Pc and the CuPc molecule placed individually on an InAs(111)A-(2×2) surface and an adjacent STM tip. Gating is achieved by repositioning charged indium adatoms on the surface and bringing them close to the molecule.

Many of the observations of this experiment have been explained in this chapter within a schematic model of incoherent transport through a single level. The phthalocyanine molecule has been modelled as a semiconductor quantum dot attached to two electron reservoirs formed by the STM tip and the InAs(111)A surface. Allowing for thermally-induced switching between two conformational states, electron transport through the molecule has been calculated via a master equation approach which describes the coupled dynamics of charge and conformational transitions. The corresponding rates have been calculated within Fermi's golden rule. We have assumed that the neutral and negatively charged molecules possess different ground state conformations and that tunnelling-induced switching is suppressed by Franck-Condon physics. While the stationary solution of the master equation has explained

the observed current at different bias and gate voltages and its pronounced conductance gap, the non- stationary solution with a linearly changing bias voltage and fixed gate voltage has explained the observed hysteretic behaviour.

Some features of the experiment, however, are not captured in the theoretical description and require a more refined model. In the present model, for instance, the calculated transition line, which defines the switching in the current–voltage diagram [cf. Eq. (5.31) and the blue line in Fig. 5.8], shows a small kink around zero bias voltage. This characteristic behaviour is not observed in the experiment presumably due to the fact that this kink is located in the region where the hysteretic behaviour is most pronounced. Furthermore, the extrapolated lines which separate the regions of zero and nonzero current in the current–voltage diagram cross at zero bias voltage. This can be seen from Eqs. (5.29) and (5.30) and is illustrated in Fig. 5.8. The observations in Fig. 5.4, however, do not show this feature, where the extrapolated lines cross at finite bias. In principle, this can be explained by current-induced heating of the molecule. An increasing temperature has the effect of shifting the crossing point to nonzero bias voltages. But since the average waiting times between two successive electron tunnelling events are much longer than the electronic tunnelling times and the vibrational relaxation rates of the molecule [Harris et al., 1991, Lee et al., 2005], current-induced heating can be excluded in our model. Alternatively, a more accurate description of the electrostatic interaction of the molecule with its environment in principle affects the slopes and crossing points of the separation lines which distinguish the regions of zero and nonzero current. Although a more refined model can reproduce more features of the experimental observations, we have restricted ourselves to a schematic model, which explains the general observations with a minimal number of parameters.

6. Conclusion

This thesis aims at further increasing our understanding of nanoelectromechanical systems and the control of their motion. Nanoelectromechanical systems are characterised by strong electron-phonon interactions and, therefore, are manipulated by driving the system out of equilibrium via imposing a bias voltage and running an electric current through the device. In this context, understanding the forces exerted by the electrons on the nanosystem is of fundamental importance. Based on the recently obtained expressions of the adiabatic reaction forces in terms of the scattering matrix and its first adiabatic correction [Bode et al., 2011, Bode et al., 2012b], we present a rederivation of these adiabatic reaction forces in the present thesis. Our derivation is more direct and efficient and thus provides further understanding of the nature of the forces. With our derivation, we generalise previous works to a generic classical system coupled to a quantum environment which can be of both fermionic or bosonic nature. This opens a wider range of applications including possible applications in optomechanical systems, spintronics or ultra-cold atoms.

The derivation of the adiabatic reaction forces in this thesis is based on an adiabatic expansion within the methods of scattering theory. The starting point closely follows the seminal work in Ref. [Berry and Robbins, 1993] on environment-induced forces for closed quantum systems, with a discrete energy spectrum. This enables a direct comparison to our work, in particular concerning the absence of dissipation for closed quantum systems. For nanoelectromechanical systems, in contrast, friction naturally occurs when opening the system by attaching leads to it. At a mathematical level, opening the system is accompanied by a continuous energy spectrum which then allows for a friction term, as shown in this thesis. A further advantage of our approach is that it gives an explicit expression of the first adiabatic correction of the scattering matrix in terms of scattering states. This expression strongly simplifies direct calculations for specific realisations, which is essential for applications. Moreover, our derivation specifies the limits of validity. For closed quantum system an adiabatic expansion is performed under the condition that the level spacing of the quantum system is large compared to the frequency of the oscillator. The adiabatic condition for open systems with a continuous spectrum, on

the other hand, requires the inverse dwell time of the quantum system to be large compared to the frequency of the resonator.

Understanding the effect of the environment driven out of equilibrium is essential for the ultimate aim of controlling quantum systems. In nanoelectromechanical systems, out-of-equilibrium situations enable a negative friction coefficient and a non-conservative Born-Oppenheimer force. The latter condition opens the possibility to exert work on the system [Dundas et al., 2009, Brandbyge, 2009, Todorov et al., 2010]. This is the basic idea of an electronically driven molecular motor. Recent experiments motivate the importance of a theoretical description of reaction forces on the path towards creating directed translational [Kudernac et al., 2011] or rotational motion [Tierney et al., 2011] on the molecular scale. The knowledge gained in this thesis provides further insight towards creating directed forces which control the motion of such systems. In particular, the Born-Oppenheimer force plays a crucial role for the basic idea of constructing an adiabatic quantum motor. This is due to the fact that the work exerted by the Born-Oppenheimer force when the system is forced to move on a cyclic path is proportional to the pumped charge through the system when adiabatically varying its parameters [Bustos-Marún et al., 2013].

Understanding the interaction of a classical system, which moves in a quantum environment, is further deepened in the present thesis by reversing the point of view and studying the effect of the classical system on the quantum environment. Due to the Anderson orthogonality catastrophe it is known that small changes of a classical system can have a profound impact on a large quantum environment. We have studied the fidelity amplitude and its absolute square value, the Loschmidt echo, which represent dynamical measures of the Anderson orthogonality catastrophe. In particular, we have expressed these microscopic quantities in the small-distance regime in terms of the mesoscopic adiabatic reaction forces, that is the Born-Oppenheimer force, the friction coefficient and the correlator of the stochastic force. To this end, we have made use of the achieved knowledge and expressions of the environment-induced forces in terms of both the scattering matrix and its first order adiabatic correction and, equivalently, in terms of non-equilibrium Green functions.

A relation between the friction coefficient and the Anderson orthogonality exponent has been found in Ref. [Schönhammer, 1991] for finite quantum systems in the small-distance limit. In this thesis, we have generalised this idea to nanoelectromechanical systems, which can be driven out of equilibrium, by considering infinite quantum systems with a continuous energy spectrum and a finite imposed bias voltage. We have found that the coloured noise of the classical degrees of freedom determines the behaviour of the Loschmidt echo at all times. Using the

fluctuation-dissipation theorem, we have then recovered a power-law decay of the Loschmidt echo in equilibrium and at zero temperature with an exponent proportional to the dissipation. This reflects the Anderson orthogonality. Since a noise correlator, which is delta-correlated in time, implies an exponential decay of the Loschmidt echo, the power-law behaviour signals the breakdown of the semiclassical description of the Markovian Langevin equation.

To linear order in the bias voltage, we have shown that an exponential decay of the Loschmidt echo suppresses the power-law behaviour at times, which are larger than the inverse bias voltage. The exponential decay is consistent with a white-noise assumption to lowest order and the power-law behaviour characterises the next-order correction term. While the exponential decay is determined by the shot-noise fluctuations, we have found that the power-law exponent is given by a competition between fluctuations and dissipation, which ultimately determines the sign of the exponent.

Furthermore, we have analysed the effect of finite temperatures. We have recovered an exponential decay of the Loschmidt echo in the classical limit of large temperatures, which is a manifestation of the classical fluctuation-dissipation theorem. Moreover, we have illustrated the applicability to nanoelectromechanical systems by applying the derived formulas to a concrete example of a single level, which is attached to two leads and coupled to one vibrational mode. This example represents, for instance, a quantum dot confined on an oscillating nanotube.

The use of scattering theory in the derivation of the adiabatic environment-induced forces and in the analysis of the Loschmidt echo limits the validity of the results to non-interacting scattering particles. Interactions can be included at a mean-field level. Generally, taking interactions into account may yield interesting departures from the results discussed in this thesis. Moreover, interesting features are expected by studying a quantum system instead of a classical system which is coupled to a fermionic or bosonic environment.

The ultimate limit of miniaturisation and control is reached by electronic devices on the atomic or molecular scale, where individual electrons sequentially tunnel through the system. This thesis provides a theoretical model of a transistor on the molecular scale recently realised in Ref. [Martínez-Blanco et al., 2015]. This experiment uses the techniques of bottom-up molecular manipulations by STM [Stroscio and Eigler, 1991] and by this provides a technique to reach atomically precise gating. The transistor consists of a phthalocyanine molecule (free base phthalocyanine or copper phthalocyanine) on an InAs(111)A-(2×2) surface and an adjacent STM tip. By construction, a low coverage of additional positively charged native donor-

type indium adatoms is absorbed on the substrate. As these adatoms are weakly bound to the substrate, they can be repositioned by the STM tip and change the local electrostatic potential on the phthalocyanine molecule. Thus, they serve as an analogue of a gate electrode with atomic precision. A bias voltage applied between the STM tip and the InAs surface then creates a current running through the system which is controlled by the position of the indium adatoms. Remarkably, the current as a function of applied bias and gate voltage shows a pronounced gap instead of the expected charge degeneracy point.

Motivated by the experimental observations, we have explained the occurrence of the gap by the existence of two distinct conformational states of the phthalocyanine molecule. We have introduced a schematic model which treats the phthalocyanine molecule as a semiconductor quantum dot and explains the general experimental observations. The tip and the substrate have been treated as electron reservoirs kept at different chemical potentials in the presence of the bias voltage. Tunnelling through the molecule has then been described by the solution of the rate equations which involve transition rates between the two different conformational states and rates changing the charge state of the molecule. These coupled dynamics show the presence of new features and explain the the occurrence of the gap in the current–voltage diagram, which extends the established understandings of sequential transport in transistors on the molecular scale. We have further confirmed this conclusion by a quantitative calculation of the experimentally observed features.

The present thesis discusses nanoelectromechanical systems ranging from nanostructures, such as oscillating graphene sheets or nanotubes, to electronic devices made up of individual molecules. The ultimate goal is to manipulate and control these miniaturised devices on the nanoscale. Our study of both the adiabatic reaction forces and the single-molecule transistor deepens our understanding of transport through these materials and thus enables interesting perspectives for the future. On the one hand, an exciting perspective is the creation of directed adiabatic reaction forces which is essential for the construction molecular machines. On the other hand, single-molecule transistors are fundamental devices in the field of nanotechnology as they provide a way to control transport in molecular materials. By this, they open the door towards the construction of electric circuits with elements made up of individual molecules.

A. Loschmidt echo within scattering theory

In this appendix, we derive Eqs. (4.46) to (4.49) purely within the methods of scattering theory which gives the relation of the Loschmidt echo to the adiabatic reaction forces to linear response in the bias at zero temperature. Throughout the appendix we frequently refer to the definition of the frozen scattering matrix in Eq. (3.24) and its relation to the A-matrix via Eqs. (3.35). Furthermore Eq. (3.53) is used to identify the derivative of the scattering matrix with respect to the classical degree of freedom.

We begin with the identification of the friction tensor $\boldsymbol{\gamma} = \boldsymbol{\gamma}^{eq} + \boldsymbol{\gamma}^{neq}$. For an expansion to linear response in the bias voltage we use the notation

$$\boldsymbol{\gamma}^{eq} = \boldsymbol{\gamma}_0^{eq} + \boldsymbol{\gamma}_1^{eq} \tag{A.1}$$

$$\boldsymbol{\gamma}^{neq} = \boldsymbol{\gamma}_1^{neq} \tag{A.2}$$

introduced in the main text where the index denotes the order in $\Delta\mu\,\tau_D$. There is no term $\boldsymbol{\gamma}_0^{neq}$ since the term $\boldsymbol{\gamma}^{neq}$ represents a pure out-of-equilibrium contribution. The friction tensor is expressed in terms of the S- and A-matrix in Eq. (3.64) where the first term equals $\boldsymbol{\gamma}^{eq}$ and the second term gives $\boldsymbol{\gamma}^{neq}$. It is straightforward to show for two leads with chemical potentials $\mu_L = \mu + \Delta\mu/2$ and $\mu_R = \mu - \Delta\mu/2$ that the above contributions to the friction tensor in linear response read

$$(\boldsymbol{\gamma}_0^{eq})_{\alpha\beta} = \frac{1}{4\pi}\sum_{\alpha\beta} \mathrm{tr}\left\{\partial_\alpha S_t^\dagger(\mu)\cdot\partial_\beta S_t(\mu)\right\}_s, \tag{A.3}$$

$$(\boldsymbol{\gamma}_1^{eq})_{\alpha\beta} = \frac{1}{8\pi}\sum_{\alpha\beta}\partial_\varepsilon\left[\left(\partial_\alpha S_t^\dagger(\varepsilon)\cdot\partial_\beta S_t(\varepsilon)\right)_{LL} - \left(\partial_\alpha S_t^\dagger(\varepsilon)\cdot\partial_\beta S_t(\varepsilon)\right)_{RR}\right]_{\varepsilon=\mu}, \tag{A.4}$$

$$\begin{aligned}(\boldsymbol{\gamma}_1^{neq})_{\alpha\beta} = \frac{1}{4\pi i}\sum_{\alpha\beta}\Big\{&\left(\partial_\alpha S_t^\dagger(\mu)\cdot A_t^\beta(\mu) - A_t^{\beta\dagger}(\mu)\cdot\partial_\alpha S_t(\mu)\right)_{LL}\\ &-\left(\partial_\alpha S_t^\dagger(\mu)\cdot A_t^\beta(\mu) - A_t^{\beta\dagger}(\mu)\cdot\partial_\alpha S_t(\mu)\right)_{RR}\Big\}_s.\end{aligned} \tag{A.5}$$

Essential for a derivation of Eqs. (4.46) to (4.49) is an expression of the function $\mathbf{K}_{kn}(\varepsilon) = \mathbf{K}_{kn}(\varepsilon,\varepsilon)$ in terms of the scattering matrix. From the definition in Eq. (4.36) together with Eq. (4.35) and by twice inserting the resolution $1 = \int \frac{\mathrm{d}\varepsilon}{2\pi} \sum_m |\psi_m^{\mathbf{X}-}(\varepsilon)\rangle\langle\psi_m^{\mathbf{X}-}(\varepsilon)|$ of the advanced scattering states we find

$$\begin{aligned} K_{kn}^{\alpha\beta}(\varepsilon) &= \langle\psi_k^{\mathbf{X}+}(\varepsilon)|\partial_\alpha V_{\mathbf{X}}|\psi_n^{\mathbf{X}+}(\varepsilon)\rangle\langle\psi_n^{\mathbf{X}+}(\varepsilon)|\partial_\beta V_{\mathbf{X}}|\psi_k^{\mathbf{X}+}(\varepsilon)\rangle \\ &= \Big(\partial_\alpha S_t^\dagger(\varepsilon)\cdot S_t(\varepsilon)\Big)_{kn}\Big(S_t^\dagger(\varepsilon)\cdot\partial_\beta S_t(\varepsilon)\Big)_{nk} . \end{aligned} \tag{A.6}$$

Since the scattering matrix is unitary, so that $S_t^\dagger(\varepsilon)\cdot S_t(\varepsilon) = 1$, we conclude that

$$\frac{1}{4\pi}\sum_{kn} K_{kn}^{\alpha\beta}(\mu) = \frac{1}{4\pi}\mathrm{tr}\left\{\partial_\alpha S_t^\dagger(\mu)\cdot\partial_\beta S_t(\mu)\right\}_s = (\boldsymbol{\gamma}_0^{eq})_{\alpha\beta} . \tag{A.7}$$

The last step follows by comparing to Eq. (A.3) and gives the first desired Eq. (4.46).

Next, we address the identification of the coefficient $\boldsymbol{\gamma}_1^{eq}$. We note that $K_{kn}^{\alpha\beta}(\varepsilon) = K_{nk}^{\alpha\beta}(\varepsilon)$ is symmetric under exchanging the indices k and n, which readily follows from the symmetric summation over the indices of the classical degree of freedom, that is α and β. We deduce the relations $\partial^s K_{kn}^{\alpha\beta}(\varepsilon) = \frac{1}{2}\,\partial_\varepsilon K_{kn}^{\alpha\beta}(\varepsilon)$ and $\partial^s K_{kn}^{\alpha\beta}(\varepsilon) = \partial^s K_{nk}^{\alpha\beta}(\varepsilon)$. By referring to the linear response expression in Eq. (A.4) we conclude that

$$\begin{aligned} \frac{\Delta\mu}{4\pi}\Big[\partial^s K_{LL}^{\alpha\beta}(\mu) - \partial^s K_{RR}^{\alpha\beta}(\mu)\Big] &= \frac{\Delta\mu}{8\pi}\sum_{n=L,R}\partial_\varepsilon\Big[K_{Ln}^{\alpha\beta}(\varepsilon) - K_{Rn}^{\alpha\beta}(\varepsilon)\Big]_{\varepsilon=\mu} \\ &= \frac{\Delta\mu}{8\pi}\partial_\varepsilon\left\{\Big[\Big(\partial_\alpha S_t^\dagger(\varepsilon)\cdot\partial_\beta S_t(\varepsilon)\Big)_{LL} - \Big(\partial_\alpha S_t^\dagger(\varepsilon)\partial_\beta S_t(\varepsilon)\Big)_{RR}\Big]_{\varepsilon=\mu}\right\}_s \\ &= (\boldsymbol{\gamma}_1^{eq})_{\alpha\beta} , \end{aligned} \tag{A.8}$$

which proves the relation in Eq. (4.48).

The identification of the pure out-of-equilibrium contribution to the friction tensor in linear response requires an expression of the antisymmetric energy derivative of the function $\mathbf{K}_{kn}$ in terms of the S- and the A-matrix. Similar to the previous cases,

we insert the resolution $1 = \int \frac{\mathrm{d}\varepsilon}{2\pi} \sum_m |\psi_m^{\mathbf{X}-}(\varepsilon)\rangle\langle\psi_m^{\mathbf{X}-}(\varepsilon)|$ twice and get

$$\begin{aligned}
\partial^a K_{kn}^{\alpha\beta}(\varepsilon) &= \frac{1}{2}\left(\partial_\varepsilon - \partial_{\varepsilon'}\right) K_{kn}^{\alpha\beta}(\varepsilon,\varepsilon')\Big|_{\varepsilon'=\varepsilon} \\
&= \frac{1}{2}\Big\{\langle\partial_\varepsilon\psi_k^{\mathbf{X}+}(\varepsilon)|\partial_\alpha V_{\mathbf{X}}|\psi_n^{\mathbf{X}+}(\varepsilon)\rangle\langle\psi_n^{\mathbf{X}+}(\varepsilon)|\partial_\beta V_{\mathbf{X}}|\psi_k^{\mathbf{X}+}(\varepsilon)\rangle \\
&\quad + \langle\psi_k^{\mathbf{X}+}(\varepsilon)|\partial_\alpha V_{\mathbf{X}}|\psi_n^{\mathbf{X}+}(\varepsilon)\rangle\langle\psi_n^{\mathbf{X}+}(\varepsilon)|\partial_\beta V_{\mathbf{X}}|\partial_\varepsilon\psi_k^{\mathbf{X}+}(\varepsilon)\rangle \\
&\quad - \langle\psi_k^{\mathbf{X}+}(\varepsilon)|\partial_\alpha V_{\mathbf{X}}\,\partial_\varepsilon\Big[|\psi_n^{\mathbf{X}+}(\varepsilon)\rangle\langle\psi_n^{\mathbf{X}+}(\varepsilon)|\Big]\,\partial_\beta V_{\mathbf{X}}|\psi_k^{\mathbf{X}+}(\varepsilon)\rangle\Big\}_s \\
&= -\frac{1}{2}\sum_{ml}\Big\{\partial_\alpha S_t^{\dagger,km}(\varepsilon)\,\partial_\varepsilon\Big[S_t^{mn}(\varepsilon)\,S_t^{\dagger,nl}(\varepsilon)\Big]\,\partial_\beta S_t^{lk}(\varepsilon)\Big\}_s \\
&\quad - \frac{1}{i}\sum_{ml}\Big\{\Big(\partial_\alpha S_t^\dagger(\varepsilon)\cdot S_t(\varepsilon)\Big)_{kn}\Big(S_t^\dagger(\varepsilon)A_t^\beta(\varepsilon)\Big)_{nk} \\
&\quad - \Big(A_t^{\beta\,\dagger}(\varepsilon)\cdot S_t(\varepsilon)\Big)_{kn}\Big(S_t^\dagger(\varepsilon)\cdot\partial_\alpha S_t(\varepsilon)\Big)_{nk}\Big\}_s\,. \qquad \text{(A.9)}
\end{aligned}$$

Now we are ready to identify the coefficient $\boldsymbol{\gamma}_1^{neq}$. We note that $\partial^a K_{kn}^{\alpha\beta}(\varepsilon) = -\partial^a K_{nk}^{\alpha\beta}(\varepsilon)$ is antisymmetric under exchanging the lead indices and in particular we deduce that $\partial^a K_{nn}^{\alpha\beta}(\varepsilon) = 0$. Hence we have

$$\begin{aligned}
\frac{\Delta\mu}{4\pi}\Big[\partial^a K_{RL}^{\alpha\beta}(\mu) - \partial^a K_{LR}^{\alpha\beta}(\mu)\Big] &= \frac{\Delta\mu}{4\pi}\sum_{n=L,R}\Big[\partial^a K_{Rn}^{\alpha\beta}(\mu) - \partial^a K_{Ln}^{\alpha\beta}(\mu)\Big] \\
&= \frac{\Delta\mu}{4\pi i}\Big\{\Big(\partial_\alpha S_t^\dagger(\mu)\cdot A_t^\beta(\mu) - A_t^{\beta\dagger}(\mu)\cdot\partial_\alpha S_t(\mu)\Big)_{LL} \\
&\quad - \Big(\partial_\alpha S_t^\dagger(\mu)\cdot A_t^\beta(\mu) - A_t^{\beta\dagger}(\mu)\cdot\partial_\alpha S_t(\mu)\Big)_{RR}\Big\}_s \\
&= (\boldsymbol{\gamma}_1^{neq})_{\alpha\beta}\,, \qquad \text{(A.10)}
\end{aligned}$$

which shows Eq. (4.49). Here we have used that $\mathrm{tr}\{\partial_\alpha S_t^\dagger \cdot A_t^\beta - A_t^{\beta\dagger}\cdot\partial_\alpha S_t\} = 0$ which expresses the vanishing of $\boldsymbol{\gamma}_0^{neq} = 0$.

Finally, we address the derivation of Eq. (4.47) which involves the relation to the zero-frequency noise correlator, $\mathbf{D}_{[T,\Delta\mu]} = \mathbf{D}(\mathbf{X})$. At zero frequency the we deduce from Eq. (4.38) that

$$D_{\alpha\beta}(\mathbf{X}) = \int\frac{\mathrm{d}\varepsilon}{2\pi}\sum_{k,m=L,R} f_m(\varepsilon)\,[1-f_k(\varepsilon)]\,K_{mk}^{\alpha\beta}(\varepsilon)\,. \qquad \text{(A.11)}$$

We note that this expression is consistent with the expression of the classical noise correlator in Eq. (3.69). For small temperatures T we can write the product of the Fermi functions as $f_k(\varepsilon)\,[1-f_k(\varepsilon)] = -T\,\partial_\varepsilon f_k(\varepsilon) = T\,\delta(\varepsilon-\mu_k)$. Consequently, in

linear response we find

$$D_{\alpha\beta}(\mathbf{X}) = \frac{T}{2\pi}\left(\sum_{k,m=L,R} K^{\alpha\beta}_{mk}(\mu) + \frac{\Delta\mu}{2}\left[\partial_\varepsilon K^{\alpha\beta}_{LL}(\varepsilon) - \partial_\varepsilon K^{\alpha\beta}_{RR}(\varepsilon)\right]_{\varepsilon=\mu}\right) \tag{A.12}$$

$$+ \frac{\Delta\mu}{4\pi}\left[K^{\alpha\beta}_{LR}(\mu) + K^{\alpha\beta}_{RL}(\mu)\right], \tag{A.13}$$

because $K^{\alpha\beta}_{km}(\varepsilon) = K^{\alpha\beta}_{mk}(\varepsilon)$. With $\frac{1}{2}\,\partial_\varepsilon = \partial^s$ we readily deduce from the second term the validity of Eq. (4.47) at zero temperature.

B. Loschmidt echo within Green function formalism

This appendix is devoted to the derivation of Eqs. (4.64) to (4.67) within the methods of non-equilibrium Green functions which provides an alternative derivation compared to the derivation based on scattering theory. We conclude this appendix by showing the equivalence of both methods.

We start the derivation with the expression of the full friction tensor in terms of the adiabatic lesser and greater Green functions of the dot [Bode et al., 2011, Bode et al., 2012b]

$$\boldsymbol{\gamma}_{\alpha\beta} = \int \frac{\mathrm{d}\varepsilon}{2\pi} \,\mathrm{tr}\Big\{ \Lambda_\alpha \, G_D^{>}(\varepsilon) \, \Lambda_\beta \, \partial_\varepsilon G_D^{<}(\varepsilon) \Big\}_s \,. \tag{B.1}$$

Out-of-equilibrium enters in this expression via the Green functions, which can be expressed in terms the Fermi functions and the retarded and advanced Green functions of the dot via Langreth rule, cf. Eqs. (4.58) and (4.59). In equilibrium, we find with the definition of the function $\tilde{\mathbf{K}}$ in Eq. (4.62) at zero temperature that

$$\begin{aligned}
(\boldsymbol{\gamma}_0^{eq})_{\alpha\beta} = \int \frac{\mathrm{d}\varepsilon}{4\pi} \sum_{kn=L,R} \mathrm{tr} \Big\{ & \Lambda_\alpha \, G_D^R(\varepsilon) W^\dagger(\mu) \, \Pi_k(\mu) \, W(\mu) \\
& \times G_D^A(\mu) \, \Lambda_\beta \, G_D^R(\mu) \, W^\dagger(\mu) \, \Pi_n(\mu) \, W(\mu) \, G_D^A(\mu) \Big\}_s \qquad \text{(B.2)} \\
= \frac{1}{4\pi} \sum_{k,n=L,R} & \tilde{K}_{kn}^{\alpha\beta}(\mu) \,, \qquad \text{(B.3)}
\end{aligned}$$

which is equal to Eq. (4.64). For the linear response term $\boldsymbol{\gamma}_1^{eq} + \boldsymbol{\gamma}_1^{neq}$ we expand the Fermi function of the left and right lead as $f_{L/R}(\varepsilon) = f(\varepsilon) \mp \Delta\mu/2 \, \partial_\varepsilon f(\varepsilon)$. Inserting Eqs. (4.58) and (4.59) into Eq. (B.1) we find to linear order in the bias voltage after

integrating by parts

$$
\begin{aligned}
(\boldsymbol{\gamma}_1^{eq}+\boldsymbol{\gamma}_1^{neq})_{\alpha\beta} = {} & \frac{\Delta\mu}{8\pi}\,\partial_\varepsilon\,\Big(\tilde{K}^{\alpha\beta}_{LL}(\mu,\varepsilon)+\tilde{K}^{\alpha\beta}_{LR}(\varepsilon,\mu)\Big)_{\varepsilon=\mu} \\
& -\frac{\Delta\mu}{8\pi}\,\partial_\varepsilon\,\Big(\tilde{K}^{\alpha\beta}_{RL}(\mu,\varepsilon)+\tilde{K}^{\alpha\beta}_{RR}(\varepsilon,\mu)\Big)_{\varepsilon=\mu} + \frac{\Delta\mu}{8\pi}\,\partial_\varepsilon\,\Big(\tilde{K}^{\alpha\beta}_{LL}(\mu,\varepsilon)+\tilde{K}^{\alpha\beta}_{RL}(\varepsilon,\mu)\Big)_{\varepsilon=\mu} \\
& -\frac{\Delta\mu}{8\pi}\,\partial_\varepsilon\,\Big(\tilde{K}^{\alpha\beta}_{LR}(\mu,\varepsilon)+\tilde{K}^{\alpha\beta}_{RR}(\varepsilon,\mu)\Big)_{\varepsilon=\mu} \\
& +\int\frac{\mathrm{d}\varepsilon}{2\pi}\,(\partial_\varepsilon f(\varepsilon))^2\,\Big(\tilde{K}^{\alpha\beta}_{LL}(\varepsilon,\varepsilon)+\tilde{K}^{\alpha\beta}_{LR}(\varepsilon,\varepsilon)-\tilde{K}^{\alpha\beta}_{RL}(\varepsilon,\varepsilon)-\tilde{K}^{\alpha\beta}_{RR}(\varepsilon,\varepsilon) \\
& -\tilde{K}^{\alpha\beta}_{LL}(\varepsilon,\varepsilon)-\tilde{K}^{\alpha\beta}_{RL}(\varepsilon,\varepsilon)+\tilde{K}^{\alpha\beta}_{LR}(\varepsilon,\varepsilon)+\tilde{K}^{\alpha\beta}_{RR}(\varepsilon,\varepsilon)\Big)
\end{aligned}
\tag{B.4}
$$

at zero temperature. We note that the terms in the last two lines cancel each other because $\tilde{\mathbf{K}}_{kn}(\varepsilon,\varepsilon)=\tilde{\mathbf{K}}_{nk}(\varepsilon,\varepsilon)$ which readily follows from the definition of the function $\tilde{\mathbf{K}}_{kn}$. We are thus left with

$$
(\boldsymbol{\gamma}_1^{eq}+\boldsymbol{\gamma}_1^{neq})_{\alpha\beta} = \frac{\Delta\mu}{4\pi}\,\Big(\partial^s\tilde{K}^{\alpha\beta}_{LL}(\mu)-\partial^s\tilde{K}^{\alpha\beta}_{RR}(\mu)\Big)+\frac{\Delta\mu}{4\pi}\,\Big(\partial^a\tilde{K}^{\alpha\beta}_{RL}(\mu)-\partial^a\tilde{K}^{\alpha\beta}_{LR}(\mu)\Big)\,. \tag{B.5}
$$

The first term corresponds to the coefficient $\boldsymbol{\gamma}_1^{eq}$ and the second terms to the coefficient $\boldsymbol{\gamma}_1^{neq}$. This leads to the desired Eqs. (4.48) and (4.67).

We now turn to the zero-frequency noise correlator $\mathbf{D}_{[T,\Delta\mu]}=\mathbf{D}(\mathbf{X})$. In terms of lesser and greater Green functions of the dot the noise correlator reads [Bode et al., 2011, Bode et al., 2012b]

$$
D_{\alpha\beta}(\mathbf{X}) = \int\frac{\mathrm{d}\varepsilon}{2\pi}\,\mathrm{tr}\{\Lambda_\alpha\,G_D^{>}(\varepsilon)\,\Lambda_\beta\,G_D^{<}(\varepsilon)\}_s\,. \tag{B.6}
$$

Similar to the identification of the friction tensor, we continue by applying Langreth rule, that is we make use of Eqs. (4.58) and (4.59). We identify the function $\tilde{\mathbf{K}}$ by referring to Eq. (4.62) and deduce at zero temperature with the aid of $f_R(\varepsilon)\,(1-f_L(\varepsilon))=0$ that

$$
\begin{aligned}
D_{\alpha\beta}(\mathbf{X}) &= \int\frac{\mathrm{d}\varepsilon}{2\pi}\sum_{k,n=L,R} f_k(\varepsilon)\,[1-f_n(\varepsilon)]\,\tilde{K}^{\alpha\beta}_{kn}(\varepsilon,\varepsilon) \\
&= \frac{\Delta\mu}{4\pi}\,\Big(\tilde{K}^{\alpha\beta}_{LR}(\mu)+\tilde{K}^{\alpha\beta}_{RL}(\mu)\Big)
\end{aligned}
\tag{B.7}
$$

to linear response in the bias. Here we have used that $\tilde{\mathbf{K}}_{kn}(\varepsilon)=\tilde{\mathbf{K}}_{nk}(\varepsilon)$. The last line agrees with Eq. (4.65).

We conclude this appendix by explicitly showing the equivalence between the function $\mathbf{K}_{kn}(\varepsilon,\varepsilon')$, defined in Eq. (4.36) in terms of scattering states, and the function $\tilde{\mathbf{K}}_{kn}(\varepsilon,\varepsilon')$, introduced in Eq. (4.62) in terms of Green functions. To show the

equivalence, we follow similar steps as in Sec. 3.4 where we have shown that the retarded scattering states and the retarded Green function of the dot are related via Eq. (3.76). A similar equation holds for the advanced scattering states and their relation to the advanced Green function of the dot. Inserting Eq. (3.76) into the definition of the function $\mathbf{K}_{kn}$ in Eq. (4.36), we get

$$K_{kn}^{\alpha\beta}(\varepsilon,\varepsilon') = \Big\{ \langle\phi_k(\varepsilon)|\, W(\varepsilon)\, G_D^A(\varepsilon)\, \lambda_\alpha\, G_D^R(\varepsilon')\, W^\dagger(\varepsilon')\, |\phi_n(\varepsilon')\rangle\langle\phi_n(\varepsilon')|\, W(\varepsilon')\, G_D^A(\varepsilon') \\ \times \lambda_\beta\, G_D^R(\varepsilon)\, W^\dagger(\varepsilon)\, |\phi_k(\varepsilon)\rangle \Big\}_s \tag{B.8}$$

since $\partial_\alpha V_{\mathbf{X}} = \Pi_D\, \partial_\alpha h_0(\mathbf{X})\, \Pi_D$ and $\lambda_\alpha = \partial_\alpha h_0$, cf. Sec. 3.4. With $\Pi_n(\varepsilon') = |\phi_n(\varepsilon')\rangle\langle\phi_n(\varepsilon')|$ and making use of the symmetry in the indices α and β, we deduce that

$$\begin{aligned} K_{kn}^{\alpha\beta}(\varepsilon,\varepsilon') &= \mathrm{tr}\, \big\{ \partial_\alpha H_{\mathbf{X}}\, G_D^R(\varepsilon')\, W^\dagger(\varepsilon')\, \Pi_n(\varepsilon')\, W(\varepsilon')\, G_D^A(\varepsilon') \\ &\quad \times \partial_\beta H_{\mathbf{X}}\, G_D^R(\varepsilon)\, W^\dagger(\varepsilon)\, \Pi_k(\varepsilon)\, W(\varepsilon)\, G_D^A(\varepsilon) \big\}_s \\ &\equiv \tilde{K}_{kn}^{\alpha\beta}(\varepsilon,\varepsilon') \end{aligned}$$

by referring to Eq. (4.62). Hence we have shown that the functions $\mathbf{K}_{kn}(\varepsilon,\varepsilon')$ and $\tilde{\mathbf{K}}_{kn}(\varepsilon,\varepsilon')$ are identical. This shows that the present Green function approach is equivalent to the formulation in terms of scattering states.

Bibliography

[Abanin and Levitov, 2004] Abanin, D. A. and Levitov, L. S. *Tunable fermi-edge resonance in an open quantum dot.* Phys. Rev. Lett. **93**, 126802 (2004).

[Abanin and Levitov, 2005] Abanin, D. A. and Levitov, L. S. *Fermi-edge resonance and tunneling in nonequilibrium electron gas.* Phys. Rev. Lett. **94**, 186803 (2005).

[Agraït et al., 2003] Agraït, N., Yeyati, A., and Van Ruitenbeek, J. *Quantum properties of atomic-sized conductors.* Phys. Rep. **377**, 81 (2003).

[Aleiner et al., 2002] Aleiner, I., Brouwer, P., and Glazman, L. *Quantum effects in coulomb blockade.* Physics Reports **358**, 309 (2002).

[Anderson, 1967] Anderson, P. W. *Infrared catastrophe in fermi gases with local scattering potentials.* Phys. Rev. Lett. **18**, 1049 (1967).

[Arrachea et al., 2014] Arrachea, L., Bode, N., and von Oppen, F. *Vibrational cooling and thermoelectric response of nanoelectromechanical systems.* Phys. Rev. B **90**, 125450 (2014).

[Avron et al., 2001] Avron, J. E., Elgart, A., Graf, G. M., and Sadun, L. *Optimal quantum pumps.* Phys. Rev. Lett. **87**, 236601 (2001).

[Bailey et al., 2008] Bailey, S. W. D., Amanatidis, I., and Lambert, C. J. *Carbon nanotube electron windmills: A novel design for nanomotors.* Phys. Rev. Lett. **100**, 256802 (2008).

[Beenakker, 1991] Beenakker, C. W. J. *Theory of coulomb-blockade oscillations in the conductance of a quantum dot.* Phys. Rev. B **44**, 1646 (1991).

[Bennett et al., 2010] Bennett, S. D., Maassen, J., and Clerk, A. A. *Scattering approach to backaction in coherent nanoelectromechanical systems.* Phys. Rev. Lett. **105**, 217206 (2010), See also *Phys. Rev. Lett.* **106**, 199902 (2011).

[Benyamini et al., 2014] Benyamini, A., Hamo, A., Viola Kusminskiy, S., von Oppen, F., and Ilani, S. *Real-space tailoring of the electron-phonon coupling in ultraclean nanotube mechanical resonators.* Nature Physics **10**, 151 (2014).

[Berry and Robbins, 1993] Berry, M. V. and Robbins, J. M. *Chaotic classical and half-classical adiabatic reactions: Geometric magnetism and deterministic friction.* Proc. R. Soc. Lond. A **442**, 659 (1993).

[Besteman et al., 2003] Besteman, K., Lee, J.-O., Wiertz, F. G. M., Heering, H. A., and Dekker, C. *Enzyme-coated carbon nanotubes as single-molecule biosensors.* Nano Letters **3**, 727 (2003).

[Binnig et al., 1986] Binnig, G., Quate, C. F., and Gerber, C. *Atomic force microscope.* Phys. Rev. Lett. **56**, 930 (1986).

[Binnig et al., 1982a] Binnig, G., Rohrer, H., Gerber, C., and Weibel, E. *Surface studies by scanning tunneling microscopy.* Phys. Rev. Lett. **49**, 57 (1982a).

[Binnig et al., 1982b] Binnig, G., Rohrer, H., Gerber, C., and Weibel, E. *Tunneling through a controllable vacuum gap.* Appl. Phys. Lett. **40**, 178 (1982b).

[Blanter and Büttiker, 2000] Blanter, Y. M. and Büttiker, M. *Shot noise in mesoscopic conductors.* Physics Rep9orts **336**, 1 (2000).

[Bode, 2012] Bode, N. *Coherent electrons and collective modes in quantum-transport through nanostructures.* PhD thesis, Freie Universität Berlin (2012).

[Bode et al., 2012a] Bode, N., Arrachea, L., Lozano, G. S., Nunner, T. S., and von Oppen, F. *Current-induced switching in transport through anisotropic magnetic molecules.* Phys. Rev. B **85**, 115440 (2012a).

[Bode et al., 2011] Bode, N., Viola Kusminskiy, S., Egger, R., and von Oppen, F. *Scattering theory of current-induced forces in mesoscopic systems.* Phys. Rev. Lett. **107**, 036804 (2011).

[Bode et al., 2012b] Bode, N., Viola Kusminskiy, S., Egger, R., and von Oppen, F. *Current-induced forces in mesoscopic systems: A scattering-matrix approach.* Beilstein J. Nanotechnol. **3**, 144 (2012b).

[Born and Oppenheimer, 1927] Born, M. and Oppenheimer, R. *Zur quantentheorie der molekeln.* Annalen der Physik **389**, 457 (1927).

[Brandbyge, 2009] Brandbyge, M. *Atomic waterwheels go to work.* Nature Nanotechnology **4**, 81 (2009).

[Brandbyge et al., 1995] Brandbyge, M., Schiøtz, J., Sørensen, M. R., Stoltze, P., Jacobsen, K. W., Nørskov, J. K., Olesen, L., Laegsgaard, E., Stensgaard, I., and Besenbacher, F. *Quantized conductance in atom-sized wires between two metals.* Phys. Rev. B **52**, 8499 (1995).

[Brataas et al., 2008] Brataas, A., Tserkovnyak, Y., and Bauer, G. E. W. *Scattering theory of gilbert damping.* Phys. Rev. Lett. **101**, 037207 (2008).

[Brataas et al., 2011] Brataas, A., Tserkovnyak, Y., and Bauer, G. E. W. *Magnetization dissipation in ferromagnets from scattering theory.* Phys. Rev. B **84**, 054416 (2011).

[Brouwer, 1998] Brouwer, P. W. *Scattering approach to parametric pumping.* Phys. Rev. B **58**, R10135 (1998).

[Bruus and Flensberg, 2004] Bruus, H. and Flensberg, K. *Many-Body Quantum Theory in Condensed Matter Physics.* Oxford University Press, Oxford, United Kingdom (2004).

[Bunch et al., 2004] Bunch, J., Rhodin, T., and McEuen, P. *Noncontact-afm imaging of molecular surfaces using single-wall carbon nanotube technology.* Nanotechnology **15**, 76 (2004).

[Bunch et al., 2007] Bunch, J. S., van der Zande, A. M., Verbridge, S. S., Frank, I. W., Tanenbaum, D. M., Parpia, J. M., Craighead, H. G., and McEuen, P. L. *Electromechanical resonators from graphene sheets.* Science **315**, 490 (2007).

[Bustos-Marún et al., 2013] Bustos-Marún, R., Refael, G., and von Oppen, F. *Adiabatic quantum motors.* Phys. Rev. Lett. **111**, 060802 (2013).

[Büttiker, 1990] Büttiker, M. *Scattering theory of thermal and excess noise in open conductors.* Phys. Rev. Lett. **65**, 2901 (1990).

[Büttiker, 1992] Büttiker, M. *Scattering theory of current and intensity noise correlations in conductors and wave guides.* Phys. Rev. B **46**, 12485 (1992).

[Büttiker, 1993] Büttiker, M. *Capacitance, admittance, and rectification properties of small conductors.* Journal of Physics: Condensed Matter **5**, 9361 (1993).

[Büttiker et al., 1985] Büttiker, M., Imry, Y., Landauer, R., and Pinhas, S. *Generalized many-channel conductance formula with application to small rings.* Phys. Rev. B **31**, 6207 (1985).

[Büttiker et al., 1994] Büttiker, M., Thomas, H., and Prêtre, A. *Current partition in multiprobe conductors in the presence of slowly oscillating external potentials.* Zeitschrift für Physik B Condensed Matter **94**, 133 (1994).

[Champagne et al., 2005] Champagne, A. R., Pasupathy, A. N., and Ralph, D. C. *Mechanically adjustable and electrically gated single-molecule transistors.* Nano Letters **5**, 305 (2005).

[Chen et al., 2006] Chen, Y., Wang, X., Erramilli, S., Mohanty, P., and Kalinowski, A. *Silicon-based nanoelectronic field-effect ph sensor with local gate control.* Appl. Phys. Lett. **89**, 223512 (2006).

[Cimalla et al., 2006] Cimalla, V., Niebelschütz, F., Tonisch, K., Foerster, C., Brueckner, K., Cimalla, I., Friedrich, T., Pezoldt, J., Stephan, R., Hein, M., and Ambacher, O. *Nanoelectromechanical devices for sensing applications.* Sensors and Actuators B: Chemical **126**, 24 (2006).

[Craig and Linke, 2009] Craig, E. M. and Linke, H. *Mechanochemical model for myosin v.* PNAS **106**, 18261 (2009).

[Craighead, 2000] Craighead, H. G. *Nanoelectromechanical systems.* Science **24**, 1532 (2000).

[Cucchietti et al., 2003] Cucchietti, F. M., Dalvit, D. A. R., Paz, J. P., and Zurek, W. H. *Decoherence and the Loschmidt Echo.* Phys. Rev. Lett. **91**, 210403 (2003).

[Cui et al., 2001] Cui, Y., Wei, Q., Park, H., and Lieber, C. M. *Nanowire nanosensors for highly sensitive and selective detection of biological and chemical species.* Science **293**, 1289 (2001).

[Dalibard et al., 2011] Dalibard, J., Gerbier, F., Juzeliūnas, G., and Öhberg, P. *Colloquium: Artificial gauge potentials for neutral atoms.* Rev. Mod. Phys. **83**, 1523 (2011).

[Danilov et al., 2006] Danilov, A. V., Kubatkin, S. E., Kafanov, S. G., Flensberg, K., and Bjørnholm, T. *Electron transfer dynamics of bistable single-molecule junctions.* Nano Letters **6**, 2184 (2006).

[De Volder et al., 2013] De Volder, M. F. L., Tawfick, S. H., Baughman, R. H., and Hart, A. J. *Carbon nanotubes: Present and future commercial applications.* Science **339**, 535 (2013).

[Dietrich, 1986] Dietrich, J. S. *Tiny tale gets grand.* Engineering and Science **49**, 25 (1986).

[Dóra et al., 2011] Dóra, B., Haque, M., and Zaránd, G. *Crossover from adiabatic to sudden interaction quench in a luttinger liquid.* Phys. Rev. Lett. **106**, 156406 (2011).

[Dóra et al., 2013] Dóra, B., Pollmann, F., Fortágh, J., and Zaránd, G. *Loschmidt echo and the many-body orthogonality catastrophe in a qubit-coupled luttinger liquid.* Phys. Rev. Lett. **111**, 046402 (2013).

[Dundas et al., 2009] Dundas, D., McEniry, E. J., and Todorov, T. N. *Current-driven atomic waterwheels.* Nature Nanotechnology **4**, 99 (2009).

[Ebbesen and Ajayan, 1992] Ebbesen, T. W. and Ajayan, P. M. *Large-scale synthesis of carbon nanotubes.* Nature **358**, 220 (1992).

[Engel, 1997] Engel, M. K. *Single-crystal and solid-state molecular structures of phthalocyanine complexes.* Kawamura Rikagaku Kenkyusho Hokoku **8**, 11 (1997).

[Entin-Wohlman et al., 2002] Entin-Wohlman, O., Aharony, A., and Levinson, Y. *Adiabatic transport in nanostructures.* Phys. Rev. B **65**, 195411 (2002).

[Eom et al., 2011] Eom, K., Park, H. S., Yoon, D. S., and Kwon, T. *Nanomechanical resonators and their applications in biological/chemical detection: Nanomechanics principles.* Physics Reports **503**, 115 (2011), and references therein.

[Fennimore et al., 2003] Fennimore, A. M., Yuzvinsky, T. D., Han, W.-Q., Fuhrer, M. S., Cumings, J., and Zettl, A. *Rotational actuators based on carbon nanotubes.* Nature **424**, 408 (2003).

[Fernández-Torrente et al., 2012] Fernández-Torrente, I., Kreikemeyer-Lorenzo, D., Stróżecka, A., Franke, K. J., and Pascual, J. I. *Gating the charge state of single molecules by local electric fields.* Phys. Rev. Lett. **108**, 036801 (2012).

[Fert, 2008] Fert, A. *Nobel lecture: Origin, development, and future of spintronics.* Rev. Mod. Phys. **80**, 1517 (2008).

[Feynman et al., 1963] Feynman, R., Leighton, R., and Sands, M. *The Feynman Lectures on Physics*, volume 1. Addison-Wesley Publishing Company, Inc., Reading, Massachusetts (1963).

[Feynman, 1960] Feynman, R. P. *There's plenty of room at the bottom.* Engineering and Science **23**, 22 (1960).

[Feynman, 1993] Feynman, R. P. *Infinitesimal machinery.* Journal of Microelectromechanical Systems **2**, 4 (1993).

[Fölsch et al., 2014] Fölsch, S., Martínez-Blanco, J., Yang, J., Kanisawa, K., and Erwin, S. C. *Quantum dots with single-atom precision.* Nature Nanotechnology **9**, 505 (2014).

[Friedel, 1952] Friedel, J. *The distribution of electrons round impurities in monovalent metals.* Philosophical Magazine Series 7 **43**, 153 (1952).

[Fulton and Dolan, 1987] Fulton, T. A. and Dolan, G. J. *Observation of single-electron charging effects in small tunnel junctions.* Phys. Rev. Lett. **59**, 109 (1987).

[Galperin et al., 2007] Galperin, M., Ratner, M. A., and Nitzan, A. *Molecular transport junctions: vibrational effects.* Journal of Physics: Condensed Matter **19**, 103201 (2007).

[Glazman and Pustilnik, 2005] Glazman, L. I. and Pustilnik, M. *Nanophysics: Coherence and Transport.* Elsevier, New York (2005).

[Gorin et al., 2004] Gorin, T., Prosen, T., Seligman, T. H., and Strunz, W. T. *Connection between decoherence and fidelity decay in echo dynamics.* Phys. Rev. A **70**, 042105 (2004).

[Gorin et al., 2006] Gorin, T., Prosen, T., Seligman, T. H., and Žnidarič, M. *Dynamics of loschmidt echoes and fidelity decay.* Phys. Rep. **435**, 33 (2006).

[Gorter, 1951] Gorter, C. J. *A possible explanation of the increase of the electrical resistance of thin metal films at low temperatures and small field strengths.* Physica **17**, 777 (1951).

[Haake, 2010] Haake, F. *Quantum signatures of chaos.* Springer, Berlin Heidelberg, 3 edition (2010).

[Hamill et al., 2014] Hamill, J. M., Wang, K., and Xu, B. *Characterizing molecular junctions through the mechanically controlled break-junction approach.* Reports in Electrochemistry **4**, 1 (2014).

[Hänggi and Marchesoni, 2009] Hänggi, P. and Marchesoni, F. *Artificial brownian motors: Controlling transport on the nanoscale.* Rev. Mod. Phys. **81**, 387 (2009).

[Harris et al., 1991] Harris, A. L., Rothberg, L., Dhar, L., Levinos, N. J., and Dubois, l. H. *Vibrational energy relaxation of a polyatomic adsorbate on a metal surface: methyl thiolate (ch3s) on ag(111).* J. Chem. Phys. **94**, 2438 (1991).

[Heikkilä, 2013] Heikkilä, T. T. *The Physics of Nanoelectronics: Transport and Fluctuation Phenomena at Low Temperatures.* Oxford University Press, Oxford, United Kingdom (2013).

[Hipps, 2001] Hipps, K. W. *It's all about contacts.* Science **294**, 536 (2001).

[Husain et al., 2003] Husain, A., Hone, J., Postma, H. W. C., Huang, X. M. H., Drake, T., Barbic, M., Scherer, A., and Roukes, M. L. *Nanowire-based very-high-frequency electromechanical resonator.* Appl. Phys. Lett. **83**, 1240 (2003).

[Hüttel et al., 2009] Hüttel, A. K., Steele, G. A., Witkamp, B., Poot, M., Kouwenhoven, L. P., and van der Zant, H. S. J. *Carbon nanotubes as ultrahigh quality factor mechanical resonators.* Nano Letters **9**, 2547 (2009).

[Iijima, 1991] Iijima, S. *Helical microtubules of graphitic carbon.* Nature **354**, 56 (1991).

[Imambekov et al., 2012] Imambekov, A., Schmidt, T. L., and Glazman, L. I. *One-dimensional quantum liquids: Beyond the luttinger liquid paradigm.* Rev. Mod. Phys. **84**, 1253 (2012).

[Jalabert and Pastawski, 2001] Jalabert, R. A. and Pastawski, H. M. *Environment-independent decoherence rate in classically chaotic systems.* Phys. Rev. Lett. **86**, 2490 (2001).

[Jauho et al., 1994] Jauho, A.-P., Wingreen, N. S., and Meir, Y. *Time-dependent transport in interacting and noninteracting resonant-tunneling systems.* Phys. Rev. B **50**, 5528 (1994).

[Journet et al., 1997] Journet, C., Maser, W. K., Bernier, P., Loiseau, A., Lamy

de la Chapelle, M., Lefrant, S., Deniard, P., Lee, R., and Fischer, J. E. *Large-scale production of single-walled carbon nanotubes by the electric-arc technique.* Nature **388**, 756 (1997).

[Kane et al., 1994] Kane, C. L., Matveev, K. A., and Glazman, L. I. *Fermi-edge singularities and backscattering in a weakly interacting one-dimensional electron gas.* Phys. Rev. B **49**, 2253 (1994).

[Karkuszewski et al., 2002] Karkuszewski, Z., Jarzynski, C., and Zurek, W. *Quantum chaotic environments, the butterfly effect, and decoherence.* Phys. Rev. Lett. **89**, 170405 (2002).

[Karzig, 2012] Karzig, T. *Low dimensional electron systems out of equilibrium.* PhD thesis, Freie Universität Berlin (2012).

[Ke and Espinosa, 2005] Ke, C. and Espinosa, H. D. *Handbook of Theoretical and Computational Nanotechnology: Nanoelectromechanical systems and modeling*, volume 1. American Scientific Publishers; 1 edition, Valencia, California (2005).

[Kelly et al., 1998] Kelly, T. R., Sestelo, J. P., and Tellitu, I. *New molecular devices: In search of a molecular ratchet.* J. Org. Chem. **63**, 3655 (1998).

[Kelly et al., 1997] Kelly, T. R., Tellitu, I., and Sestelo, J. P. *In search of molecular ratchets.* Angew. Chem. Int. Ed. Engl. **36**, 1866 (1997).

[Kippenberg and Vahala, 2008] Kippenberg, T. J. and Vahala, K. J. *Cavity optomechanics: Back-action at the mesoscale.* Science **321**, 1172 (2008).

[Knap et al., 2012] Knap, M., Shashi, A., Nishida, Y., Imambekov, A., Abanin, D. A., and Demler, E. *Time-dependent impurity in ultracold fermions: Orthogonality catastrophe and beyond.* Phys. Rev. X **2**, 041020 (2012).

[Koch and von Oppen, 2005] Koch, J. and von Oppen, F. *Franck-Condon blockade and giant fano factors in transport through single molecules.* Phys. Rev. Lett. **94**, 206804 (2005).

[Koch et al., 2006] Koch, J., von Oppen, F., and Andreev, A. V. *Theory of the Franck-Condon blockade regime.* Phys. Rev. B **74**, 205438 (2006).

[Kouwenhoven et al., 1997] Kouwenhoven, L., Marcus, C., McEuen, P., Tarucha, S., Westervelt, R., and Wingreen, N. *Electron transport in quantum dots.* Pro-

ceedings of the NATO Advanced Study Institute on Mesoscopic Electron Transport, Curaçao, Netherlands Antilles (1997).

[Kouwenhoven et al., 2001] Kouwenhoven, L. P., Austing, D. G., and Tarucha, S. *Few-electron quantum dots.* Rep. Prog. Phys. **64**, 701 (2001).

[Krans et al., 1993] Krans, J. M., Muller, C. J., Yanson, I. K., Govaert, T. C. M., Hesper, R., and van Ruitenbeek, J. M. *One-atom point contacts.* Phys. Rev. B **48**, 14721 (1993).

[Krive et al., 2010] Krive, I. V., Palevski, A., Shekhter, R. I., and Jonson, M. *Resonant tunneling of electrons in quantum wires (review).* Low Temperature Physics **36**, 119 (2010).

[Kubatkin et al., 2003] Kubatkin, S., Danilov, A., Hjort, M., Cornil, J., Brédas, J.-L., Stuhr-Hansen, N., Hedegård, P., and Bjørnholm, T. *Single-electron transistor of a single organic molecule with access to several redox states.* Nature **425**, 698 (2003).

[Kudernac et al., 2011] Kudernac, T., Ruangsupapichat, N., Parschau, M., Maciá, B., Katsonis, N., Harutyunyan, S. R., Ernst, K.-H., and Feringa, B. L. *Electrically driven directional motion of a four-wheeled molecule on a metal surface.* Nature **479**, 208 (2011).

[Kupferschmidt et al., 2006] Kupferschmidt, J. N., Adam, S., and Brouwer, P. W. *Theory of the spin-torque-driven ferromagnetic resonance in a ferromagnet/normal-metal/ferromagnet structure.* Phys. Rev. B **74**, 134416 (2006).

[Laird et al., 2011] Laird, E. A., Pei, F., Tang, W., Steele, G. A., and Kouwenhoven, L. P. *A high quality factor carbon nanotube mechanical resonator at 39 ghz.* Nano Letters **12**, 193 (2011).

[Landau, 1957a] Landau, L. D. *Oscillations in a fermi-liquid.* Sov. Phys. JETP **5**, 101 (1957a).

[Landau, 1957b] Landau, L. D. *Theory of fermi-liquids.* Sov. Phys. JETP **3**, 920 (1957b).

[Landau, 1959] Landau, L. D. *On the theory of the fermi-liquid.* Sov. Phys. JETP **8**, 70 (1959).

[Landauer, 1957] Landauer, R. *Spatial variation of currents and fields due to localized scatterers in metallic conduction.* IBM J. Res. Dev. **1**, 223 (1957).

[Landauer, 1970] Landauer, R. *Electrical resistance of disordered one-dimensional lattices.* Philos. Mag. **21**, 863 (1970).

[Landauer, 1975] Landauer, R. *Residual resistivity dipoles.* Zeitschrift für Physik B Condensed Matter **21**, 247 (1975).

[Langer and Ambegaokar, 1961] Langer, J. S. and Ambegaokar, V. *Friedel sum rule for a system of interacting electrons.* Phys. Rev. **121**, 1090 (1961).

[Lassagne et al., 2009] Lassagne, B., Tarakanov, Y., Kinaret, J., Garcia-Sanchez, D., and Bachtold, A. *Coupling mechanics to charge transport in carbon nanotube mechanical resonators.* Science **325**, 1107 (2009).

[Lee et al., 2005] Lee, H. J., Lee, J. H., and Ho, W. *Vibronic transitions in single metalloporphyrins.* ChemPhysChem **6**, 971 (2005).

[Lee et al., 2007] Lee, W. C., Cho, Y.-H., and Pisano, A. P. *Nanomechanical protein concentration detector using a nanogap squeezing actuator with compensated displacement monitoring electrodes.* Journal of Microelectromechanical Systems **16**, 802 (2007).

[LeRoy et al., 2004] LeRoy, B. J., Lemay, S. G., Kong, J., and Dekker, C. *Electrical generation and absorption of phonons in carbon nanotubes.* Nature **432**, 371 (2004).

[Leturcq et al., 2009] Leturcq, R., Stampfer, C., Inderbitzin, K., Durrer, L., Hierold, C., Mariani, E., Schultz, M. G., von Oppen, F., and Ensslin, K. *Franck-Condon blockade in suspended carbon nanotube quantum dots.* Nature **5**, 327 (2009).

[Li et al., 1996] Li, W. Z., Xie, S. S., Qian, L. X., Chang, B. H., Zou, B. S., Zhou, W. Y., Zhao, R. A., and Wang, G. *Large-scale synthesis of aligned carbon nanotubes.* Science **274**, 1701 (1996).

[Liang et al., 2002] Liang, W., Shores, M. P., Bockrath, M., Long, J. R., and Park, H. *Kondo resonance in a single-molecule transistor.* Nature **417**, 725 (2002).

[Lotze et al., 2012] Lotze, C., Corso, M., Franke, K. J., von Oppen, F., and Pas-

cual, J. I. *Driving a macroscopic oscillator with the stochastic motion of a hydrogen molecule.* Science **338**, 779 (2012).

[Lü et al., 2010] Lü, J.-T., Brandbyge, M., and Hedegård, P. *Blowing the fuse: Berry's phase and runaway vibrations in molecular conductors.* Nano Letters **10**, 1657 (2010).

[Lü et al., 2012] Lü, J.-T., Brandbyge, M., Hedegård, P., Todorov, T. N., and Dundas, D. *Current-induced atomic dynamics, instabilities, and raman signals: Quasiclassical langevin equation approach.* Phys. Rev. B **85**, 245444 (2012).

[Lü et al., 2011] Lü, J.-T., Hedegård, P., and Brandbyge, M. *Laserlike vibrational instability in rectifying molecular conductors.* Phys. Rev. Lett. **107**, 046801 (2011).

[Madou, 1997] Madou, M. *Fundamentals of Micofabrication.* CRC Press, New York (1997).

[Mahan, 1967] Mahan, G. D. *Excitons in metals: Infinite hole mass.* Phys. Rev. **163**, 612 (1967).

[Martínez-Blanco et al., 2015] Martínez-Blanco, J. Nacci, C., Erwin, S. C., Kanisawa, K., Locane, E., Thomas, M., von Oppen, F., Brouwer, P., and Fölsch, S. *Gating a single-molecule transistor with individual atoms.* accepted for publication in Nature Physics (2015).

[Mello and Kumar, 2004] Mello, P. A. and Kumar, N. *Quantum Transport in Mesoscopic Systems: Complexity and Statistical Fluctuations (Mesoscopic Physics and Nanotechnology).* Oxford University Press, Oxford, United Kingdom (2004).

[Misiorny and Barnaś, 2009] Misiorny, M. and Barnaś, J. *Switching of molecular magnets.* Phys. Status Solidi B **246**, 695 (2009).

[Moskalets and Büttiker, 2004] Moskalets, M. and Büttiker, M. *Adiabatic quantum pump in the presence of external ac voltages.* Phys. Rev. B **69**, 205316 (2004).

[Moskalets and Büttiker, 2005] Moskalets, M. and Büttiker, M. *Magnetic-field symmetry of pump currents of adiabatically driven mesoscopic structures.* Phys. Rev. B **72**, 035324 (2005).

[Moskalets, 2011] Moskalets, M. V. *Scattering Matrix Approach to Non-Stationary Quantum Transport.* Imperial College Press, London, United Kingdom (2011).

[Mozyrsky et al., 2006] Mozyrsky, D., Hastings, M. B., and Martin, I. *Intermittent polaron dynamics: Born-oppenheimer approximation out of equilibrium.* Phys. Rev. B **73**, 035104 (2006).

[Muller et al., 1992] Muller, C. J., van Ruitenbeek, J. M., and de Jongh, L. J. *Conductance and supercurrent discontinuities in atomic-scale metallic constrictions of variable width.* Phys. Rev. Lett. **69**, 140 (1992).

[Münder et al., 2012] Münder, W., Weichselbaum, A., Goldstein, M., Gefen, Y., and von Delft, J. *Anderson orthogonality in the dynamics after a local quantum quench.* Phys. Rev. B **85**, 235104 (2012).

[Muzykantskii et al., 2003] Muzykantskii, B., d'Ambrumenil, N., and Braunecker, B. *Fermi-edge singularity in a nonequilibrium system.* Phys. Rev. Lett. **91**, 266602 (2003).

[Nacci et al., 2012] Nacci, C., Erwin, S. C., Kanisawa, K., and Fölsch, S. *Controlled switching within an organic molecule deliberately pinned to a semiconductor surface.* ACS Nano **6**, 4190 (2012).

[Naik et al., 2006] Naik, A., Buu, O., LaHaye, M. D., Armour, A. D., Clerk, A. A., and Blencowe, M. P.and Schwab, K. C. *Cooling a nanomechanical resonator with quantum back-action.* Nature **443**, 193 (2006).

[Nazarov and Blanter, 2010] Nazarov, Y. V. and Blanter, Y. M. *Quantum Transport: Introduction to Nanoscience.* Cambridge University Press, Cambridge, UK (2010).

[Ng, 1995] Ng, T.-K. *X-ray-edge singularity in nonequilibrium systems.* Phys. Rev. B **51**, 2009 (1995).

[Ng, 1996] Ng, T.-K. *Fermi-edge singularity in nonequilibrium systems.* Phys. Rev. B **54**, 5814 (1996).

[Nozières and de Dominicis, 1969] Nozières, P. and de Dominicis, C. T. *Singularities in the x-ray absorption and emission of metals. iii. one-body theory exact solution.* Phys. Rev. **178**, 1097 (1969).

[Ogawa et al., 1992] Ogawa, T., Furusaki, A., and Nagaosa, N. *Fermi-edge singularity in one-dimensional systems.* Phys. Rev. Lett. **68**, 3638 (1992).

[Ohnishi et al., 1998] Ohnishi, H., Kondo, Y., and Takayanagi, K. *Quantized conductance through individual rows of suspended gold atoms.* Nature **395**, 780 (1998).

[Park et al., 2000] Park, H., Park, J., Lim, A. K. L., Anderson, E. H., Alivisatos, A. P., and McEuen, P. L. *Nanomechanical oscillations in a single-c60 transistor.* Nature **407**, 57 (2000).

[Park et al., 2002] Park, J., Pasupathy, A. N., Goldsmith, J. I., Chang, C., Yaish, Y., Petta, J. R., Rinkoski1, M., Sethna, J. P., Abruña, H. D., McEuen, P. L., and Ralph, D. C. *Coulomb blockade and the kondo effect in single-atom transistors.* Nature **417**, 722 (2002).

[Pecchia et al., 2007] Pecchia, A., Romano, G., and Di Carlo, A. *Theory of heat dissipation in molecular electronics.* Phys. Rev. B **75**, 035401 (2007).

[Peres, 1984] Peres, A. *Stability of quantum motion in chaotic and regular systems.* Phys. Rev. A **30**, 1610 (1984).

[Perrin et al., 2013] Perrin, M. L., Verzijl, C. J. O., Martin, C. A., Shaikh, A. J., Eelkema, R., van Esch, J. H., van Ruitenbeek, J. M., Thijssen, J. M., van der Zant, H. S. J., and Dulić, D. *Large tunable image-charge effects in single-molecule junctions.* Nature Nanotechnology **8**, 282 (2013).

[Pistolesi et al., 2008] Pistolesi, F., Blanter, Y. M., and Martin, I. *Self-consistent theory of molecular switching.* Phys. Rev. B **78**, 085127 (2008).

[Ponomarev et al., 2009] Ponomarev, A. V., Denisov, S., and Hänggi, P. *ac-driven atomic quantum motor.* Phys. Rev. Lett. **102**, 230601 (2009).

[Qi and Zhang, 2009] Qi, X.-L. and Zhang, S.-C. *Field-induced gap and quantized charge pumping in a nanoscale helical wire.* Phys. Rev. B **79**, 235442 (2009).

[Ralph and Stiles, 2008] Ralph, D. C. and Stiles, M. D. *Spin transfer torques.* J. Magn. Magn. Mater. **320**, 1190 (2008).

[Rauch et al., 1998] Rauch, C., Strasser, G., Unterrainer, K., Boxleitner, W.,

Gornik, E., and Wacker, A. *Transition between coherent and incoherent electron transport in* GaAs/GaAlAs *superlattices.* Phys. Rev. Lett. **81**, 3495 (1998).

[Reimann, 2002] Reimann, P. *Brownian motors: noisy transport far from equilibrium.* Physics Reports **361**, 57 (2002).

[Rivier and Simanek, 1971] Rivier, N. and Simanek, E. *Exact calculation of the orthogonality catastrophe in metals.* Phys. Rev. Lett. **26**, 435 (1971).

[Roch et al., 2008] Roch, N., Florens, S., Bouchiat, V., Wernsdorfer, W., and Balestro, F. *Quantum phase transition in a single-molecule quantum dot.* Nature **453**, 633 (2008).

[Roman, 1965] Roman, P. *Advanced Quantum Theory: An Outline of the Fundamental Ideas.* Addison-Wesley Publishing Company, Inc., Reading, Massachusetts (1965).

[Roukes, 2000] Roukes, M. *Technical Digest of the 2000 Solid State Sensor and Actuator Workshop.* Transducers Research Foundation, Cleveland, Ohio (2000).

[Sachdeva et al., 2014] Sachdeva, R., Nag, T., Agarwal, A., and Dutta, A. *Finite-time interaction quench in a luttinger liquid.* Phys. Rev. B **90**, 045421 (2014).

[Safavi-Naeini et al., 2012] Safavi-Naeini, A. H., Chan, J., Hill, J. T., Alegre, T. P. M., Krause, A., and Painter, O. *Observation of quantum motion of a nanomechanical resonator.* Phys. Rev. Lett. **108**, 033602 (2012).

[Sakurai, 1994] Sakurai, J. J. *Modern Quantum Mechanics (Revised Edition).* Addison-Wesley Publishing Company, Inc., Reading, Massachusetts (1994).

[Salger et al., 2009] Salger, T., Kling, S., Hecking, T., Geckeler, C., Morales-Molina, L., and Weitz, M. *Directed transport of atoms in a hamiltonian quantum ratchet.* Science **27**, 1241 (2009).

[Sapmaz et al., 2006] Sapmaz, S., Jarillo-Herrero, P., Blanter, Y. M., Dekker, C., and van der Zant, H. S. J. *Tunneling in suspended carbon nanotubes assisted by longitudinal phonons.* Phys. Rev. Lett. **96**, 026801 (2006).

[Schönhammer, 1991] Schönhammer, K. *Orthogonality exponent and the friction coefficient of an electron gas.* Phys. Rev. B **43**, 11323 (1991).

[Schotte and Schotte, 1969] Schotte, K. D. and Schotte, U. *Tomonaga's model and the threshold singularity of x-ray spectra of metals.* Phys. Rev. **182**, 479 (1969).

[Schuler et al., 2013] Schuler, B., Liu, W., Tkatchenko, A., Moll, N., Meyer, G., Mistry, A., Fox, D., and Gross, L. *Adsorption geometry determination of single molecules by atomic force microscopy.* Phys. Rev. Lett. **111**, 106103 (2013).

[Schulze et al., 2008] Schulze, G., Franke, K. J., and Pascual, J. I. *Resonant heating and substrate-mediated cooling of a single c60 molecule in a tunnel junction.* New Journal of Physics **10**, 065005 (2008).

[Sebastian, 2000] Sebastian, K. L. *Molecular ratchets: Verification of the principle of detailed balance and the second law of dynamics.* Phys. Rev. E **61**, 937 (2000).

[Segal et al., 2007] Segal, D., Reichman, D. R., and Millis, A. J. *Nonequilibrium quantum dissipation in spin-fermion systems.* Phys. Rev. B **76**, 195316 (2007).

[Silva, 2008] Silva, A. *Statistics of the work done on a quantum critical system by quenching a control parameter.* Phys. Rev. Lett. **101**, 120603 (2008).

[Sindona et al., 2013] Sindona, A., Goold, J., Lo Gullo, N., Lorenzo, S., and Plastina, F. *Orthogonality catastrophe and decoherence in a trapped-fermion environment.* Phys. Rev. Lett. **111**, 165303 (2013).

[Sols and Guinea, 1987] Sols, F. and Guinea, F. *Bulk and surface diffusion of heavy particles in metals: A path-integral approach.* Phys. Rev. B **36**, 7775 (1987).

[Song et al., 2009] Song, H., Kim, Y., Jang, Y. H., Jeong, H., Reed, M. A., and Lee, T. *Observation of molecular orbital gating.* Nature **462**, 1039 (2009).

[Sotthewes et al., 2014] Sotthewes, K., Geskin, V., Heimbuch, R., Kumar, A., and Zandvliet, H. J. W. *Research update: Molecular electronics: The single-molecule switch and transistor.* APL Materials **2**, 010701 (2014).

[Splettstoesser et al., 2006] Splettstoesser, J., Governale, M., König, J., and Fazio, R. *Adiabatic pumping through a quantum dot with coulomb interactions: A perturbation expansion in the tunnel coupling.* Phys. Rev. B **74**, 085305 (2006).

[Steele et al., 2009] Steele, G. A., Hüttel, A. K., Witkamp, B., Poot, M., Meerwaldt, H. B., Kouwenhoven, L. P., and van der Zant, H. S. J. *Strong coupling*

between single-electron tunneling and nanomechanical motion. Science **325**, 1103 (2009).

[Stettenheim et al., 2010] Stettenheim, J., Thalakulam, M., Pan, F., Bal, M., Ji, Z., Xue, W., Pfeiffer, L., West, K., Blencowe, M. P., and Rimberg, A. J. *A macroscopic mechanical resonator driven by mesoscopic electrical back-action.* Nature **466**, 86 (2010).

[Stöckmann, 2006] Stöckmann, H.-J. *Quantum chaos: an introduction.* ambridge University Press, New York (2006).

[Stroscio and Eigler, 1991] Stroscio, J. A. and Eigler, D. M. *Atomic and molecular manipulation with the scanning tunneling microscope.* Science **254**, 1319 (1991).

[Swart et al., 2011] Swart, I., Sonnleitner, T., and Repp, J. *Charge state control of molecules reveals modification of the tunneling barrier with intramolecular contrast.* Nano Letters **11**, 1580 (2011).

[Terrones, 2003] Terrones, M. *Science and technology of the twenty-first century: Synthesis, properties, and applications of carbon nanotubes.* Annu. Rev. Mater.Res. **33**, 419 (2003).

[Thess et al., 1996] Thess, A., Lee, R., Nikolaev, P., Dai, H., Petit, P., Robert, J., Xu, C., Lee, Y. H., Kim, S. G., Rinzler, Andrew G.and Colbert, D. T., Scuseria, G. E., Tománek, D., Fischer, J. E., and Smalley, R. E. *Crystalline ropes of metallic carbon nanotubes.* Science **26**, 483 (1996).

[Thomas et al., 2015] Thomas, M., Karzig, T., and Viola Kusminskiy, S. *Langevin dynamics of a heavy particle and orthogonality effects.* arXiv:1506.06061 (2015).

[Thomas et al., 2012] Thomas, M., Karzig, T., Viola Kusminskiy, S., Zaránd, G., and von Oppen, F. *Scattering theory of adiabatic reaction forces due to out-of-equilibrium quantum environments.* Phys. Rev. B **86**, 195419 (2012).

[Tierney et al., 2011] Tierney, H. L., Murphy, C. J., Jewell, A. D., Baber, A. E., Iski, E. V., Khodaverdian, H. Y., McGuire, A. F., Klebanov, N., and Sykes, E. C. H. *Experimental demonstration of a single-molecule electric motor.* Nat. Nano. **6**, 625 (2011).

[Todorov et al., 2010] Todorov, T. N., Dundas, D., and McEniry, E. J. *Nonconservative generalized current-induced forces.* Phys. Rev. B **81**, 075416 (2010).

[Tserkovnyak et al., 2002] Tserkovnyak, Y., Brataas, A., and Bauer, G. E. W. *Enhanced gilbert damping in thin ferromagnetic films.* Phys. Rev. Lett. **88**, 117601 (2002).

[van Wees et al., 1988] van Wees, B. J., van Houten, H., Beenakker, C. W. J., Williamson, J. G., Kouwenhoven, L. P., van der Marel, D., and Foxon, C. T. *Quantized conductance of point contacts in a two-dimensional electron gas.* Phys. Rev. Lett. **60**, 848 (1988).

[Vavilov et al., 2001] Vavilov, M. G., Ambegaokar, V., and Aleiner, I. L. *Charge pumping and photovoltaic effect in open quantum dots.* Phys. Rev. B **63**, 195313 (2001).

[Wang et al., 2012] Wang, Y., Wu, K., Kröger, J., and Berndt, R. *Review article: Structures of phthalocyanine molecules on surfaces studied by STM.* AIP Advances **2**, 041402 (2012).

[Weiss, 1999] Weiss, U. *Quantum Dissipative Systems*, volume 10. World Scientific Publishing Co. Pte. Ltd., Singapore (1999).

[Wharam et al., 1988] Wharam, D. A., Thornton, T. J., Newbury, R., Pepper, M., Ahmed, H., Frost, J. E. F., Hasko, D. G., Peacock, D. C., Ritchie, D. A., and Jones, G. A. C. *One-dimensional transport and the quantisation of the ballistic resistance.* Journal of Physics C: Solid State Physics **21**, L209 (1988).

[Wigner, 1955] Wigner, E. P. *Lower limit for the energy derivative of the scattering phase shift.* Phys. Rev. **98**, 145 (1955).

[Woodside and McEuen, 2002] Woodside, M. T. and McEuen, P. L. *Scanned probe imaging of single-electron charge states in nanotube quantum dots.* Science **296**, 1098 (2002).

[Yamada and Yosida, 1982] Yamada, K. and Yosida, K. *Orthogonality catastrophe for a system of interacting electrons. iii.* Progr. of Theor. Phys. **68**, 1504 (1982).

[Yanson et al., 1998] Yanson, A. I., Rubio Bollinger, G., van den Brom, H. E., and Agraït, N. andvan Ruitenbeek, J. M. *Formation and manipulation of a metallic wire of single gold atoms.* Nature **395**, 783 (1998).

[Yu et al., 2004] Yu, L. H., Keane, Z. K., Ciszek, J. W., Cheng, L., Stewart, M. P.,

Tour, J. M., and Natelson, D. *Inelastic electron tunneling via molecular vibrations in single-molecule transistors.* Phys. Rev. Lett. **93**, 266802 (2004).

[Yu and Natelson, 2004] Yu, L. H. and Natelson, D. *The kondo effect in c60 single-molecule transistors.* Nano Letters **4**, 79 (2004).

[Yuval and Anderson, 1970] Yuval, G. and Anderson, P. W. *Exact results for the kondo problem: One-body theory and extension to finite temperature.* Phys. Rev. B **1**, 1522 (1970).

[Zurek, 2001] Zurek, W. H. *Sub-Planck structure in phase space and its relevance for quantum decoherence.* Nature **412**, 712 (2001).

Publications

The main part of the present thesis is based on the following publications/projects.

M. Thomas, T. Karzig, S. Viola Kusminskiy, G. Zaránd, and F. von Oppen. "Scattering theory of adiabatic reaction forces due to out-of-equilibrium quantum environments". *Physical Review B* **86**, 195419 (2012), DOI: 10.1103/PhysRevB.86.195419. [Thomas et al., 2012]

M. Thomas, T. Karzig, and S. Viola Kusminskiy. "Langevin dynamics of a heavy particle and orthogonality effects". *arXiv*:1506.06061 (2015). [Thomas et al., 2015]

J. Martínez-Blanco, C. Nacci, S. C. Erwin, K. Kanisawa, E. Locane, M. Thomas, F. von Oppen, P. Brouwer, and S. Fölsch. "Gating a single-molecule transistor with individual atoms". accepted for publication in *Nature Physics* (2015). [Martínez-Blanco et al., 2015]

Curriculum vitae

For reasons of data protection, the *curriculum vitae* is not included in the online version of this thesis.

Acknowledgements

This work would not have been possible without the support of many people. First and foremost, I owe deep gratitude to my advisor Felix von Oppen. I am grateful to him for his supervision and for offering me the opportunity for my PhD studies. Especially his intuitive way of addressing difficult physical problems has soon begun to fascinate me and will definitely accompany and encourage me in my further studies. I furthermore would like to express my thankfulness to him for inviting me to the California Institute of Technology in Pasadena during his sabbatical, where I greatly benefited from.

Besides to my advisor, I would like to deeply thank my co-workers who contributed to this work, that is Torsten Karzig (Caltech), Silvia Viola Kusminskiy (FU Berlin), Gergely Zaránd (BME Budapest), Piet Brouwer (FU Berlin), Elina Locane (FU Berlin), Christophe Nacci (PDI Berlin), Steven C. Erwin (CMS Washington, DC), Kiyoshi Kanisawa (NTT Basic Research Laboratories), Stefan Fölsch (PDI Berlin) and Jesús Martínez-Blanco (PDI Berlin), for sharing their knowledge and for innumerable interesting and instructive discussions. Moreover, I would like to thank Stefan Fölsch and Jesús Martínez-Blanco for providing me experimental data on the single-molecule transistor.

In addition, my sincere thanks also go to Tamara Nunner for co-refereeing this thesis.

Furthermore, I am grateful to all my friends and colleagues of the Dahlem Center of Complex Quantum Systems, the Sfb 658 and visiting friends for useful discussions and for creating a remarkably friendly working atmosphere. My thanks also go to Brigitte Odeh for supporting me in administration matters.

Finally, I acknowledge financial support by the Deutsche Forschungsgemeinschaft through Sfb 658.